1-1-2006

Shear design and behavior of Ultra-High Performance Concrete

Brian Everett Degen
Iowa State University

Shear design and behavior of

Ultra-High Performance Concrete

by

Brian Everett Degen

A thesis submitted to the graduate faculty

in partial fulfillment of the requirements for the degree of

MASTER OF SCIENCE

Major: Civil Engineering (Structural Engineering)

Program of Study Committee:
Brent Phares, Co-major Professor
Sri Sritharan, Co-major Professor
Terry Wipf
Lester Schmerr

Iowa State University

Ames, Iowa

2006

Graduate College
Iowa State University

This is to certify that the master's thesis of

Brian Everett Degen

has met the thesis requirements of Iowa State University

Signatures have been redacted for privacy

TABLE OF CONTENTS

ABSTRACT

Research is presented herein describing the behavior of a newly developed material called Ultra-High Performance Concrete (UHPC). The two primary objectives of this research are to develop a shear design procedure for possible code adoption and to provide a performance evaluation of structural testing to ensure the viability of the first UHPC bridge design in the United States. Two other secondary objectives will be helpful in this pursuit including: defining of material properties and understanding of flexural behavior. In order to obtain information in these areas several tests have been carried out including material testing, large-scale laboratory flexure testing, large-scale laboratory shear testing, large-scale laboratory flexure-shear testing, small-scale laboratory shear testing, and field testing. In addition future field testing will be completed on the UHPC bridge. Experimental and analytical results of the described tests are presented herein. Analytical models of flexure and shear behavior have been developed using iterative computer based procedures. Previous research has been referenced explaining a simplified flexural design procedure and a simplified pure shear design procedure. This work describes a shear design procedure based on the Modified Compression Field Theory (MCFT) which can be used for UHPC. The main difference in the procedure for use with UHPC is the consideration of residual tensile strength of the concrete after cracking. Finally, conclusions are provided about the viability of the UHPC bridge and recommendations are made for future research.

ACKNOWLEDGEMENTS

Throughout this research many people have been helpful in many different ways. My family and friends have supported me personally throughout my college experience. My committee members have facilitated my research and my education. The Iowa State University professors and staff have imparted educational and practical knowledge that have been useful in my research. The Center for Transportation Research and Education has provided facilities to support a working environment. The Iowa Department of Transportation and Wapello County have supplied financial capabilities, design expertise, and research collaboration. In particular Dean Bierwagen from the Iowa Department of Transportation and Brian Moore from Wapello County have had instrumental involvement with this project. Lafarge North America has shared expertise on the construction, research and design of Ultra-High Performance Concrete. The Federal Highway Administration has provided research collaboration and test equipment. Thank you to all who have been involved.

LIST OF FIGURES

LIST OF TABLES

LIST OF NOTATION

a: maximum aggregate diameter
A: gross cross-sectional area
A_b: area below centroid
A_c: area of bottom flange
A_e: effective area
A_n: area of nodal face
A_p: area of strands
A_p: area of strands in bottom flange
A_{pc}: area of strands within bottom flange
A_q: second order quadratic equation coefficient
A_s: area of mild reinforcement
A_{sbf}: area of mild reinforcement in bottom flange
A_{st}: area of strut
A_t: area of top flange
A_v: area of shear reinforcement within distance s
A_w: area of web
b: width of section
b_w: width of web
B: tensile stress factor
B_q: first order quadratic equation coefficient
c: distance from centroid
c_c: distance from composite centroid
c_t: distance from transformed centroid
c_T: prestressing ratio
c_v: maximum distance from shear reinforcement in transverse direction
c_x: maximum distance from longitudinal reinforcement in vertical direction
C_q: constant quadratic equation coefficient
d: depth
d_{bv}: diameter of shear reinforcement
d_{bx}: diameter of longitudinal reinforcement
e: eccentricity of axial force
E_c: modulus of concrete
E_{cf}: modulus of composite fiber
E_{ci}: initial modulus of concrete
E_{cs}: modulus of composite concrete and strands
E_p: modulus of strand
E_s: modulus of mild reinforcement
f_c: compressive stress
f'_c: maximum compressive strength of concrete
f_{cr}: cracking tensile strength of concrete
f_{cs}: maximum stress of composite concrete and strands
f_{max}: maximum tensile strength of concrete
f_p: stress in strand
f_{ps}: stress in strand at nominal strength [9]
f_{pu}: ultimate strand strength
f_{py}: yield strength of strand
f_s: stress in mild reinforcement
f_v: stress in shear reinforcement

f_{vy}: yield strength of shear reinforcement
f_y: yield strength of mild reinforcement
F: applied flexural cracking load
F_{bf}: tensile force resultant in bottom flange
F_c: compressive force
F_{nn}: nominal nodal force
F_{ns}: nominal strut force
F_{nt}: nominal tie force
G: shear modulus
h: distance above bottom of section
H: height
I: moment of inertia
I_t: transformed moment of inertia
I_c: composite moment of inertia
j: lever arm percentage of depth
k_1: 0.4 for deformed bars and 0.8 for plain bars or bonded strands
K: creep coefficient
L: span
L_f: length of fiber
M: applied external moment
M_c: moment applied to composite section
M_{cr}: cracking moment
M_{dl}: dead load moment
M_i: internal moment
M_{ll}: live load moment
M_n: nominal moment strength
M_t: moment applied to transformed section
M_u: factored ultimate moment
N: axial force
N_p: axial force from moment
N_u: factored ultimate axial force
p: prestressing equivalent external pressure
P: applied axial force
P_f: prestressing force final
P_{max}: maximum applied compressive force
Q: second moment of area
Q_t: transformed second moment of area
Q_c: composite second moment of area
s: spacing of shear reinforcement
s_{mx}: crack spacing in longitudinal direction
$s_{m\theta}$: crack spacing in direction of principal compressive stress
s_{mv}: crack spacing in vertical direction
s_x: spacing of longitudinal reinforcement in transverse direction
u: unit weight of concrete
V: applied shear
V_c: concrete shear contribution
V_c: shear applied to composite section
V_f: fiber shear contribution
V_p: shear force provide by strands

V_n: nominal shear strength
V_{n1}: nominal shear strength
V_{n2}: nominal shear strength
V_s: reinforcement shear contribution
V_t: shear applied to transformed section
V_u: factored ultimate shear force
w: crack width
x: position along length of beam
α: thermal expansion coefficient
α_1: 1.0 for deformed, 0.7 for plain, and 0 for unbonded reinforcement
α_2: 1.0 for short-term monotonic loading and 0.7 for sustained and/or repeated loads
β: crack angle
β_n: node factor
β_{st}: strut factor
Δ: deflection due to moment and shear
Δ_m: deflection due to moment
ΔT: change in temperature
Δ_v: deflection due to shear
$\varepsilon`_c$: strain associated with $f`_c$
ε_{cr}: cracking tensile strain of concrete
ε_l: strain limit
ε_{max}: maximum magnitude of strain corresponding to f_{max}
ε_{min}: minimum magnitude of strain corresponding to f_{max}
ε_{p1}: principal tensile strain
ε_{p2}: principal compressive strain
ε_{sh}: total shrinkage strain
ε_x: longitudinal strain
ε_{xa}: allowable longitudinal strain
ε_{xb}: longitudinal strain at bottom of section
ε_y: vertical strain
γ: final prestressing percentage
γ_{bf}: partial safety factor
γ_{max}: maximum shear strain
γ_{xy}: shear strain in the x-y plane
φ: strength reduction factor
ρ_v: shear reinforcement ratio
ρ_x: longitudinal reinforcement ratio
χ: curvature
σ_f: final stress due to prestress after losses
σ_{p1}: principal tensile stress
σ_{p2}: principal compressive stress
σ_{p2m}: maximum principal compressive stress
σ_x: longitudinal stress
σ_{xc}: longitudinal stress based on constitutive properties
σ_y: vertical stress
τ_{ci}: shear stress at crack
τ_{cr}: cracking shear stress
τ_{max}: maximum shear stress
τ_{xy}: shear stress in the x-y plane

θ: principal compressive stress angle
υ: poisson's ratio
ξ_1: first softening coefficient
ξ_2: second softening coefficient

CHAPTER 1: INTRODUCTION

1.1 BACKGROUND

In 2003 the Iowa Department of Transportation (Iowa DOT) and Wapello County, Iowa began planning for a bridge replacement project. At that time, the bridge (see Fig. 1.1) known as FHWA structure #330530 100th Ave. over Little Soap Creek was closed due to durability and strength concerns. This bridge was a steel truss bridge with a timber deck and timber abutments. The need and timing for a bridge replacement presented an opportunity to use a newly developed material called Ultra-High Performance Concrete (UHPC). Ultimately, this became the first UHPC bridge constructed in the United States and construction was partially funded through the Federal Highway Administration's (FHWA) Innovative Bridge Research and Construction (IBRC) program.

Figure 1.1. Wapello County truss bridge prior to replacement.

1.2 CONCRETE TYPES

One general way of classifying concrete is within the following three categories: conventional concrete, High Performance Concrete, and UHPC. Conventional concrete generally has compressive strengths of at least 2,000 psi with maximum design strengths of approximately 6,000 psi. In general the material components include coarse aggregate, fine aggregate, cement, and water. Fundamentally, the cement and water undergo a chemical reaction thereby creating a hardened paste that binds the aggregate together.

Generally, High Performance Concrete (HPC) has compressive strengths of approximately 6,000 psi to 16,000 psi. In addition to the material components of conventional concrete, HPC can contain silica fume, fly ash, retarder, and superplasticizer. Silica fume and fly ash act as extremely fine aggregate filling voids in the concrete mix and thereby creating a denser and stronger material. Generally in all concretes, the less water compared with the amount of cement that exists the stronger the concrete. Accelerator is a chemical that allows the water to cement ratio to be reduced by delaying the concrete from setting up to allow time to place the material. Superplasticizer is a chemical that allows the water to cement ratio to be further reduced by liquefying the concrete, thus allowing placement of the material with improved workability.

The compressive strength of UHPC is generally 16,000 psi to 30,000 psi. Also, the tensile strength which is normally negligible and therefore neglected in other concretes can be as high as 1,700 psi. Refer to section 2.1 on the material properties of UHPC. The material components of UHPC can include all of the materials previously listed except for coarse aggregate. The exclusion of coarse aggregate filler material, which is generally weaker than other components, makes a stronger concrete possible. UHPC also contains small fibers either steel or organic randomly mixed within the concrete. The steel fibers used for this research constitute 2% of the mix by volume and their size is 0.5 in. long by 0.006 in. diameter. These fibers increase both the material's tensile strength and its ductility. Refer to Table 1.1 for a typical material composition of UHPC. For comparison Fig. 1.2 shows samples of UHPC and conventional concrete. The darker colored square samples are composed of UHPC and the presence of steel fibers is apparent. The conventional concrete, in the light circular samples shows the presence of coarse aggregate which is not a component of UHPC.

Table 1.1. Typical UHPC material composition [1].

Material	Amount (lb/cubic yard)
Portland Cement	1200
Fine Sand	1720
Silica Fume	390
Ground Quartz	355
Superplasticizer	51.8
Accelerator	50.5
Steel Fibers	263
Water	184

Figure 1.2. Samples of UHPC and conventional concrete.

UHPC materials may be referred to by several names. The term Reactive Powder Concrete is sometimes used in the academic world to describe UHPC. UHPC may also be identified as Fiber Reinforced Concrete referring to the use of the fibers. All the research summarized herein referring to UHPC has been conducted on one specific brand name of UHPC manufactured by Lafarge North America and known as Ductal®.

1.3 ADVANTAGES AND DISADVANTAGES OF UHPC

Several characteristics of UHPC make it a desirable construction material. With increased compressive and tensile strengths the material lends itself well to structural applications by allowing greater loads to be supported. By utilizing the higher strengths, traditional structural components can also be reduced in size and weight. A secondary benefit of UHPC is the high density of the material making it essentially impermeable to water and chlorides, thus making the material highly durable. These are important characteristics in areas of high impact and where water or chloride ions can corrode steel reinforcement.

Although not discussed in detail here, the life-cycle cost of UHPC may prove to be lower than other concretes. UHPC material itself is more costly than some other concretes due to the elimination of the less expensive coarse aggregate material, use of more cement, and the addition of fibers.

However, the labor cost associated with creating a structural component such as a beam can be reduced. This is because the steel fibers are mixed within the concrete matrix in a random orientation as compared to other concretes where larger steel reinforcing bars must be hand placed in specific orientations. Additionally, in some cases steel reinforcement may potentially be eliminated completely. Furthermore, by reducing the size and weight of structural components, less material will be required and lower transportation costs may be realized at the same time. Because of the enhanced impermeability and durability characteristics of the material, long term costs associated with the deterioration of structural components may also be reduced. Refer to Table 1.2 for a summary of advantages and disadvantages.

Table 1.2. Advantages and disadvantages of UHPC.

Advantages	Disadvantages
High Compressive Strength	Short-Term Costs
High Tensile Strength	material cost
High Shear Strength	mixing time
High Impermeability	casting bed time
High Durability	heat treatment
Self Leveling	Cast-In-Place Construction
Self Healing Unhydrated Cement	is not Desirable
Long-Term Costs	
eliminate labor installing strirrups	
fewer deck replacements	
reduced weight for shipping	

1.4 RESEARCH OBJECTIVES

Previous research has not extensively investigated shear behavior of UHPC. One primary objective is to acquire knowledge on the shear behavior of UHPC for the purpose of developing a shear design procedure. The second primary objective is to complete a structural performance evaluation of a UHPC girder for use in the Wapello County bridge to assure the viability of the bridge design and verify design assumptions. One secondary objective is to define the material properties of UHPC more extensively than has been previously published. The other secondary objective is to more fully understand the flexural behavior of a UHPC girder. This understanding is necessary for the development of an UHPC shear design procedure because of flexure-shear interaction and it is also necessary for ensuring a viable design for the Wapello County bridge girders.

1.5 CONVENTIONS

Consistent sign conventions are followed throughout this report. Refer to Table 1.3 for the specific conventions. In addition, when using the square root of the compressive strength in computations, the numerical value of the compressive strength should be used in psi units. The result of the square root of the compressive strength will also be in psi units.

Table 1.3. Sign conventions.

Quantity	Positive	Negative
Stress / Strain	Compression	Tension
Vertical Position	Upward	Downward
Deflection	Downward	Upward
Moment	Causing (+) Deflection	Causing (-) Deflection
Curvature	Causing (+) Deflection	Causing (-) Deflection
Slope	Counter Clockwise	Clockwise

1.6 REPORT CONTENT

This report summarizes information about the various aspects of the overall research program. A literature review is provided in Chapter 2 describing: UHPC material properties, UHPC flexural strength, UHPC and conventional concrete shear strengths, UHPC structural testing, and UHPC prestress bond. The first UHPC bridge constructed in the United States is described in Chapter 3. The adequacy of the design for this bridge was verified through an experimental test program completed at Iowa State University (ISU) and described in Chapter 4. The program has the following components: material testing, large-scale laboratory testing, small-scale laboratory testing, and field testing. Chapter 5 describes computational methods associated with the research including analytical modeling of UHPC in flexure and shear. Analytical and experimental results are presented in Chapter 6. Chapter 7 recommends a shear design procedure to be used with UHPC for both the service limit state and the ultimate limit state. Finally, Chapter 8 concludes the report discussing an overall summary, performance evaluation of the bridge beam design, and future research of UHPC.

CHAPTER 2: LITERATURE REVIEW

Previous research is provided herein on UHPC material properties, flexural strength, shear strength, structural testing, and prestress bond. Little research has currently been conducted on the shear strength of UHPC therefore information has been provided on approaches to determining shear strength for conventional concrete.

2.1 MATERIAL PROPERTIES

The constitutive material properties of UHPC need to be known to define a stress-stain relationship which can be used to predict responses and strengths of UHPC members. The constitutive properties used for this report are idealizations of data from a number of sources and are summarized in Fig. 2.1, Fig. 2.2, and Table 2.1. The modulus of elasticity was defined by Chuang and Ulm [2]. The cracking tensile stress used was also defined by Chuang and Ulm [2]. The general shape of Fig. 2.1 was obtained from the Association Francaise de Genie Civil (French Association of Civil Engineering) (AFGC) [3], but has been represented by a parabola to facilitate computations that will be discussed herein. The tensile data used were from Bristow and Sritharan [4] with the cracking stress and strain altered slightly to adhere to the previously stated modulus of elasticity and cracking tensile strength.

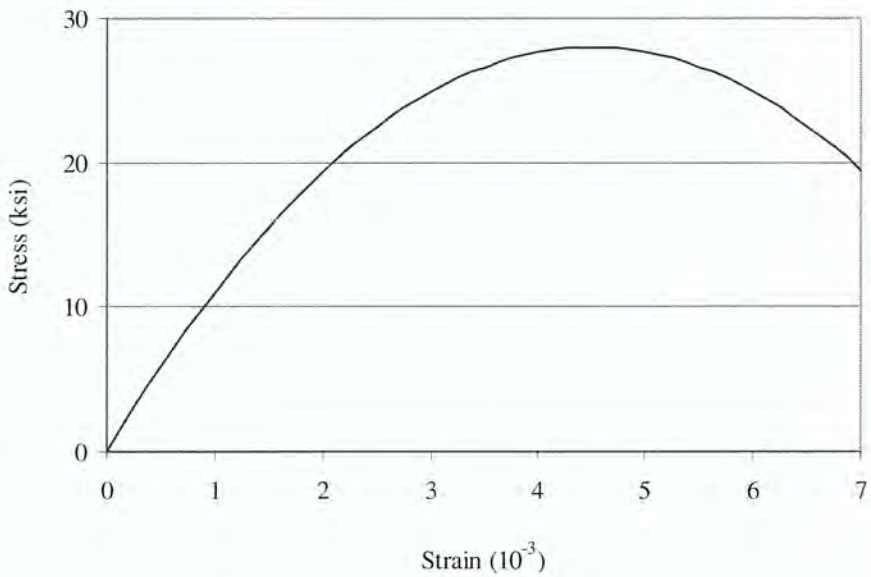

Figure 2.1. Compressive constitutive properties of UHPC.

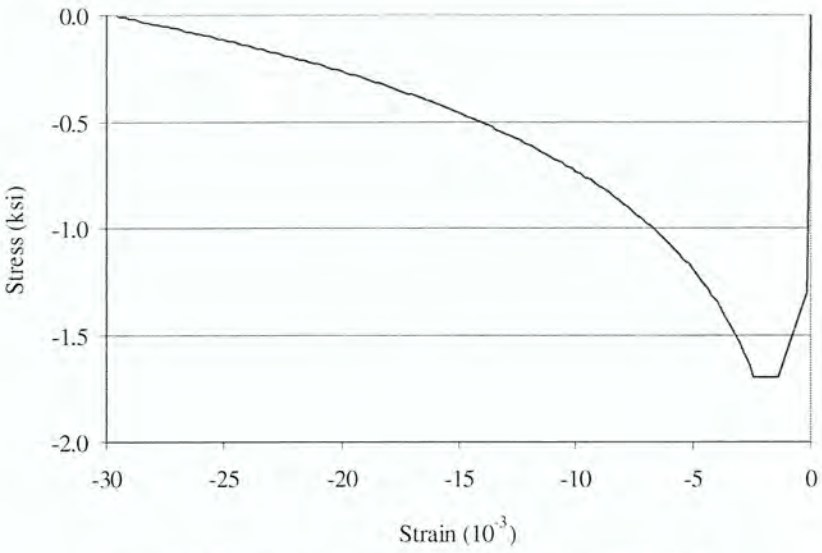

Figure 2.2. Tensile constitutive properties of UHPC.

Table 2.1. Compressive and tensile constitutive properties of UHPC.

Stress (ksi)	Strain (10^{-3})
$f`_c[2(\text{Strain}/\varepsilon`_c)-(\text{Strain}/\varepsilon`_c)^2]$	> 0
-1.100 (f_{cr})	-0.141
-1.700 (f_{max})	-1.400 (ε_{min})
-1.700 (f_{max})	-2.400 (ε_{max})
(0.672)LN(-Strain)+2.362 < 0	< -2.400

In addition, other material properties are also useful for structural engineering concepts. The following values are followed by their referenced source and are used throughout this work.

- E_c = 7820 ksi — modulus of concrete [2]
- E_{ci} = 5700 ksi — initial modulus of concrete [3]
- E_{cf} = 0 ksi — modulus of composite fiber [5]
- E_p = 28,500 ksi — modulus of strand [6]
- $f`_c$ = 28 ksi — maximum compressive strength of concrete [2]
- f_{cr} = -1.1 ksi — cracking tensile strength of concrete [2]
- f_{max} = -1.7 ksi — maximum tensile strength of concrete [4]
- f_{pu} = 270 ksi — ultimate strand strength [6]
- K = 0.3 — creep coefficient [3]

- L_f = 0.25 in. — length of fiber [5]
- u = 156 pcf — unit weight of concrete [3]
- α = 6.55×10^{-6} per °F — thermal expansion coefficient [3]
- $\varepsilon`_c$ = 0.0045 — strain associated with f`c [3]
- ε_{max} = -0.0024 — maximum magnitude of strain corresponding to f_{max} [4]
- ε_{min} = -0.0014 — minimum magnitude of strain corresponding to f_{max} [4]
- ε_{sh} = 5.50×10^{-4} — total shrinkage strain [3]
- γ_{bf} = 1.3 — partial safety factor [7]
- υ = 0.2 — poisson's ratio [3]

The constitutive properties of UHPC in compression are generally better known than for tension. Generally, research has shown the compressive strength of UHPC to be around 28 ksi as shown by research by Graybeal and Hartmann [1] in Table 2.2.

Table 2.2. Compressive strength of 3x6 in. UHPC cylinders tested by Graybeal and Hartmann [1].

Curing Method	Samples	Compressive Strength (ksi)	Standard Deviation (ksi)
Steam	96	28.0	2.1
Ambient Air	44	18.0	1.8
Tempered Steam	18	25.2	1.3
Delayed Steam	18	24.9	1.5

The constitutive properties of UHPC in tension are difficult to quantify with research still investigating this issue and with different researchers formulating slightly different conclusions. Graybeal and Hartmann [1] determined the cracking strength of UHPC, agreeing fairly well with other researchers, as shown in Table 2.3 for three different tensile tests and for four different curing conditions. Chuang and Ulm [2] attempted to define the tensile constitutive properties of UHPC as shown in Fig. 2.3 using a notched tensile plate test. However, the stress-strain relationship is not fully defined because results are not provided past the peak stress. The AFGC [3] also defined the tensile properties of UHPC. However, the recommendations require arbitrary determinations in order to obtain a complete stress-strain curve.

Table 2.3. Tensile cracking strength of UHPC tested by Graybeal and Hartmann [1].

Curing Method	Mortar Briquette (ksi)	Split Cylinder (ksi)	Direct Tension (ksi)
Steam	1.20	1.70	1.60
Air	0.90	1.30	0.82
Tempered Steam	1.45	1.60	1.14
Delayed Steam	1.00	1.60	1.62

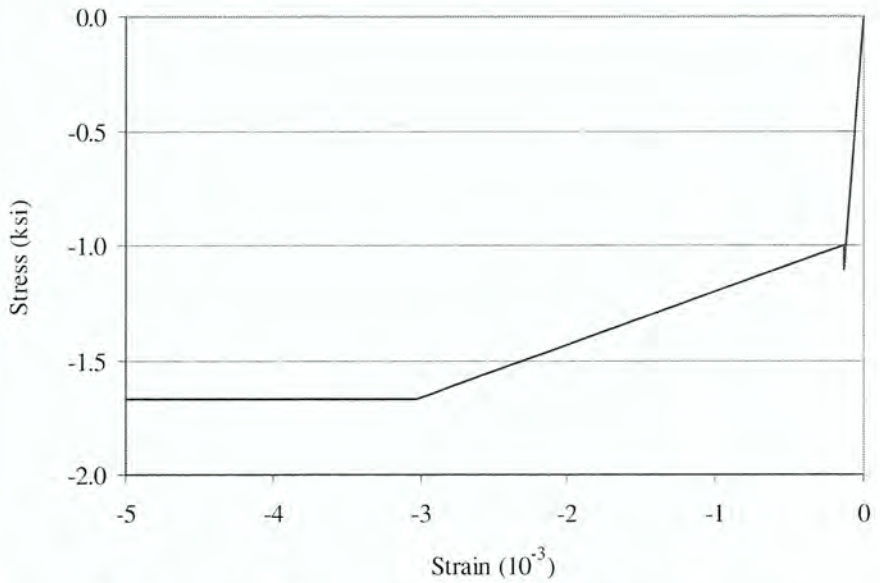

Figure 2.3. Tensile constitutive properties of UHPC tested by Chuang and Ulm [2].

Some researches have suggested a limiting flexural tensile strain value based on the height of the specimen undergoing flexural loads. The reason for limiting the strain is because as the crack width grows large in comparison to the length of the fibers, it is postulated that tension stresses will not be transferred across the crack. Gowripalan and Gilbert [5] have proposed a limiting strain value shown in equation 2.1. The AFGC [3] recommends a similar limiting strain value shown in equation 2.2.

$$\varepsilon_l = -\frac{L_f}{1.2 \cdot d} \geq 0.001 \quad \text{strain limit} \tag{2.1}$$

Where: L_f = length of fibers (in.)

d = depth (in.)

$$\varepsilon_l = -\frac{3L_f}{8 \cdot H} \quad \text{strain limit} \tag{2.2}$$

Where: H = height (in.)

Research has also been conducted at Iowa State University (ISU) separate from the work summarized herein by Bristow and Sritharan [4]. In that work direct tension tests using dog-bone-shaped samples were conducted to determine the constitutive tensile properties of UHPC. The properties established in that work matched relatively well with the properties determined by Chuang and Ulm [2]. However, Bristow and Sritharan's results are extended to a larger strain level. Figure 2.2 and Table 2.1 show the stress-strain relationship as linear to a stress of 1.3 ksi at which point the stress increases to 1.7 ksi, flattens off and then declines gradually.

2.2 FLEXURAL STRENGTH

Previous research by Park, Chuang and Ulm [6] and Ulm and Chuang [7] has been completed concerning the flexural capacity of an UHPC member. Equations 2.3 to 2.13 summarized below were proposed by the authors to ensure that a given section is acceptable under given loading conditions.

$$c_T = \frac{A_{pc}}{A_c} \quad \text{prestressing ratio} \tag{2.3}$$

Where: A_{pc} = area of strands within bottom flange (in.^{2})

A_c = area of bottom flange (in.^{2})

$$\gamma = \frac{P_f}{A_p \cdot f_{pu}} \quad \text{final prestressing percentage} \tag{2.4}$$

Where: P_f = prestressing force final (kips)

A_p = area of strands (in.^{2})

$$p = \gamma \cdot f_{pu} \cdot c_T \quad \text{prestressing equivalent external pressure (ksi)} \tag{2.5}$$

$$\varepsilon_l = \max\left(-\frac{3 \cdot L_f}{8 \cdot H}, -\frac{3}{200}\right) \quad \text{strain limit} \tag{2.6}$$

$$E_{cs} = E_{cf} + c_T \cdot \left(E_p - E_{cf}\right) \quad \text{modulus of composite concrete and strands (ksi)} \tag{2.7}$$

$$f_{cs} = \min\left\{\left|f_{\max}\right| + c_T \cdot \left[(1-\gamma)\cdot f_{pu} - \left|f_{\max}\right|\right], \left[E_{cs} + M \cdot \left(1 + \frac{E_{cs}}{E_c}\right)\right] \cdot \left|\varepsilon_l\right| + \left(1 + \frac{E_{cs}}{E_c}\right) \cdot \left|f_{cr}\right|\right\}$$

maximum stress of composite concrete and strands (ksi) (2.8)

Where: M = applied external moment (in.- kips)

$$j = \frac{M}{d \cdot (p + f_{cs}) \cdot A_c} \quad \text{lever arm percentage of depth} \tag{2.9}$$

$$M_i = M - p \cdot A_c \cdot j \cdot d \quad \text{internal moment (in.- kips)} \tag{2.10}$$

$$F_c = \frac{M_i}{j \cdot d} \quad \text{compressive force (kips)} \tag{2.11}$$

$$f_c = \frac{F_c}{A_t} \quad \text{compressive stress (ksi)} \tag{2.12}$$

Where: A_t = area of top flange (in.^{2})

$$f_c < f`_c \tag{2.13}$$

2.3 SHEAR STRENGTH

One simple procedure to compute an estimated ultimate shear strength of an UHPC structure has been developed by Chuang and Ulm [7] using previous information from the AFGC [3] as shown in equations 2.14 through 2.16. The basic concept of this procedure is to simply add the concrete contribution and fiber contribution to determine an ultimate shear strength. In this formulation, the concrete shear strength is determined empirically as the square root of the compressive strength. The fiber contribution is determined based on the tensile strength acting perpendicular to a crack. The crack occurs over the moment arm height and the web width. The height of the moment arm is estimated to be 90% of the depth. The tangent term is derived by finding the vertical component of the tensile strength that acts over the diagonal length of the crack. A partial safety factor is used to account for the degree to which the strength of this new material is still unknown. It should be pointed out that this procedure does not provide any information about the response of the structure. Refer to equation 5.9 for the computation of the crack angle.

$$V_c = 1.7 \cdot b_w \cdot d\sqrt{f`_c} \quad \text{concrete shear contribution (kips)} \tag{2.14}$$

Where: b_w = width of web (in.)

d = depth (in.)

$$V_f = \frac{0.9 \cdot b_w \cdot d \cdot |f_{\max}|}{\gamma_{bf} \cdot \tan\beta} \quad \text{fiber shear contribution (kips)} \tag{2.15}$$

Where: γ_{bf} = partial safety factor = 1.3

β = crack angle (degrees)

$$V_n = V_c + V_f \quad \text{nominal shear strength (kips)} \tag{2.16}$$

Research has been completed by Padmarajaiah and Ramaswamy [8] using a truss model to determine shear capacity for high strength fiber reinforced concrete. In addition, strut and tie models [9], [10] and plasticity models [10] have been used by many different individuals to determine shear capacity of conventional concrete. Once again, these procedures do not provide information about the response of the structure.

The main advantage of using a strut and tie model is for analyzing and designing the D-regions of a structure that do not satisfy the assumption that plane sections remain plane. This assumption may not be true for regions with discontinuities in loading or geometry. St. Venant's Principle states that the D-region extends a distance away from a discontinuity equal to the overall height of the member.

When designing using a strut and tie model, a truss model should be created. This model should include struts where compression forces are expected, ties where tensile forces are expected, and nodes at the intersection of the struts and ties. Figure 2.4 demonstrates a possible truss model for a simply supported deep beam loaded with a concentrated load. Several different truss models may be possible for a single structure, but each will be acceptable if the following procedures are followed. The determination of the geometry of the truss may be somewhat iterative. Once the truss model is developed, the forces in each of the nodes, struts, and ties should be determined. The design strength of each component should be greater than the applied loads. According to the American Concrete Institute (ACI) code [9], the design strength is found by multiplying the nominal strength by a strength reduction factor of 0.75.

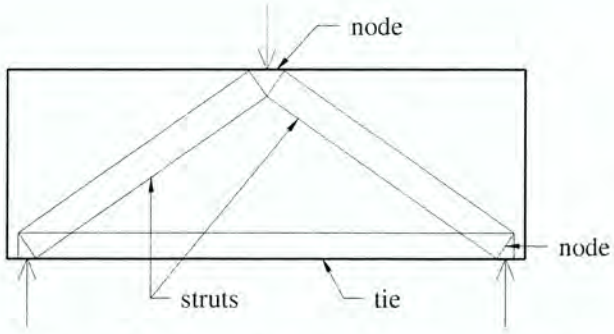

Figure 2.4. General strut and tie truss model.

The nodes should be examined to ensure sufficient strength. The nodes rely on compression of the concrete to resist the forces of the struts and ties. The nominal compression strength at the face of a

nodal zone is defined by ACI in equation 2.17. The node factor is 1.0, 0.8, or 0.6 for a node with no ties, one tie, or two ties respectively. If one is examining a two dimensional structure, the area of the nodal face may be determined by using the width of the member in one direction. The size of the node in the other direction should be increased until the design strength is equal to or greater than the applied force. At this point iteration may take place if the change in size of the nodes affects the geometry of the truss model.

$$F_{nn} = 0.85 \cdot \beta_n \cdot f`_c \cdot A_n \quad \text{nominal nodal force (kips)} \tag{2.17}$$

Where: β_n = node factor

A_n = area of nodal face (in.^{2})

The strength of the struts should be examined to ensure sufficient strength. ACI has determined the nominal compressive strength of the strut according to equation 2.18. The strut factor is 1.0 for struts with uniform cross section, 0.75 for bottle-shaped struts with adequate reinforcement, 0.4 for struts passing through cracks of a tensile zone, and conservatively 0.6 for struts within beam webs where struts are likely to be crossed by inclined cracks. The area of the strut should equate to the area of its nodal face.

$$F_{ns} = 0.85 \cdot \beta_{st} \cdot f`_c \cdot A_{st} \quad \text{nominal strut force (kips)} \tag{2.18}$$

Where: β_{st} = strut factor

A_{st} = area of strut (in.^{2})

The strength of the ties should be adequate for design. ACI has determined the nominal strength according to equation 2.19. Included is strength from mild reinforcement and prestressing strands.

$$F_{nt} = A_s \cdot f_y + A_p \cdot f_p \quad \text{nominal tie force (kips)} \tag{2.19}$$

Where: A_s = area of mild reinforcement (in.^{2})

f_y = yield strength of mild reinforcement (ksi)

A_p = area of strands (in.^{2})

f_p = stress in strand (ksi)

ACI also has recommendations for the amount of transverse reinforcement to be used. In addition, anchorage of the ties is discussed. Refer to the reference [9] for further information.

There are four major models that have been developed for conventional reinforced concrete that can predict both capacity and response of an element under shear or combined flexure and shear. They are the compression field theory (CFT) [11], the modified compression field theory (MCFT) [11] , the rotating angle softened truss model (RASTM) [10], and the fixed angle softened truss model (FASTM) [10]. The basic idea of each of the approaches is to be able to predict the capacity and response of an element by using equations of equilibrium, equations of compatibility, and constitutive stress-strain relationships of concrete compression, concrete tension, and reinforcement. The models have some unique characteristics that differentiate each from one another. The CFT assumes that after cracking, no tensile stress is carried by the concrete across cracks; this is generally an overly conservative assumption. The MCFT accounts for a realistic concrete tensile stress after cracking. The compression field theories provide information on how to apply the models in a simplified sectional approach to analysis. The truss models, however, are designed more for a finite element analysis which has not been used herein. The specific difference between the two truss models is that the FASTM assumes that the final angle of the principal compressive stress coincides with the angle of the initial cracks while a rotationg angle is assumed for the RASTM (and the compression field models). A rotating angle means that the angle of the principal compressive stress increases as the ratio of applied shear to moment increases. In addition the FASTM introduces another constitutive relationship between shear stress and strain.

The MCFT is the model that will principally be used for this research. Application of the MCFT for analytical modeling of UHPC beams is described in Chapter 5 based upon fundamentals of the MCFT as described by Collins and Mitchell [11]. In addition, Chapter 7 recommends a shear design procedure using the MCFT approach coupled with equations 2.14 through 2.16. Equations 2.20 through 2.41 and related descriptions are from Collins and Mitchell [11], describing the MCFT analytical procedure for use with conventional concrete with stirrups. The solution process is carried out at the mid-height of the web using the following steps:

1) Choose a value of the principal tensile strain at which to perform the calculations.
2) Estimate the principal compressive stress angle.
3) Calculate the crack width using equation 2.25.
4) Estimate the shear reinforcement stress.
5) Calculate the principal tensile stress using equation 2.28.
6) Calculate the shear force using equation 2.32.
7) Calculate the principal compressive stress using equation 2.30.

8) Calculate the maximum principal compressive stress using equation 2.34.

9) Ensure that the principal compressive stress is less than the maximum principal compressive stress. If this is not satisfied, return to step 1 and decrease the magnitude of the principal tensile strain.

10) Calculate the principal compressive strain from equation 2.35.

11) Calculate the longitudinal and vertical strains from equations 2.36 and 2.37.

12) Calculate the shear reinforcement stress from equation 2.38.

13) Ensure that the estimated shear reinforcement stress from step 4 is near the stress calculated in step 12. If not, then return to step 4 and make a new estimate.

14) Calculate the stresses in the longitudinal mild steel reinforcement and prestressing strands using equations 2.39 and 2.40 respectively.

15) Calculate the axial force on the member using equation 2.43.

16) Ensure that the calculated axial load is equivalent to the applied axial load. If the calculated axial load is more tensile than the applied, then return to step 2 and increase the value of the principal compressive stress angle.

17) Ensure that equation 2.44 is satisfied. If not, the principal tensile stress from step 5 needs to be incrementally reduced in magnitude.

18) Calculate the sectional curvature based on a plane sections analysis (strain compatibility) using the calculated longitudinal strain from step 11.

19) To obtain the complete response of the beam, these calculations are repeated for a range of values for the principal tensile strain.

The crack spacing parameters are used to determine the crack width as suggested by the MCFT in equations 2.20 through 2.25. Equations 2.22, 2.23, and 2.26 are not applicable for UHPC. Development of such equations for UHPC should be investigated by future research.

$$\rho_x = \frac{A_s + A_p}{A} \quad \text{longitudinal reinforcement ratio} \tag{2.20}$$

Where: A_s = area of mild reinforcement (in.^{2})

A_p = area of strands (in.^{2})

A = gross cross-sectional area (in.^{2})

$$\rho_v = \frac{A_v}{b_w \cdot s} \quad \text{shear reinforcement ratio} \tag{2.21}$$

Where: A_v = area of shear reinforcement within distance s (in.^{2})

b_w = width of web (in.)

s = spacing of shear reinforcement (in.)

$$s_{mx} = 2 \cdot \left(c_x + \frac{s_x}{10} \right) + 0.25 \cdot k_1 \cdot \frac{d_{bx}}{\rho_x} \quad \text{crack spacing in longitudinal direction (in.)} \qquad (2.22)$$

Where: c_x = maximum distance from longitudinal reinforcement in vertical direction (in.)

s_x = spacing of longitudinal reinforcement in transverse direction (in.)

k_1 = 0.4 for deformed bars and 0.8 for plain bars or bonded strands

d_{bx} = diameter of longitudinal reinforcement (in.)

$$s_{mv} = 2 \cdot \left(c_v + \frac{s}{10} \right) + 0.25 \cdot k_1 \cdot \frac{d_{bv}}{\rho_v} \quad \text{crack spacing in vertical direction (in.)} \qquad (2.23)$$

Where: c_v = maximum distance from shear reinforcement in transverse direction (in.)

d_{bv} = diameter of shear reinforcement (in.)

$$s_{m\theta} = \frac{1}{\frac{\sin\theta}{s_{mx}} + \frac{\cos\theta}{s_{mv}}} \quad \text{crack spacing in direction of principal compressive stress (in.)} \qquad (2.24)$$

$$w = \left| \varepsilon_{p1} \cdot s_{m\theta} \right| \quad \text{crack width (in.)} \qquad (2.25)$$

The shear stress along a crack can be determined by the use of equation 2.26 as suggested by the MCFT based on empirical data. It can be seen that stronger concrete, smaller crack width, and larger aggregate all contribute to a higher possible shear stress along a crack. This shear stress will be used as one condition for finding the principal tensile stress.

$$\tau_{ci} = \frac{2.16 \cdot \sqrt{f`_c}}{0.3 + \frac{24 \cdot w}{a + 0.63}} \quad \text{shear stress at crack (ksi)} \qquad (2.26)$$

Where: a = maximum aggregate diameter (in.)

A second condition for finding the principal tensile stress is derived by using the calculated average stresses and the local stresses at a crack as shown in Fig. 2.5. The vertical force in the two stress states must be equivalent as described in equation 2.27 in order for the average stresses to accurately

model the local conditions. Keep in mind that tensile stresses are negative values, while compression and shear stresses are positive values. Also note that the lever arm is the distance from the tensile force resultant to the compressive force resultant. If the crack width has become large enough that the shear stress across the crack is reduced significantly, equation 2.27 can be solved to find the principal tensile stress. This is shown in the first term of equation 2.28. If the crack width has not become large, the principal tensile stress is determined through an empirical procedure developed by the MCFT and described in the second term of equation 2.28.

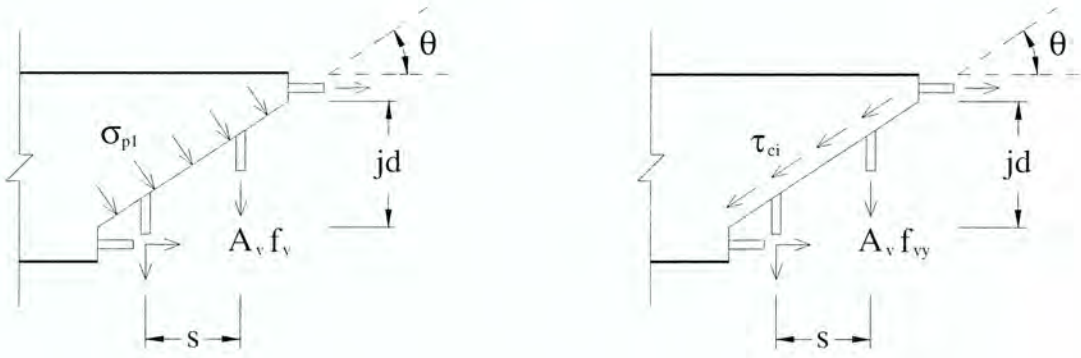

a. Calculated average stresses. b. Local stresses at crack.

Figure 2.5. Average and local stresses transmitted across cracks used by the MCFT [5].

$$A_v \cdot f_v \cdot \left(\frac{j \cdot d}{s \cdot \tan\theta}\right) + \sigma_{p1} \cdot \frac{b_w \cdot j \cdot d}{\sin\theta} = A_v \cdot f_{vy} \cdot \left(\frac{j \cdot d}{s \cdot \tan\theta}\right) - \tau_{ci} \cdot b_w \cdot j \cdot d \qquad (2.27)$$

$$\sigma_{p1} = \min\left(\frac{A_v}{s \cdot b_w} \cdot \left(f_{vy} - f_v\right) - \tau_{ci} \cdot \tan\theta, \frac{\alpha_1 \cdot \alpha_2 \cdot f_{cr}}{1 + \sqrt{500 \cdot \varepsilon_{p1}}}\right) \quad \text{principal tensile stress (ksi)} \qquad (2.28)$$

Where: α_1 = 1.0 for deformed, 0.7 for plain, and 0 for unbonded reinforcement

α_2 = 1.0 for short-term monotonic loading and 0.7 for sustained and/or repeated loads

f_{cr} = cracking tensile strength of concrete (ksi)

f_{vy} = yield strength of shear reinforcement (ksi)

The MCFT assumes a simple shear stress distribution constant over the depth of the moment arm as given in equation 2.29.

$$\tau_{xy} = \frac{V}{b_w \cdot j \cdot d} \quad \text{shear stress in the x-y plane (ksi)} \qquad (2.29)$$

Using Mohr's circle of average stresses shown in Fig. 2.6, the principal compressive stress can be developed as shown in equation 2.30.

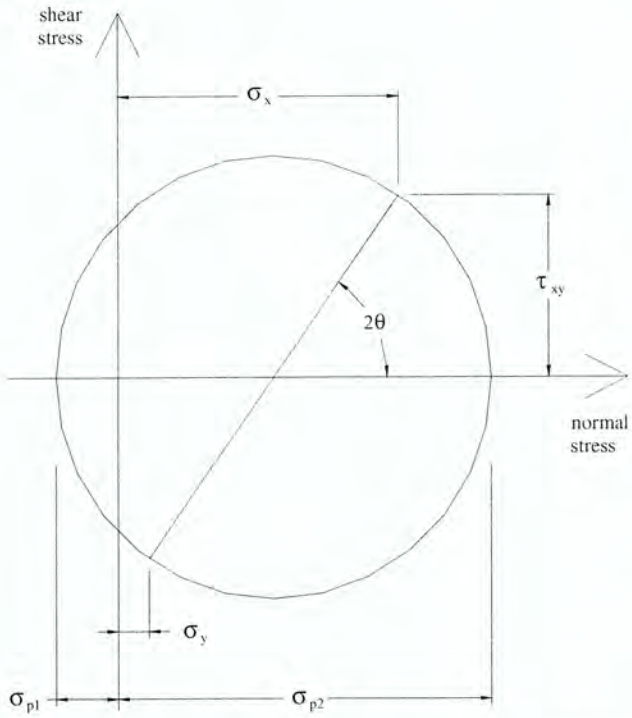

Figure 2.6. Mohr's circle of average concrete stresses in a general concrete element [5].

$$\sigma_{p2} = \left(\tan\theta + \cot\theta\right)\cdot\tau_{xy} + \sigma_{p1} \qquad \text{principal compressive stress (ksi)} \tag{2.30}$$

The principal compressive stress within a concrete member tends to push apart the top and bottom of the member while the principal tensile stress and the shear reinforcement pull the two back together. This requires a state of equilibrium in the vertical direction that is demonstrated in Fig. 2.7 and equation 2.31. When equations 2.29, 2.30, and 2.31 are combined and mathematically rearranged, equation 2.32 can be derived, describing the applied shear force.

$$A_v \cdot f_v = \left(\sigma_{p2}\cdot\sin^2\theta - \sigma_{p1}\cdot\cos^2\theta\right)\cdot b_w \cdot s \tag{2.31}$$

$$V = \sigma_{p1}\cdot b_w \cdot j\cdot d\cdot\cot\theta + \frac{A_v\cdot f_v}{s}\cdot j\cdot d\cdot\cot\theta \qquad \text{applied shear (kips)} \tag{2.32}$$

In order to calculate the principal compressive strain, two influencing factors are the principal compressive stress and the principal tensile strain. It is obvious that the principal compressive stress

is interdependent on the principal compressive strain because each is assumed to be oriented in the same direction. Typically, the relation of this stress and strain, in a uniaxial orientation would be described by the modulus of elasticity. The MCFT has described a parabolic relation between the stress and strain given in equation 2.33 that is more accurate than a straight line. However, because there is a biaxial state of stress, the same relation does not apply. In a biaxial state of stress, when a tensile strain is applied in the out-of-plane direction, the concrete will have a lower strength in the in-plane direction. This relationship is described in equation 2.34. Therefore, by substituting the maximum principal compressive stress from equation 2.34 for the compressive strength in equation 2.33 and then solving for the principal compressive strain, equation 2.35 is derived.

$$\sigma_{p2} = f`_c \cdot \left[ 2 \cdot \left( \frac{\varepsilon_{p2}}{\varepsilon`_c} \right) - \left(\frac{\varepsilon_{p2}}{\varepsilon`_c} \right)^2 \right] \quad \text{principal compressive stress (ksi)} \tag{2.33}$$

$$\sigma_{p2m} = \frac{f`_c}{0.8 + 170 \cdot \varepsilon_{p1}} \leq f`_c \quad \text{maximum principal compressive stress (ksi)} \tag{2.34}$$

$$\varepsilon_{p2} = \varepsilon`_c \cdot \left(1 - \sqrt{1 - \frac{\sigma_{p2}}{\sigma_{p2m}}} \right) \quad \text{principal compressive strain} \tag{2.35}$$

Where: $\varepsilon`_c$ = strain associated with $f`_c$

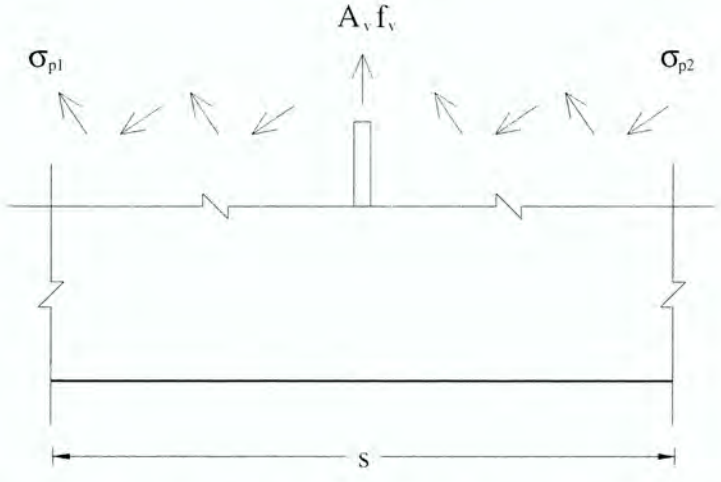

Figure 2.7. Vertical forces used in MCFT equilibrium condition.

The longitudinal and vertical strains can now be calculated as given in equations 2.36 and 2.37 based on Mohr's circle of average strains from Fig. 2.8.

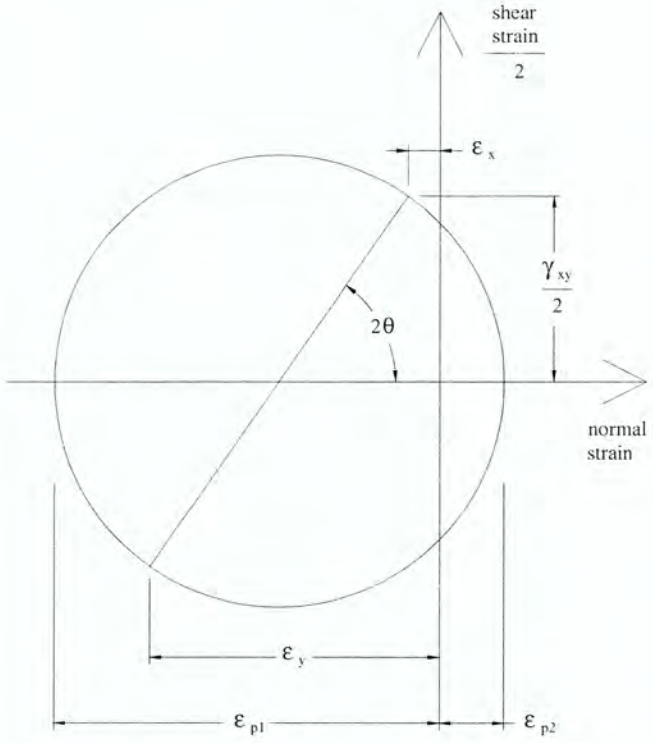

Figure 2.8. Mohr's circle of average concrete strains in a general concrete element [5].

$$\varepsilon_x = \frac{\varepsilon_{p1} \cdot \tan^2\theta + \varepsilon_{p2}}{1 + \tan^2\theta} \quad \text{longitudinal strain} \tag{2.36}$$

$$\varepsilon_y = \frac{\varepsilon_{p2} \cdot \tan^2\theta + \varepsilon_{p1}}{1 + \tan^2\theta} \quad \text{vertical strain} \tag{2.37}$$

Using these calculated strains, the stresses in the shear reinforcement, longitudinal mild reinforcement and the longitudinal prestressing strands can be calculated as described in equations 2.38 to 2.40.

$$f_v = E_s \cdot \varepsilon_y \geq f_{vy} \quad \text{stress in shear reinforcement (ksi)} \tag{2.38}$$

Where: E_s = modulus of mild reinforcement (ksi)

$$f_s = E_s \cdot \varepsilon_x \geq f_y \quad \text{stress in mild reinforcement (ksi)} \tag{2.39}$$

Where: f_y = yield strength of mild reinforcement (ksi)

$$f_p = E_p \cdot \left(\varepsilon_x - \frac{P_f}{A_p \cdot E_p} \right) \geq f_{py} \quad \text{stress in strand (ksi)} \tag{2.40}$$

Where: f_{py} = yield strength of strand (ksi)

The axial force in the member is dependent on the forces in the longitudinal reinforcement, the shear force, the stresses within the web, and the longitudinal stresses outside the web. The longitudinal stresses outside the web are only needed for compression because tension is negligible in conventional concrete. This compressive stress is described in equations 2.41 and 2.42. Then the axial force can be calculated using equation 2.43.

If $\varepsilon_x \leq 0$ then,

$$f_c = 0 \quad \text{compressive stress (ksi)} \tag{2.41}$$

If $\varepsilon_x > 0$ then,

$$f_c = f`_c \cdot \left[ 2 \cdot \left( \frac{\varepsilon_x}{\varepsilon`_c} \right) + \left(\frac{\varepsilon_x}{\varepsilon`_c} \right)^2 \right] \quad \text{compressive stress (ksi)} \tag{2.42}$$

$$N = A_s \cdot f_s + A_p \cdot f_p - V \cdot \cot\theta + \sigma_{p1} \cdot b_w \cdot j \cdot d - f_c \cdot \left(A_c - b_w \cdot j \cdot d \right) \text{ axial force (kips)} \tag{2.43}$$

In order for the previous analysis to be correct, the longitudinal reinforcement must not fail at the location of a crack and the resultant horizontal force based on the calculated average stresses and local stresses shown in Fig. 2.5 must be equivalent. This holds true if equation 2.44 is satisfied.

$$A_s \cdot f_y + A_p \cdot f_{ps} \leq A_s \cdot f_s + A_p \cdot f_p + \sigma_{p1} \cdot b_w \cdot j \cdot d + \left[\sigma_{p1} - \frac{A_v}{b_w \cdot s} \cdot \left(f_{vy} - f_v \right) \right] \cdot b_w \cdot j \cdot d \cdot \cot^2\theta \tag{2.44}$$

Where: f_{ps} = stress in strand at nominal strength [9] (ksi)

Collins and Mitchell [11] also suggest a shear design procedure for use with conventional concrete with stirrups. It is assumed that the section has already been designed based on flexure. The shear stirrups can be designed by using the following steps outlining the shear design procedure.

1) Calculate the shear stress ratio using equation 2.45.
2) Ensure that the shear stress ratio is less than 0.25. If this is not satisfied, increase the size of the section or the concrete strength.
3) Estimate the principal compressive stress angle.
4) Calculate the longitudinal strain using equation 2.46.
5) Determine θ and β using Table 2.4.

6) Ensure that the estimated principal compressive stress angle from step 3 is near the calculated value from step 5. If not, then return to step 3 and make a new estimate.

7) Calculate the concrete shear contribution using equation 2.47.

8) Calculate the reinforcement shear contribution using equation 2.48.

9) Determine the shear reinforcement spacing based on equation 2.49.

10) Ensure that yielding of the longitudinal reinforcement does not occur by satifying equation 2.50. If needed, either add more longitudinal reinforcement or revise the values of θ and β using the values for a higher longitudinal strain. These values will reduce the amount of longitudinal reinforcement but increase the amount of stirrups required.

To begin the design, the shear stress ratio and the longitudinal strain should be determined. The shear stress as earlier described is assumed to be constant over the moment arm length as shown in equation 2.45. The longitudinal strain in reinforcement can be described by prestressing, flexural, shear, and axial forces converted to stress using the area of reinforcement and converted to strain using the modulus of elasticity as described by equation 2.46. This strain is then also the strain within the concrete assuming no slip between the concrete and reinforcement.

$$\frac{\tau_{xy}}{f`_c} = \frac{V_u - V_p}{f`_c \cdot b_w \cdot j \cdot d} \quad \text{shear stress ratio} \tag{2.45}$$

Where: V_u = factored ultimate shear force (kips)

V_p = shear force provided by strands (kips)

$$\varepsilon_x = \frac{P_f - \frac{M_u}{j \cdot d} - 0.5 \cdot V_u \cdot \cot\theta + 0.5 \cdot N_u}{E_s \cdot A_s + E_p \cdot A_p} \quad \text{longitudinal strain} \tag{2.46}$$

Where: M_u = factored ultimate moment (in.- kips)

N_u = factored ultimate axial force (kips)

Using the calculated value of the longitudinal strain, the two factors defined below are determined using empirical data described by Table 2.4. The shear strength contribution of concrete can then be found using equation 2.47.

B = tensile stress factor

θ = principal compressive stress angle (degrees)

Table 2.4. MCFT shear design factors for concrete members with web reinforcement [11].

Shear Stress Ratio		Longitudinal Strain ε_x x 1000									
		0	-0.25	-0.50	-0.75	-1.00	-1.50	-2.00	-2.50	-3.00	-5.00
< 0.050	θ (deg.)	28	31	34	36	38	41	43	45	46	56
	β	5.24	3.70	3.01	2.62	2.33	1.95	1.72	1.54	1.39	0.92
0.075	θ (deg.)	28	30	30	34	36	40	42	43	43	56
	β	4.86	3.37	2.48	2.37	2.15	1.90	1.65	1.44	1.25	0.92
0.100	θ (deg.)	22	26	30	34	36	38	38	38	38	55
	β	2.71	2.42	2.31	2.27	2.08	1.72	1.39	1.16	1.00	0.95
0.125	θ (deg.)	23	27	31	34	36	36	36	36	36	55
	β	2.40	2.33	2.29	2.16	2.00	1.52	1.23	1.03	0.88	0.94
0.150	θ (deg.)	25	28	31	34	34	34	34	34	35	55
	β	2.53	2.25	2.13	2.06	1.73	1.30	1.04	0.85	0.77	0.94
0.175	θ (deg.)	26	29	32	32	32	32	34	36	38	54
	β	2.34	2.19	2.11	1.69	1.40	1.01	0.94	0.91	0.88	0.96
0.200	θ (deg.)	27	30	33	34	34	34	37	39	41	53
	β	2.16	2.13	2.09	1.82	1.52	1.08	1.11	1.04	0.99	0.98
0.225	θ (deg.)	28	31	34	34	34	37	39	42	44	-
	β	1.97	2.07	2.08	1.67	1.35	1.29	1.17	1.16	1.09	-
0.250	θ (deg.)	30	32	34	35	36	39	42	45	49	-
	β	2.26	2.00	1.87	1.63	1.45	1.37	1.32	1.28	1.24	-

$$V_c = B \cdot \sqrt{f`_c} \cdot b_w \cdot j \cdot d \qquad \text{concrete shear contribution (kips)} \tag{2.47}$$

The reinforcement shear contribution is found using equation 2.48 assuming that the design shear strength is equivalent to the applied factored shear force. The required spacing of shear reinforcement then can be described by equation 2.49.

$$V_s = \frac{V_u}{\phi} - V_p - V_c \qquad \text{reinforcement shear contribution (kips)} \tag{2.48}$$

Where: ϕ = strength reduction factor

$$s \leq \frac{A_v \cdot f_y \cdot j \cdot d \cdot \cot\theta}{V_s} \qquad \text{spacing of shear reinforcement (in.)} \tag{2.49}$$

The longitudinal reinforcement should be examined to avoid yielding. By considering all of the forces on the member, the longitudinal reinforcement will not yield if equation 2.50 is satisfied.

$$A_s \cdot f_y + A_p \cdot f_{ps} \leq 0.5 \cdot \frac{N_u}{\phi} - \frac{M_u}{\phi \cdot j \cdot d} - \left(\frac{V_u}{\phi} - 0.5 \cdot V_s - V_p \right) \cdot \cot\theta \tag{2.50}$$

Where: f_{ps} = stress in strand at nominal strength [9] (ksi)

2.4 STRUCTURAL TESTING

Structural testing of an UHPC beam has been completed at the FHWA Turner Fairbanks Highway Research Center (TFHRC) Structural Engineering Laboratory. Both flexural and shear testing procedures, instrumentation, and results have been described by Park, Chuang, and Ulm [6] and by Chuang and Ulm [12]. The test configurations are shown in Figs. 2.9 and 2.10. The tested beam was an AASHTO type II girder made of UHPC and is shown in Fig. 2.11. The Flexure Test was first performed on this beam resulting in a failure of the beam at midspan where the entire two halves of the beam separated. The Shear Test #1 and Shear Test #2 then took place on these broken portions of the original beam. Refer to Figs. 5.17 and 5.18 for some of the results of this testing.

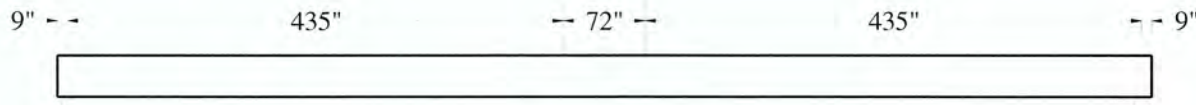

a. Flexure Test

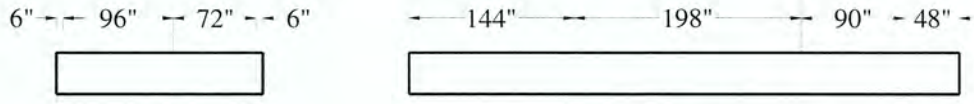

b. Shear Test #1 c. Shear Test #2

Figure 2.9. FHWA flexure and shear testing setup diagrams.

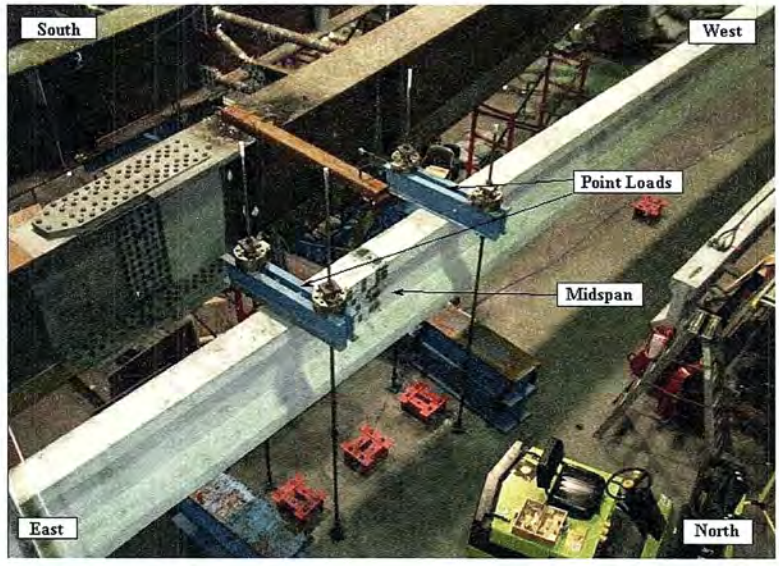

Figure 2.10. FHWA flexure test setup photograph.

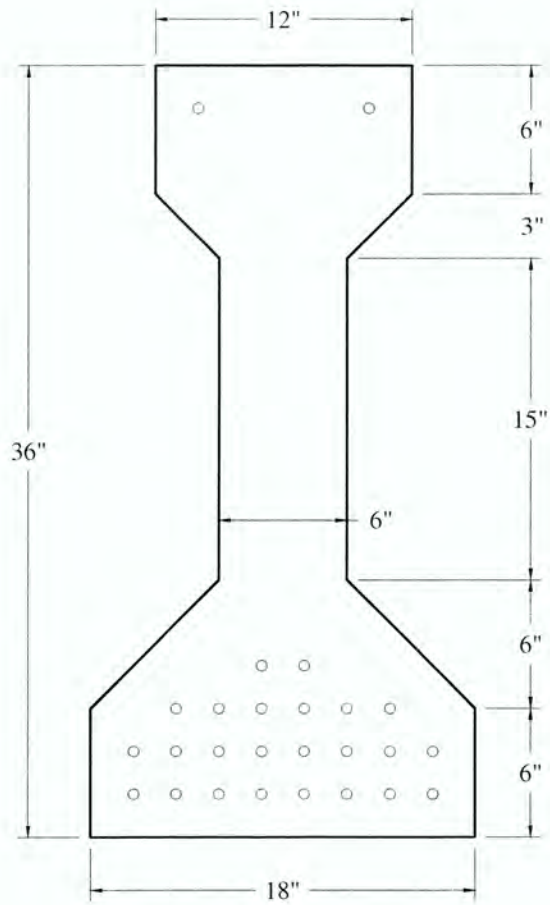

Figure 2.11. Prismatic cross section of AASHTO type II FHWA test beam.

2.5 PRESTRESS BOND

The bond between prestressing strands and UHPC has been investigated by Lubbers [13] using a pullout test with 0.5 in. and 0.5 in. oversized strands embedded within UHPC specimens that were 12 to 24 in. deep using the test setup shown in Fig. 2.12. The strands had no prestressing force applied and were spaced at 9 in. within the test specimen. Conclusions were drawn that the development length of 0.5 in. strands within UHPC is greater than 18 in. but less than 24 in. and is approximately 12 in. for the 0.5 in. oversized strands. This was based on the depth of the specimen required to cause fracturing of the strands before fully slipping. Figure 2.13 shows dead end displacement data for 0.5 in. oversized strands within 24 in. specimens of conventional concrete and 12 in. specimen of UHPC. Although the strands within UHPC fractured before fully slipping, slip of approximately 0.1 in. was observed which may be significant for some applications. There are some aspects of the testing that

may be important to relating the bond of the strands in the tests to actual structural components. In a structural component, strands are typically spaced more closely than the tested 9 in. For example, a typical strand spacing is 2 in. Also, a pretension is applied to many structural components, but not for this bond research. Also, the tension stress experienced at the bottom of a simple beam from dead and live load where the strands are located could impact the bond between the concrete and strands. These conditions were not simulated in the work by Lubbers.

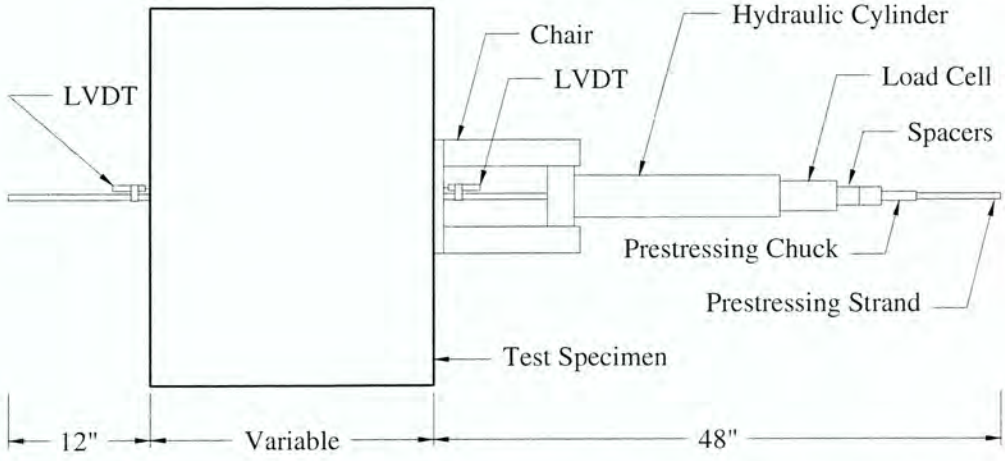

Figure 2.12. Pull-out test apparatus used by Lubbers [13].

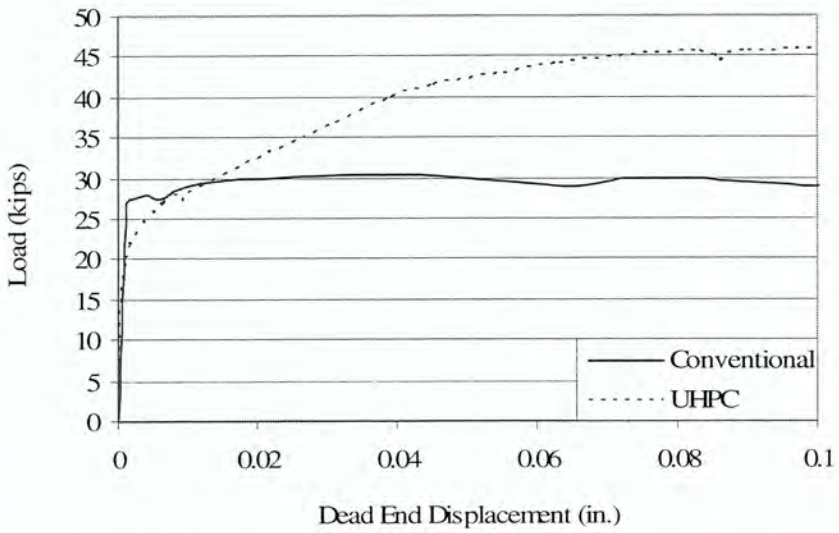

Figure 2.13. Pull-out test data for 0.5 in. oversized strands [13].

CHAPTER 3: FIELD BRIDGE DESCRIPTION

The first UHPC bridge in the United States was constructed in Wapello County, Iowa during the fall of 2005. The bridge has no horizontal curve, vertical curve, nor skew. The cross section of the bridge as a whole is shown in Fig. 3.1. The deck has a 2% transverse crown from the peak at the centerline of the roadway. The deck reinforcement consists of transverse and longitudinal steel in both the top and bottom of the deck. The transverse steel has top cover of 2.5 in. and bottom cover of 1 in. with the longitudinal steel placed inside of the transverse steel. The #7 transverse bars are spaced at 9 in. across the width of the deck in both the top and bottom of the slab. In addition, #5 transverse bars spaced at 9 in. between the #7's are in the top of the deck in the outer 6.67 ft of the deck to further strengthen the overhang. The longitudinal steel consists of #5 bars spaced at 1 ft between the beams, with the top and bottom reinforcement staggered in spacing. Similar reinforcement exists in the overhang of the deck. There is one diaphragm located at midspan of the bridge consisting of two C15x33.9 steel sections with one connecting each of the outer beams to the center beam at the mid-depth of the beams. Conventional Iowa Department of Transportation (DOT) integral abutments with wingwalls and open guard rails were used for this bridge.

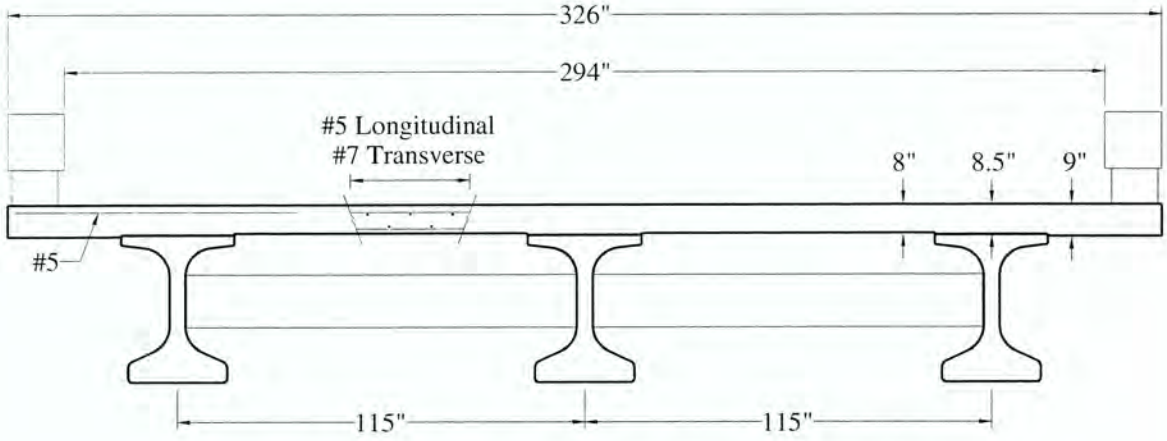

Figure 3.1. Cross section of Wapello County UHPC bridge.

The three bridge beams used on this project were modified slightly from the Iowa DOT Bulb Tee C standard with the dimensions shown in Fig. 3.2. The beams are 111 ft long with a 110 ft span. Note the solid five strands that are aligned vertically near the top of Fig. 3.1.a. These are the harped stands that decline linearly from the end cross section (Fig. 3.1.a.) to the midspan cross section (Fig. 3.1.b.) over a distance of 44.5 ft as shown in Fig 3.3. Within the central 22 ft. of the beam, all the strands

run horizontally and are located as shown in the midspan cross section. There are #5 reinforcing bars with two legs in the top of the bridge beams in order to connect the deck and beams for composite action and resist horizontal shear. The spacing of the horizontal shear bars are shown in Fig. 3.3. The last 3.5 ft of the beams on both ends have 8 strands that are debonded in the bottom flange. The last 6.5 ft of the beams on both ends have 16 strands that are debonded in the bottom flange. Debonding was used in order to reduce the stresses at the flange-web interface. No shear reinforcement is present within the beams because it has been replaced by steel fibers as described in section 1.2.

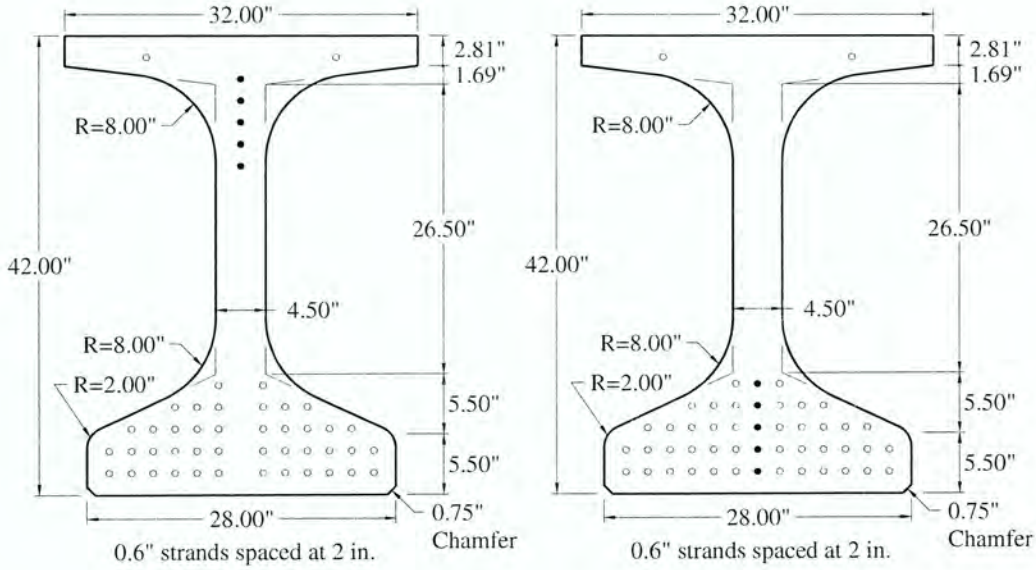

a. End cross section. b. Midspan cross section.

Figure 3.2. Cross sections of Wapello County UHPC bridge beams.

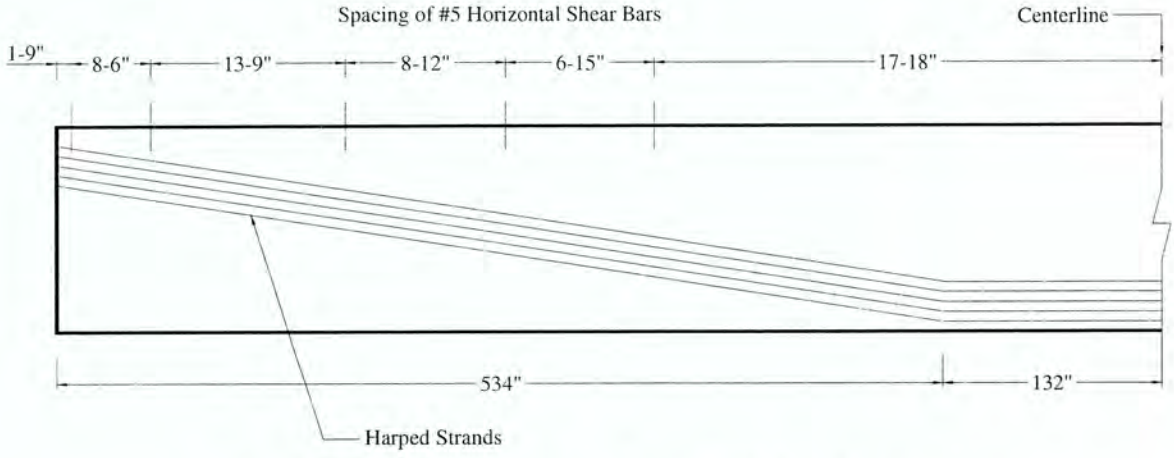

Figure 3.3. Elevation of Wapello County UHPC bridge beams.

3.1 DESIGN

Design of the bridge was completed cooperatively between the Iowa DOT, Wapello County, and ISU. Initially, a global grillage analysis was completed for determination of accurate shear and moment distribution factors for the individual beams. As no U.S. specification existed for UHPC design, the design of the beams for flexural capacity was completed using two different approaches. The procedure which will be described in section 5.2.1 was used and checked using conventional design assumptions (e.g., no tension in the concrete, a typical Whitney Stress Block, etc.) Composite action between the slab and the beams was considered. Shear design was completed using equations 2.14 to 2.16. In addition, full-scale shear testing as described in section 4.2 was completed before construction of the bridge to verify all design assumptions.

3.2 CONSTRUCTION

Each of the bridge beams were cast on separate days of June 25th, July 9th, and July 16th 2005 at a concrete plant in Winnipeg, Manitoba, Canada. The construction procedure used with UHPC is somewhat atypical of conventional concrete with some important differences in the preparation, mixing, placing, and curing.

Preparation of the beams began by pulling the prestressing strands through the end formwork and stressing them between abutments to the appropriate level. Next, the side formwork was placed, after being greased to ease removal. Bolted struts were used to hold the formwork together transversely. One of the differences of UHPC from conventional concrete is its liquidity, requiring that the formwork must be specifically prepared to prevent leaking or lifting. In this instance, all joints and prestressing holes of the formwork were sealed with putty. UHPC tends to apply high hydrostatic pressures to portions of the formwork that are "above" the concrete (such as the taper of a bottom flange). Therefore, the formwork was fastened to the ground to prevent lifting of the forms.

Batching of the concrete took place in a four motor pan mixer with a 2.6 cubic yard capacity, capable of 50 rpm. Mixing UHPC requires special specifications as compared to conventional concrete. For instance, the mixer needs to input high amounts of shear, have minimum blade clearances, be capable of variable speed, and contain an amp meter. For casting of the UHPC bridge beams, batches of 1.3 cubic yards were mixed. First, the prepackaged bags of Ductal® were emptied into the mixer. As the mixer began at low power, the water and the first portion of the admixture were added. Since the temperature was quite high during mixing, a portion of the water was replaced with ice. As the power

was increased, the rest of the admixture was added and the mixing continued. Then as the power was decreased, the steel fibers were slowly introduced. Additional mixing occurred until the concrete was ready to be placed. For this project more concrete was needed than could be mixed at once. Therefore, several batches of concrete were mixed and held in two ready mix trucks which continually agitated the fluid concrete.

Placement of the concrete occurred from only one end of the beam. If this is not done, a joint or lense may form were separate concrete pours have come together. In this case, placement was completed by placing concrete directly from the ready mix trucks into one end of the formwork as shown in Fig. 3.3. As the formwork filled, the truck was slowly moved along the length of the beam so that no overflow occurred. However, in this situation care was taken to ensure that the concrete was always placed on flowing concrete, not placed into an area of the formwork were no concrete was present. Tools like shovels and two-by-fours were used to push the surface concrete into depressed areas of the form. This was only to fill the forms as the concrete should never be troweled because it causes too much moisture to rise to the surface. At this point, inverted U-shaped mild reinforcement was installed in order to provide horizontal shear reinforcement between the beams and the bridge deck.

Figure 3.4. Placement of concrete during construction of Wapello County UHPC bridge beams.

In order to initiate the curing process and also to reduce shrinkage, the beams were tightly sealed. This was done by spraying a sealing chemical on the top surface of the freshly placed concrete. Tarps were then placed over the entire assembly to hold in moisture and heat during steam curing which was conducted for 12 hours at 140 degrees Fahrenheit. Once the concrete reached the specified strength, in this case 12 ksi as determined by cylinder testing, the strands were released. To release the strands heat was applied with an acetylene torch, causing the strands to slowly elongate and lose stress. Following release, the UHPC was heat treated at 194 degrees Fahrenheit for a period of 48 hours.

These beams were then shipped to the bridge site where conventional concrete abutments had been previously constructed. Casting of the bridge deck took place on November 8th 2005 with conventional concrete and normal construction practices. Additional construction of the guard rails, approach slab and grading of dirt took place on site in Wapello County, Iowa through the fall of 2005 with the nearly completed bridge shown in Fig. 3.4.

Figure 3.5. Elevation of Wapello County UHPC bridge.

CHAPTER 4: EXPERIMENTAL TEST PROGRAM

This chapter summarizes the experimental test program followed in this work and consists of descriptions of the test specimens, setups, and procedures. Subsequently in Chapter 6, observations and results are discussed.

4.1 MATERIAL TESTING

4.1.1 Uniaxial Compression Testing

Uniaxial compression tests on cubes were used to determine the compressive strength of the UHPC utilized in this study. Cubes were chosen instead of cylinders because the rough top surface created from casting of the concrete can be placed to the side, leaving flat, parallel surfaces on the top and bottom.

4.1.1.1 Test Specimen Description

Concrete cubes were cast on four different days when a beam was also constructed as follows: 42 specimens were cast on February 23rd 2005, 6 specimens on June 25th 2005, 6 specimens on July 9th 2005, and 9 specimens on July 16th 2005. There were three different types of curing conditions applied to the cubes. Out of the 42 specimen cast during February, 7 were cured with the beam, 14 were cured in a 194°F chamber, and 21 were cured at room temperature which was approximately 65°F. All of the cubes cast during June and July were cured with their respective UHPC beams. The cubes all had a side length of 1.97 in.

4.1.1.2 Test Configuration

Compression testing was completed following the provisions of ASTM C-109 [14]. The test was setup by placing the cube between a piece of steel and the test machine head as shown in Fig. 4.1.

4.1.1.3 Test Procedure

The test machine recorded the load and displacement of the table head throughout each test. The concrete cubes were tested at a loading rate of 300 lbs/sec. A rate above the ASTM C-109 [14] standard was required due to time constraints. A high compressive strength causes a long test duration unless the loading rate is increased.

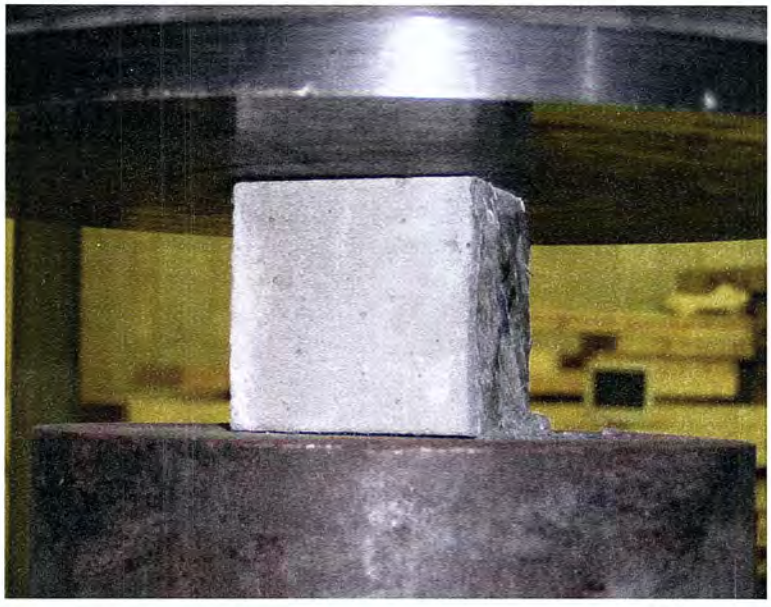

Figure 4.1. Uniaxial compression test setup used for UHPC cubes.

4.1.2 Prism Flexural Testing

Flexural tests on prisms were used to determine the cracking strength of UHPC following the guidelines of ASTM C-78 [14]. This procedure was developed for testing conventional concrete, which when unreinforced, fails at a load referred to as the cracking load. However, the same is not true of UHPC, therefore in this work; the cracking load was defined as the point where load and displacement were no longer linear.

4.1.2.1 Test Specimen Description

UHPC prisms were cast on four different days when a beam was also constructed as follows: 42 specimens were cast on February 23rd 2005, 12 specimens on June 25th 2005, 12 specimens on July 9th 2005, and 12 specimens on July 16th 2005. There were three different types of curing conditions applied to the cubes. Out of the 42 specimen cast during February, 7 were cured with the beam, 14 were cured in a 194°F chamber, and 21 were cured at room temperature which was approximately 65°F. All of the cubes cast during June and July were cured with their respective beams. The concrete prisms had dimensions of 1.57 in. x 1.57 in. x 6.30 in.

4.1.2.2 Test Configuration

The flexure testing was completed according to the provisions of ASTM C-78 [14]. The prisms were setup within a test machine head using a span length of 4.5 in. with two load points spaced 1.5 in. apart and centered within the span as shown in Fig. 4.2.

4.1.2.3 Test Procedure

The test machine recorded the load and displacement of the table head throughout each test. The prisms were tested at a loading rate of 1,000 lbs/min as it was necessary to test at a higher rate than suggested by ASTM C-78 [14] in order to reduce the time required to complete a test.

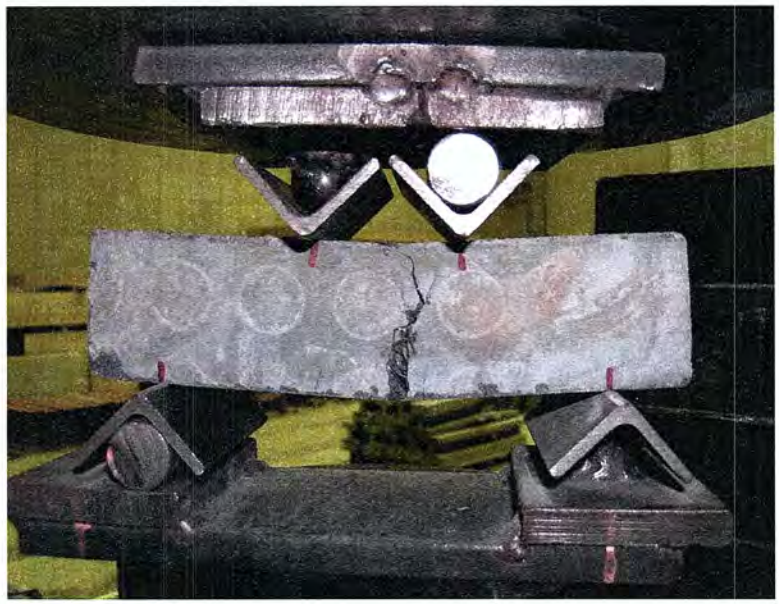

Figure 4.2. Flexure test setup used for UHPC prisms.

4.2 LARGE-SCALE LABORATORY TESTING

Large scale laboratory testing was competed to collect information about the structural performance of UHPC. In all, three tests were conducted using one full-scale specimen. First, a flexure test provided information about the service limit state capacity of the beam and allowed the prestressing losses to be estimated. Next a shear test provided information about the service and ultimate shear strength of the beam. And finally, a flexure-shear test permitted the service and ultimate shear strength of the beam to be determined when combined with significant applied moment.

4.2.1 Test Specimen Description

The cross sections of the large-scale laboratory test beam were the same as for the bridge beams shown in Fig. 3.1. The total length of the test beam was 71 ft with the harped stands varying linearly between the two cross sections which are 28.5 ft apart. The central 14 ft of the beam had the midspan cross section shown in Fig. 3.1.b. Debonding was used in the same manner as previously described for the bridge beams.

4.2.1.1 Design

The test beam design was configured with the same cross section as the Wapello County, Iowa bridge beams and limited to a practical length and weight for the Iowa State University Structural Engineering Laboratory.

4.2.1.2 Construction

On February 23rd 2005, th 71 ft long test beam was cast at a concrete plant in Winnipeg, Manitoba, Canada. The construction procedure was very similar to that described in section 3.2 with a few minor differences. As discussed previously, the UHPC mix tends to apply high hydrostatic pressures to portions of the formwork that are "above" the concrete such as the taper of a bottom flange. This pressure caused the laboratory beam formwork to lift up off its supports after the concrete was poured. Weight was added to the forms to push them back down at which point they were fastened to the ground to ensure that lifting did occur again. The test beam was sealed using plastic sheets as apposed to the preferred chemical spray.

4.2.2 Flexural Testing

4.2.2.1 Test Configuration

The flexure test setup used in this work consisted of a 70-ft span with four applied point loads centered over the midspan, creating a constant moment region of approximately 64 in. Figures 4.3 and 4.4 show the test setup.

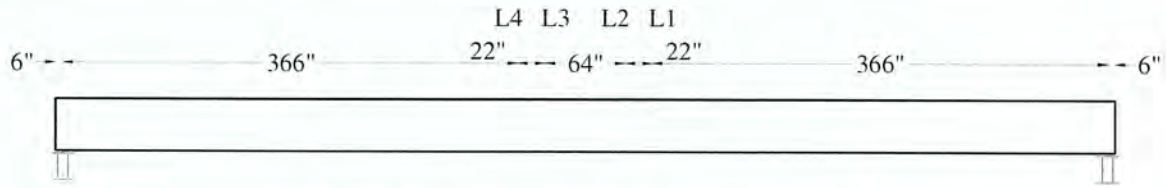

Figure 4.3. Large-scale flexure test setup diagram.

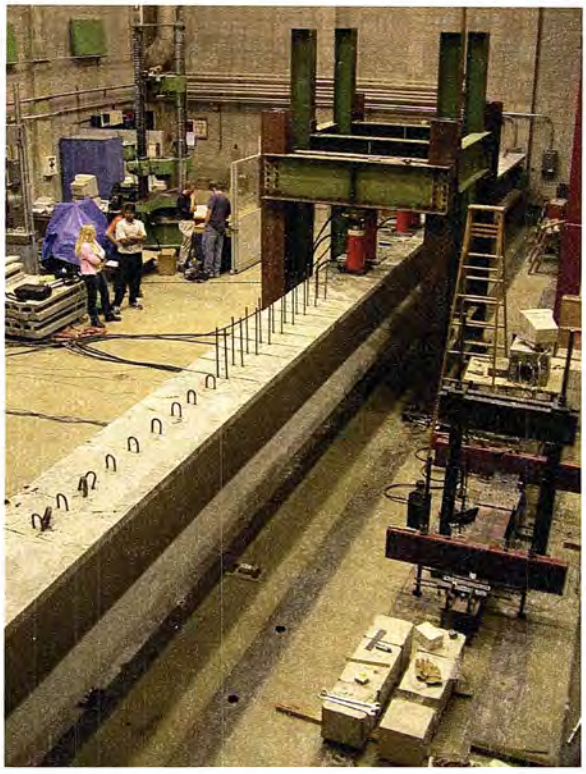

Figure 4.4. Large-scale flexure test setup photograph.

To quantify the response of the test beam, several different types of instrumentation were used and are shown in Figs. 4.5 through 4.7. The gage positions within each cross section are summarized in Table 4.1. During testing, a Megadac System and a Fiber Optic Interragator running at one hertz were used to collect data from the instruments including:

- four load cells measuring loads (L1,L2,L3,L4)
- seven strain gage rosettes measuring strains in three directions (1,2,5,6,9,13,15)
- eight linear strain gages (3,4,7,8,10,11,12,14)
- five fiber optic strain gages (F1,F2,F3,F4,F5)
- four DCDT's measuring displacement between two points on the beam (H1,H2,H3,H4)
- three DCDT's measuring strand slip (S1,S2,S3)
- eight string potentiometers measuring deflection with a designation of "a" for those placed on the north side of the beam, "b" for those placed on the south side of the beam, and no letter designation for those in the center of the beam (D1,D2,D3a,D3b,D4a,D4b,D5a,D5b)

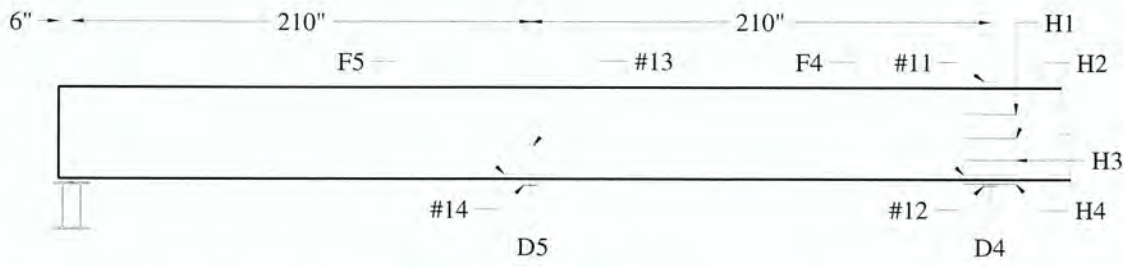

Figure 4.5. Instrumentation on east side for large-scale flexure test.

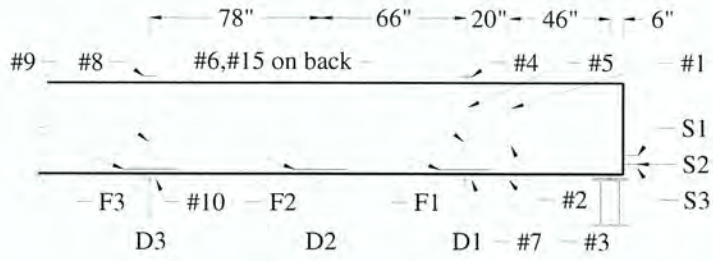

Figure 4.6. Instrumentation on west side for large-scale flexure test.

4.2.2.2 Test Procedure

Flexural testing was performed on May 11th, 2005. Two sequences of loading were applied. During the first sequence of loading a total load of 237.4 kips was applied to the beam at which point the beam was inspected for flexural cracks at midspan. Additional loading was applied to an approximate total load of 243 kips and 3 in. of midspan deflection. At this point, the beam was unloaded.

A second sequence of loading was then applied to the beam. The beam was first loaded to a total load of 256 kips and the beam was inspected for flexural cracks. Loading was resumed to a total load of 265 kips and 3.2 in. of deflection when the final inspection of the beam took place. Testing was halted at this point to maintain the structural integrity of the beam for the shear testing. It should be pointed out that the maximum applied moment is slightly under the service load condition and well under the ultimate load condition for the composite bridge beam and deck system as described in Table 6.3.

Table 4.1. Location of strain gages used in large-scale flexure test.

Gage	Vertical Position from Base (in)	Horizontal Position from West Support (in)
1	28	46
2	17	46
3	0	46
4	41	66
5	28	66
6	17	66
7	0	66
8	41	210
9	17	210
10	0	210
11	41	420
12	0	420
13	17	630
14	0	630
15	17	66
H1	28	420
H2	17	420
H3	10.9	420
H4	-1.875	420
F1	2	66
F2	2	132
F3	2	210
F4	2	420
F5	2	630

4.2.3 Shear Testing

4.2.3.1 Test Configuration

The shear test setup was configured to have a 70-ft span. The loading points were moved to the positions shown in Figs. 4.7 and 4.8. In order to reduce arching and deep beam action, a shear span to depth ratio of approximately 2.5 was used within the 90 in. region on the west end of the beam.

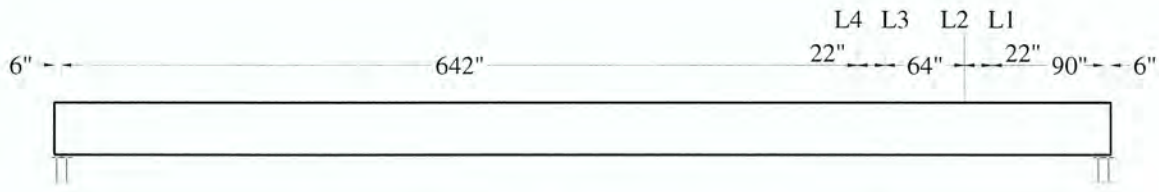

Figure 4.7. Large-scale shear test setup diagram.

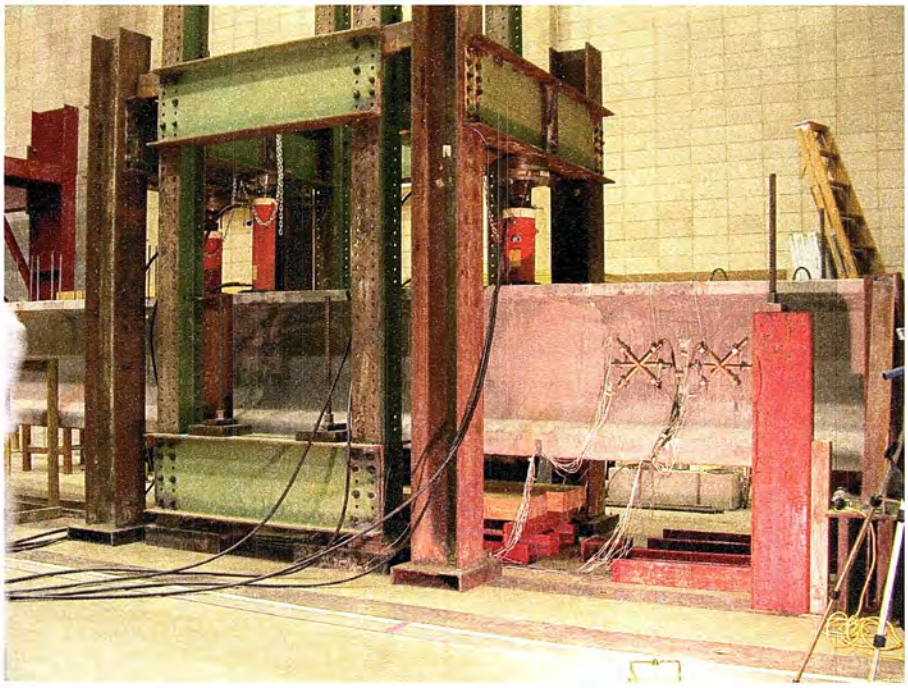

Figure 4.8. Large-scale shear test setup photograph.

Nearly the same instrumentation used during the flexural testing was also utilized during the shear testing as shown in Figs. 4.9 and 4.10 with gages 1 through 15 and F1 through F5 unchanged and some small changes. The four DCDT's (H1,H2,H3,H4) used as longitudinal strain gages at the midspan during the flexure test were moved to the end region and combined with two more for a total of six DCDT's (R1a,R1b,R1c,R2a,R2b,R2c) essentially acting as two large strain rosettes as shown in Figure 4.11. These rosettes were located at a position 22.5 in. above the bottom of the beam.

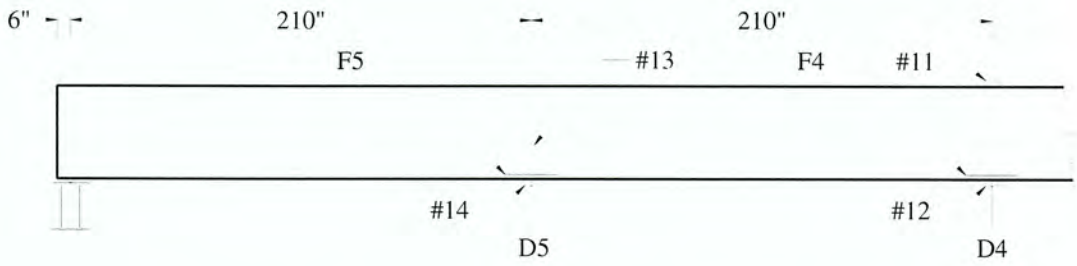

Figure 4.9. Instrumentation on east side for large-scale shear test.

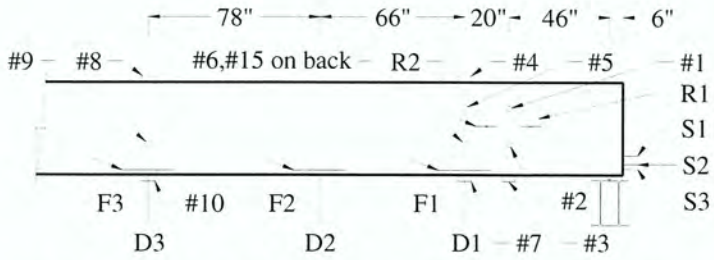

Figure 4.10. Instrumentation on west side for large-scale shear test.

4.2.3.2 Test Procedure

On June 9th, 2005 the shear test was performed. After total loads of 369.8 kips, 397.6 kips, and 594.0 kips were applied, the beam was inspected for cracks. Inspection took place at these loads due to audible cracking of the beam. The maximum total load applied during the test was 594.0 kips at which point the load began to decrease. Additional deflection was applied to the beam as the load decreased but is not significant to this research.

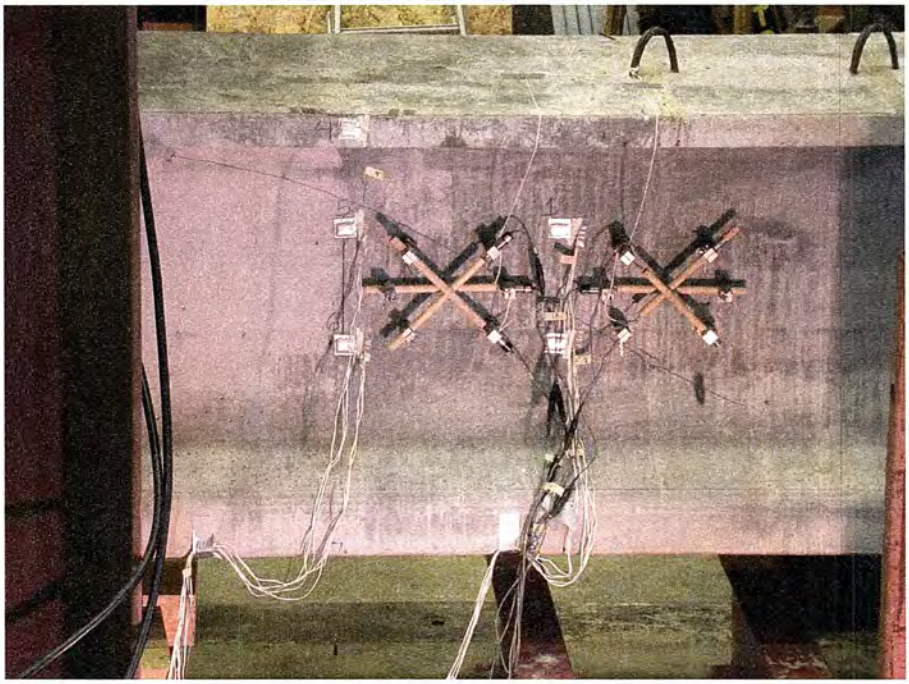

Figure 4.11. Large strain rosettes gages R1 and R2 used for large-scale shear test.

4.2.4 Flexure-Shear Testing

4.2.4.1 Test Configuration

This test was configured to have a 57-ft span as shown in Figs. 4.12 and 4.13. The end region that was damaged during the shear testing was allowed to overhang the support such as to minimize the influence on the behavior of the beam. Two factors were balanced determining an optimum loading position. The more the loads move toward the end of the beam, the more likely the beam is to fail in shear, but the less likely the moment will affect the shear strength. The selected configuration was thought to represent a typical combination of shear and bending loadings.

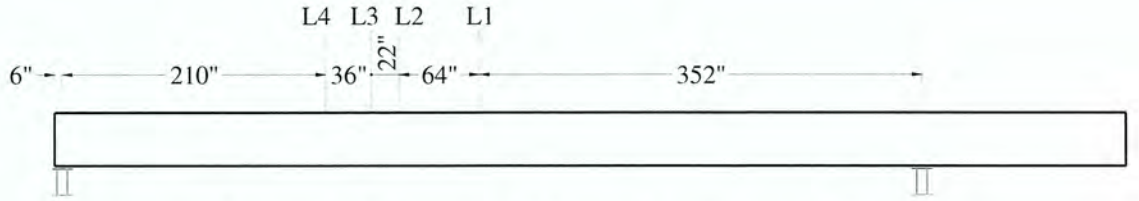

Figure 4.12. Large-scale flexure-shear test setup diagram.

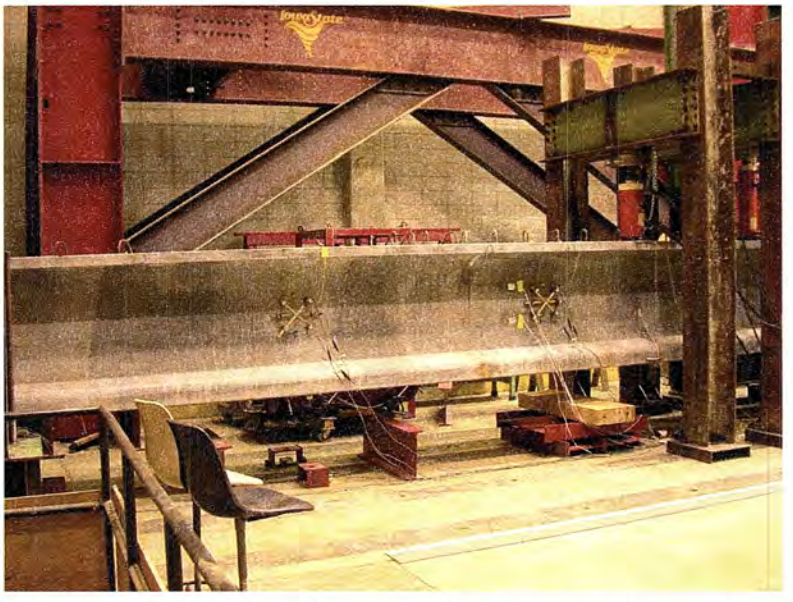

Figure 4.13. Large-scale flexure-shear test setup photograph.

The instrumentation used for the flexure-shear test, shown in Figs. 4.14 through 4.16, was somewhat different than the previous two tests although gages 1 through 15 and F1 through F5 remain unchanged. The positions of gages not previously discussed are shown in Table 4.2. A Megadac

System and a Fiber Optic Interragator running at one hertz were used to collect data from the instruments including:

- four load cells measuring load (L1,L2,L3,L4)
- six strain gage rosettes measuring strain in three directions (9,13,15,16,17,18)
- five linear strain gages (8,10,11,12,14)
- three fiber optic strain gages (F3,F4,F5)
- six DCDT's essentially acting as two large strain rosettes (R1a,R1b,R1c,R2a,R2b,R2c)
- three DCDT's measuring strand slip (S1,S2,S3)
- six string potentiometers measuring deflection with a designation of "a" for those placed on the north side of the beam, "b" for those placed on the south side of the beam, and no letter designation for those in the center of the beam (D3a,D3b,D4a,D4b,D5a,D5b)

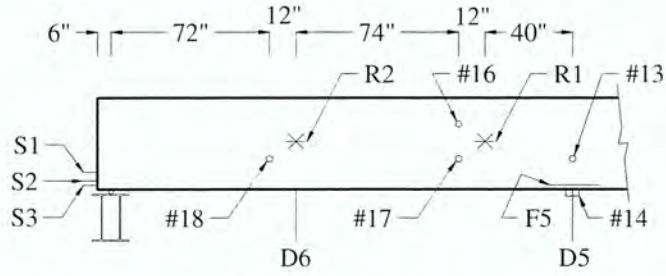

Figure 4.14. Instrumentation on east side for large-scale flexure-shear test.

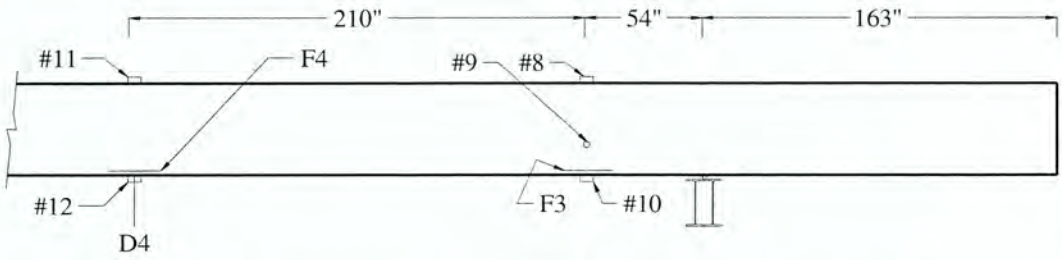

Figure 4.15. Instrumentation on west side for large-scale flexure-shear test.

Figure 4.16. Large strain rosette gage R1 used for large-scale flexure-shear test.

Table 4.2. Location of strain gages used in large-scale flexure-shear test.

Gage	Vertical Position from Base (in.)	Horizontal Position from East Support (in.)
16	28	158
17	17	158
18	17	72
R1	22.5	170
R2	22.5	84

4.2.4.2 Test Procedure

On August 5th, 2005 the flexure-shear test was performed. A total load of 367 kips was applied when the beam was first inspected for cracking. Additional inspections took place at levels of 481.8 kips and at the maximum applied load of 658.1 kips. At this point the beam may have been able to hold slight amount of additional load. However, essentially no additional load was being applied as the deflection increased to a maximum of about 8.5" at the easternmost load point. The test was then ended as the beam was unloaded.

4.3 SMALL-SCALE LABORATORY TESTING

The purpose of the small scale shear testing was to generate additional data on the shear behavior of UHPC under a variety of geometrical considerations. It was anticipated that analysis of the shear failure would provide a better definition of the shear strength of UHPC for use in design.

4.3.1 Test Specimen Description

Five different cross sections of small scale beams, with three of each beam for a total of fifteen beams were tested in the small-scale laboratory testing portion of this work. The different beams have different web widths, amount of reinforcement, and heights. The beam cross sections are shown in Fig. 4.17 with other important properties shown in Table 4.3. Sections A, B, and C have a height of 10 in. and will be collectively referred to as the 10 in. beams. Sections D and E have a height of 12 in. and will be referred to as the 12 in. beams.

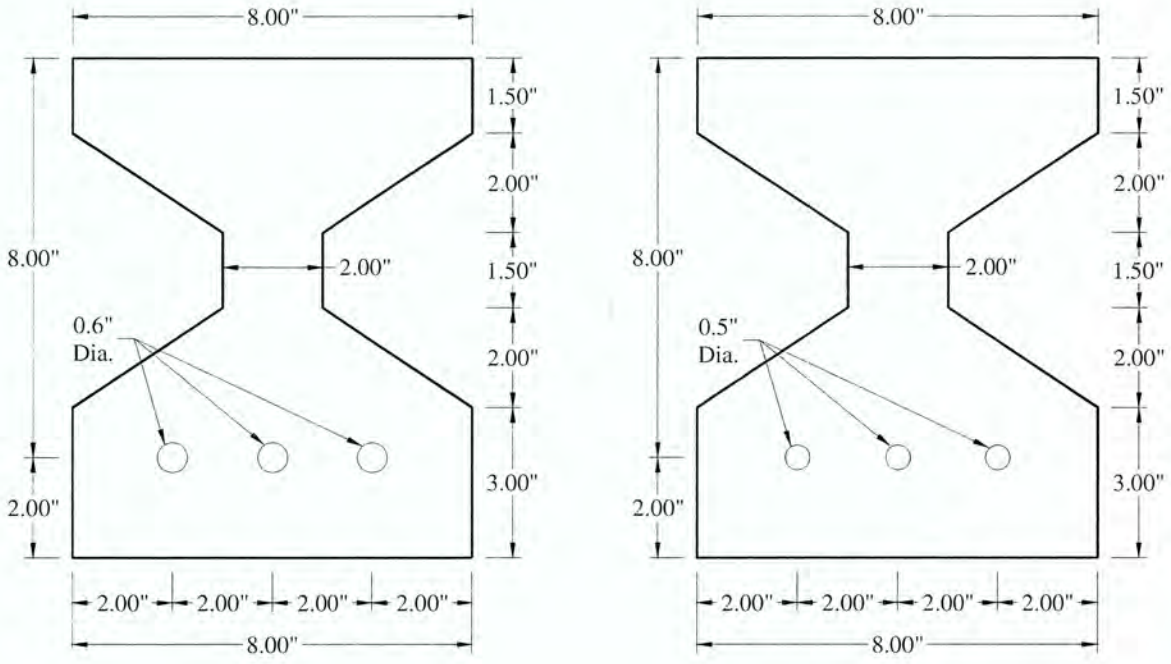

a. Section A. b. Section B.

Figure 4.17. Cross sections of small-scale test beams.

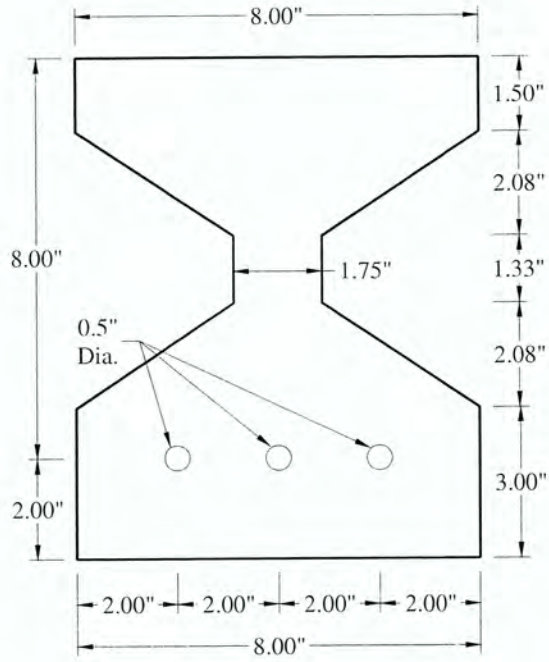

c. Section C.

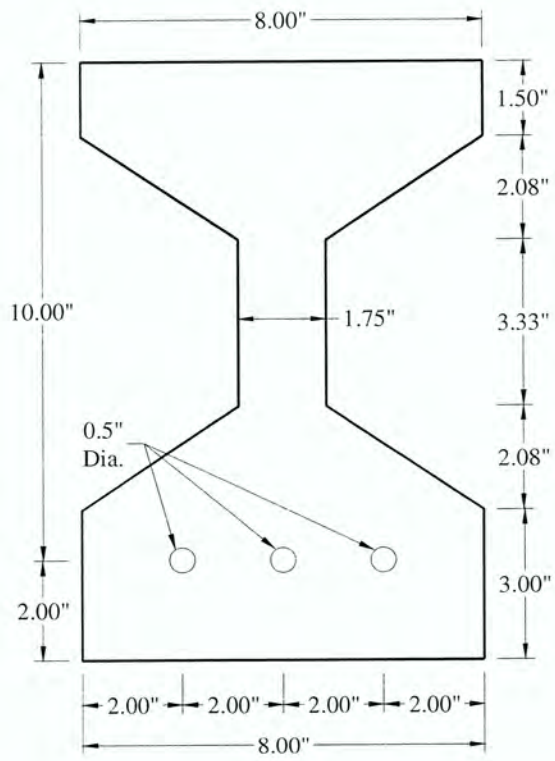

d. Section D.

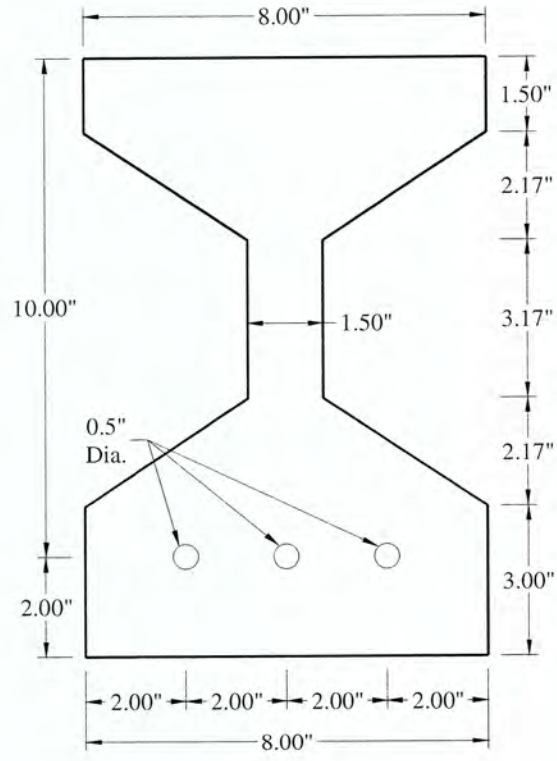

e. Section E.

Figure 4.17. Cross sections of small-scale test beams (continued).

Table 4.3. Initial prestress and length of small-scale test beams.

Section	Initial Prestress (kips)	Length (in.)
A	61.5	54
B	62.0	54
C	62.0	54
D	62.0	64
E	62.0	64

4.3.1.1 Design

In order to create a shear failure, this mode of failure needs to be weaker than the other failure modes, such as flexure or bond failure. In general, using the flexural analysis procedure which will be described in Chapter 6, the moment capacity of the beam is determined fairly accurately. The shear capacity was initially determined using equations 2.14 through 2.16. These equations are very conservative and meant for design. Therefore, the moment capacity was designed to be approximately twice that of the estimated shear capacity in order to ensure a shear failure. Using the described shear and flexure analysis, the general cross section shape and the amount of reinforcement were determined. Then, the maximum tendon stress was determined in order to stay within the limits of allowable release stresses.

4.3.1.2 Construction

Construction of the small scale shear beams took place in the days prior to the casting of the large scale test beam on February 23rd 2005. Construction was completed in a manner similar to that described in section 3.2.

4.3.2 Test Configuration

The 15 small-scale laboratory tests were all completed in a similar manner with some variations mainly between the 10 in. and 12 in. beams. Figure 4.18 shows a typical test configuration.

A computerized hydraulic system was used to test the beams as it recorded the applied load. The testing setup and instrumentation are summarized in Figs. 4.19, 4.20 and Table 4.4 for the 10 in. beams. Data were collected at one hertz for the instruments which include:

- one load cell measuring load
- five strain gage rosettes measuring strain in three directions (3,4,6,7,9)
- four linear strain gages (1,2,5,8)

- three DCDT's measuring strand slip (S1,S2,S3)
- two string potentiometers measuring deflection (D1,D2)

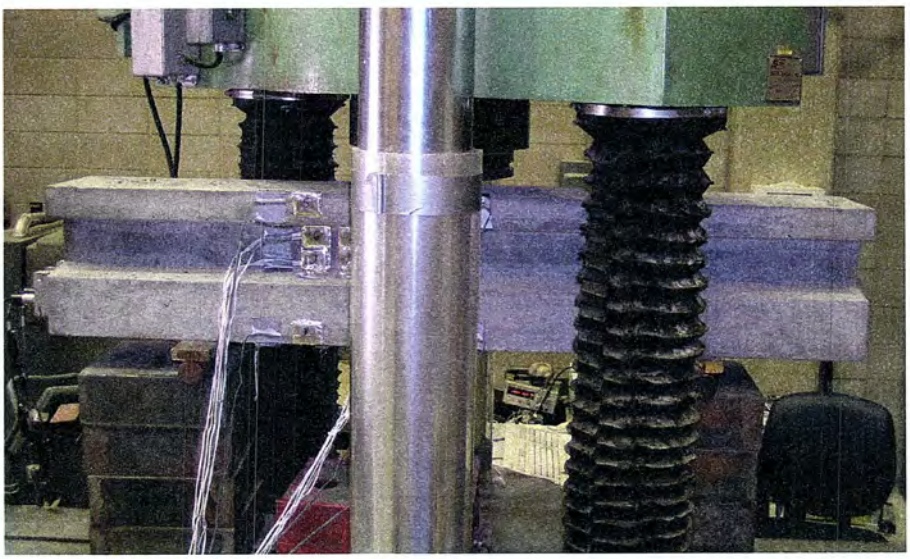

Figure 4.18. Typical small-scale test setup.

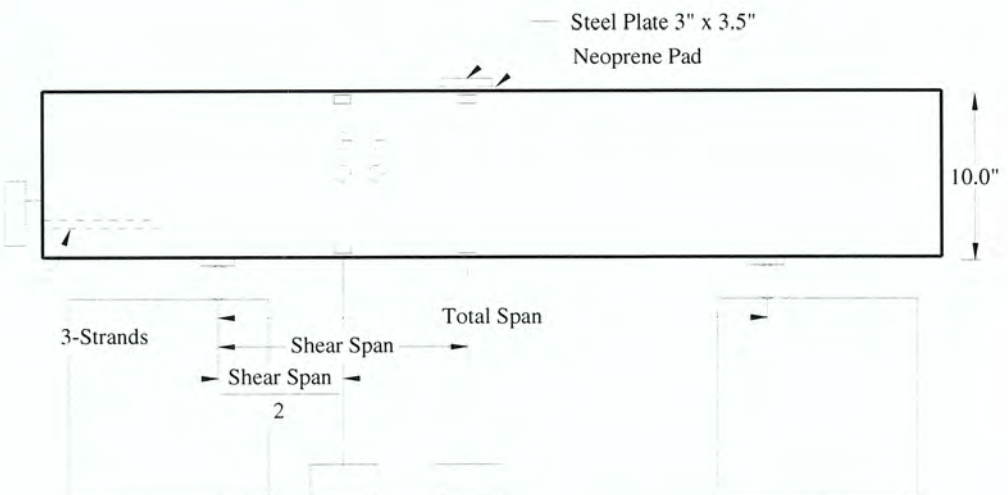

Figure 4.19. Ten inch beam test setup.

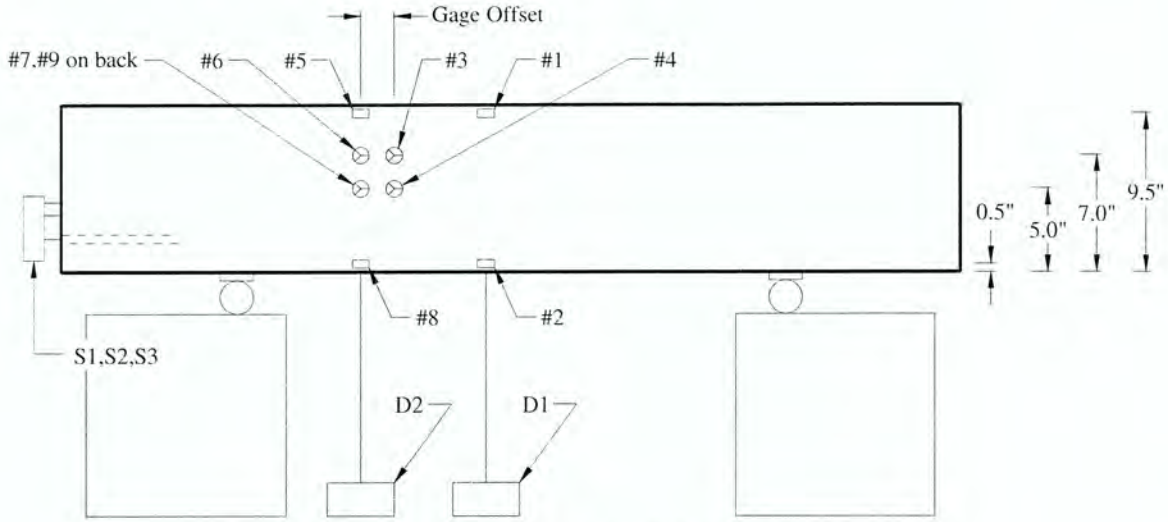

Figure 4.20. Instrumentation of ten inch beams.

Table 4.4. Variables in the setup of the ten inch small-scale test beams.

Beam	Shear Span (in)	Total Span (in)	Gage Offset (in)	Loading Device
A1	15	33	2	Pad
A2	15	33	2	Pad
A3	15	33	2	Pad
B1	20	46	4	Pin
B2	15	33	2	Pin
B3	15	33	2	Pad
C1	16	34	2	Pad
C2	15	33	2	Pad
C3	15	33	2	Pad

The 12 in. beam setup was similar to the 10 in. beams. Extra displacement devices were added to measure the deflection of the beam at the supports as well as the strand slip on both ends of the beam. In addition, four DCDT's were installed to act like large strain rosettes. The testing setup and instrumentation are further summarized in Figs. 4.21 and 4.22. For the 12 in. beams the total span length was constant at 44 in. and the shear span was 20 in. The data aquisition systems were once again used with the following instruments:

- one load cell measuring load
- five strain gage rosettes measuring strain in three directions (3,4,6,7,9)
- four linear strain gages (1,2,5,8)
- four DCDT's measuring displacement between two points on the beam (R1a,R1b,R2a,R2b)
- six DCDT's measuring strand slip (S1,S2,S3,S4,S5,S6)
- eight string potentiometers measuring deflection (E1,E2,D1a,D1b,D2a,D2b,D3a,D3b)

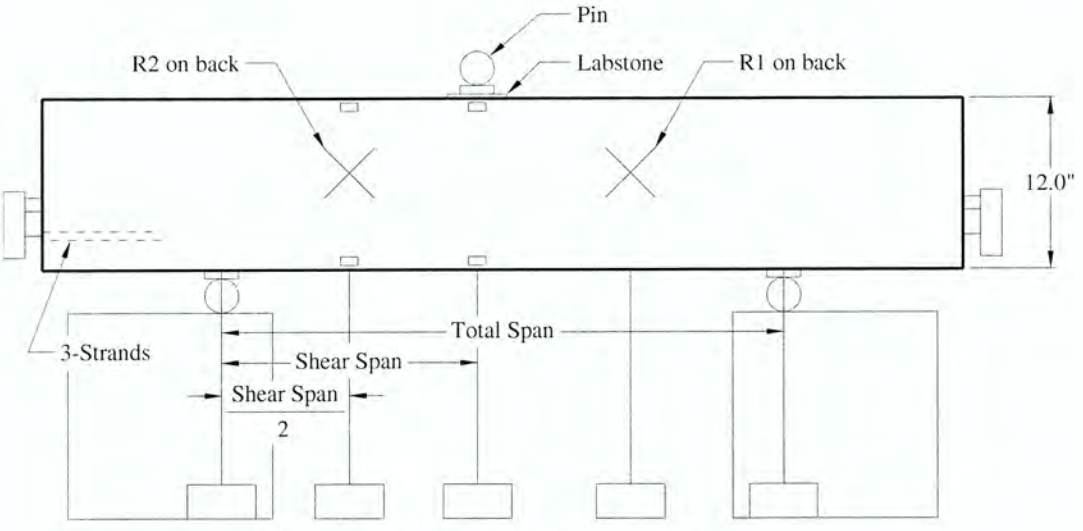

Figure 4.21. Twelve inch beam test setup.

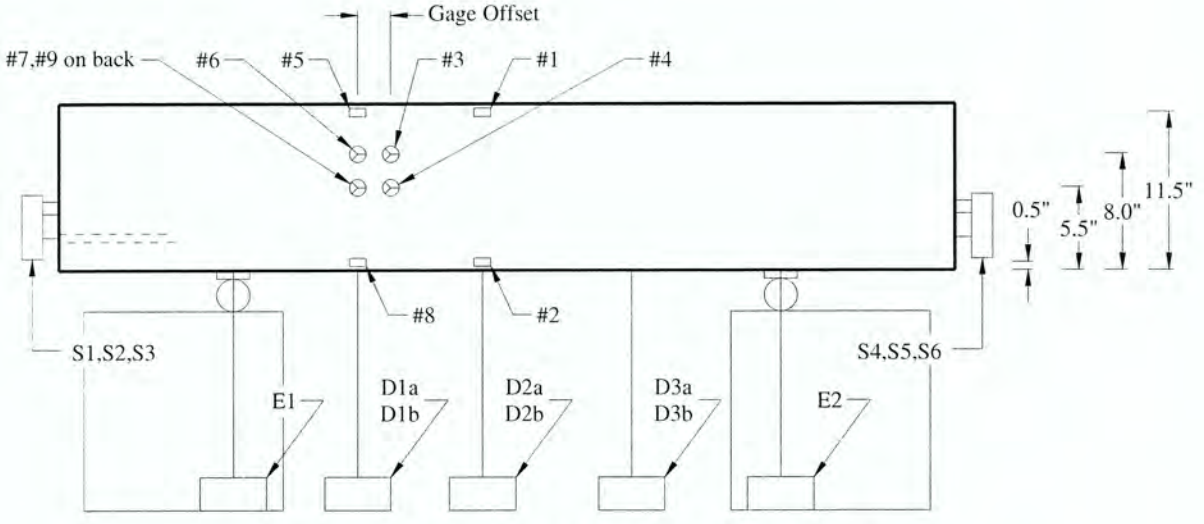

Figure 4.22. Instrumentation of twelve inch beams.

4.3.3 Test Procedure

Testing was completed on the small-scale beams using displacement control. The desired rate was input into the computer system at 0.1 in./min except for beam B1 which was 0.5 in./min. The machine automatically applied load until manually stopped. Testing was stopped after failure was evident by a significant drop in load. The beams were examined both during and after testing for indications of the response and resulting failure mode.

4.4 FIELD TESTING

Field testing consists of collection of strain data during the release of strands at the precast plant, during placement of the deck at the bridge site, and during the expected future live load testing of the completed bridge.

4.4.1 Release Testing

4.4.1.1 Test Configuration

Fiber optic gages were used to monitor the release of the strands for both the test beam and one bridge beam. Five gages were installed in both beams at the locations shown in Figs. 4.23 and 4.24.

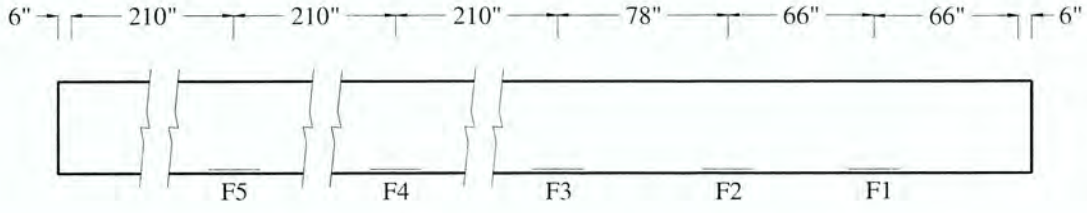

Figure 4.23. Fiber optic gage locations in the large-scale test beam.

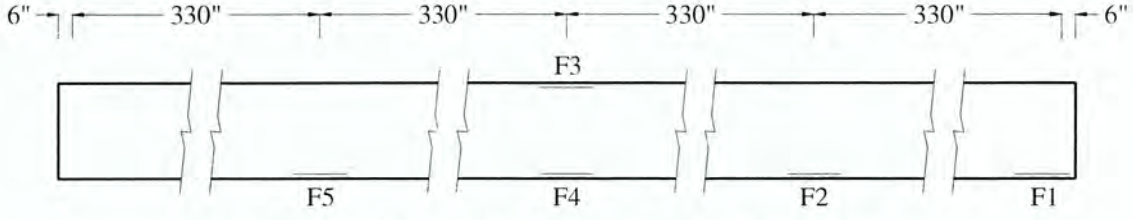

Figure 4.24. Fiber optic gage locations in the bridge beam.

4.4.1.2 Test Procedure

Testing for release stresses was completed in the precast plant for both the test beam and one of the bridge beams on Februaury 28th 2005 and July 20th 2005, respectively. The change in reflected wavelength of these gages was recorded throughout the release process for all of the gages except gage F1 of the bridge beam which was not working properly.

4.4.2 Dead Load Testing

4.4.2.1 Test Configuration

The same fiber optic gages used for release monitoring were used for dead load monitoring. Recall that the gages were located as shown in Fig. 4.24 in the west exterior beam at the center of the web except for gage F4 (bottom midspan) which was located seven inches east (toward the centerline of the entire bridge) from the horizontal center of the web.

4.4.2.2 Test Procedure

On Novemeber 8th, 2005, the Wapello Country bridge was monitored during the placement of the bridge deck concrete. Gages F1 and F2 were not working at this time and no results were collected. Initial readings were taken from gages F3 and F4 before pouring of the concrete. Slightly after the beginning of the deck pour an initial reading was also taken from gage F5. Also slightly after the beginning of the deck pour data began to be taken continuously from gage F3 and F4 until the deck pour was completed. At this point a final reading was taken from gage F5.

4.4.3 Live Load Testing

Live load testing should be completed in the future by Iowa State University and the Center for Transportation Research and Education. Future publications should contain more information.

CHAPTER 5: ANALYSIS METHODS

This chapter summarizes analysis methods used both for assessment of the collected test data and the development of a UHPC shear design procedure. Computational procedures have been developed and are summarized herein for a UHPC beam member in both its uncraked and cracked conditions. For an uncracked section, standard mechanics of materials equations are used to compute stresses, strains, and deflections. When a cracked beam is analyzed at a section, strain compatibility and the modified compression field theory (MCFT) are used. Also, a procedure for calculating deflection by applying the sectional computations of curvature across the entire member is described.

5.1 UNCRACKED BEAM ANALYSIS

5.1.1 Sectional Analysis

In this section, analysis of stresses are discussed. This is important because when the tensile principal stress reaches a value equivalent to the cracking strength of the material, the service level limit state has been reached. This is described mathematically as shown in equations 5.1 through 5.5 which can be found in any mechanics of materials text. Transformed and composite section properties are used which are described in more detail in Appendix A.

$$\sigma_x = \frac{P}{A} + \frac{P \cdot e \cdot c}{I} + \frac{M_t \cdot c_t}{I_t} + \frac{M_c \cdot c_c}{I_c} \qquad \text{longitudinal stress (ksi)} \tag{5.1}$$

Where:
- P = applied axial force (kips)
- A = gross cross-sectional area (in.^{2})
- e = eccentricity of axial force (in.)
- c = distance from centroid (in.)
- c_t = distance from transformed centroid (in.)
- c_c = distance from composite centroid (in.)
- I = moment of inertia (in.^{4})
- I_t = transformed moment of inertia (in.^{4})
- I_c = composite moment of inertia (in.^{4})
- M_t = moment applied to transformed section (in.- kips)
- M_c = moment applied to composite section (in.- kips)

σ_y = 0 vertical stress (ksi) (5.2)

$$\tau_{xy} = \frac{V_t \cdot Q_t}{I_t \cdot b} + \frac{V_c \cdot Q_c}{I_c \cdot b}$$ shear stress in the x-y plane (ksi) (5.3)

Where: V_t = shear applied to transformed section (kips)

V_c = shear applied to composite section (kips)

Q_t = transformed second moment of area (in.^{3})

Q_c = composite second moment of area (in.^{3})

b = width of section (in)

$$\sigma_{p1} = \frac{\sigma_x + \sigma_y}{2} - \sqrt{\left(\frac{\sigma_x - \sigma_y}{2}\right)^2 + \tau_{xy}^{\ 2}}$$ principal tensile stress (ksi) (5.4)

$$\sigma_{p2} = \frac{\sigma_x + \sigma_y}{2} + \sqrt{\left(\frac{\sigma_x - \sigma_y}{2}\right)^2 + \tau_{xy}^{\ 2}}$$ principal compressive stress (ksi) (5.5)

The compressive strength of UHPC was tested using a uniaxial compression test. The strength of each compression test specimen was determined using equation 5.6.

$$f`_c = \frac{P_{max}}{A}$$ maximum compressive strength of concrete (ksi) (5.6)

Where: P_{max} = maximum applied compressive force (kips)

A = gross cross-sectional area (in.^{2})

Flexural testing of prisms was completed to determine the tensile cracking strength of UHPC. The tensile cracking strength of the prisms was found using equation 5.7. There are some differences between flexural tension and direct tension, however within this work they are considered interchangeable.

$$f_{cr} = \frac{\left(\frac{F}{2} \cdot \frac{L}{3}\right) \cdot \left(-\frac{d}{2}\right)}{\left(\frac{b_w \cdot d^3}{12}\right)} = -\frac{F \cdot L}{b_w \cdot d^2}$$ cracking tensile strength of concrete (ksi) (5.7)

Where: F = applied flexural cracking load (kips)

L = span (in.)
b_w = width of web (in.)
d = depth (in.)

The service shear strength of UHPC can be determined theoretically using equation 5.4. The service shear strength is set as the shear force required to cause cracking. This occurs when the principal tensile stress is equated to the tensile cracking strength of the material. When this condition is true, the nominal service shear strength is given by equation 5.8. At this point when the concrete cracks, the crack orientation can be determined with equation 5.9 which is based upon Mohr's stress circle. This value will be used later in the formulation of ultimate shear strength.

$$V_n = V_t + V_c \quad \text{nominal shear strength (kips)} \tag{5.8}$$

Where: V_t = shear applied to transformed section (kips)

V_c = shear applied to composite section (kips)

$$\beta = \frac{1}{2} \cdot \tan^{-1}\left(\frac{2 \cdot V_n \cdot Q_c}{I_t \cdot b \cdot \sigma_x}\right) \quad \text{crack angle (degrees)} \tag{5.9}$$

Release stresses measured during release of the test beam and bridge beam can be verified using equation 5.10. This equation makes use of the mean stress method as described in reference [14] and is only valid in locations where the strand has been fully developed.

$$\sigma_f = \frac{\varepsilon_x - \varepsilon_{sh} - \alpha \cdot \Delta T + \sigma_x \cdot \left(\frac{1}{2 \cdot E_c} - \frac{K}{2 \cdot E_{ci}} - \frac{1}{2 \cdot E_{ci}}\right)}{\frac{1}{2 \cdot E_c} + \frac{K}{2 \cdot E_c} + \frac{1}{2 \cdot E_{ci}}}$$

final stress due to prestress after losses (5.10)

Where: ε_x = longitudinal strain

ε_{sh} = total shrinkage strain = 5.50×10^{-4}

α = thermal expansion coefficient = 6.55×10^{-6} per °F

ΔT = change in temperature (°F)

E_c = modulus of concrete = 7820 ksi

E_{ci} = initial modulus of concrete = 5700 ksi

K = creep coefficient = 0.3

5.1.2 Deflection Analysis

Deflections are calculated in order to compare the experimental and analytical values to ensure understanding of the structural behavior of UHPC. The total deflection can be described as the superposition of the flexural and shear deflections as shown in equation 5.11. For an uncracked elastic section, these computations have been carried out using the unit load method. Any variety of methods would be acceptable.

$$\Delta = \Delta_m + \Delta_v \quad \text{deflection due to moment and shear (in.)} \tag{5.11}$$

Where: Δ_m = deflection due to moment (in.)

Δ_v = deflection due to shear (in.)

5.2 CRACKED BEAM ANALYSIS

In this section, methods for determining many different parameters of a cracked UHPC beam are discussed including the flexural strength, shear strength, stresses, strains, and curvature at a section. Note that the curvature computed at the sectional level will be used to make deflection calculations for the beam as a whole.

5.2.1 Sectional Analysis

For a cracked section, a non-linear flexural model was developed as part of this work. This model is sometimes referred to as a strain compatibility approach by ACI [9] and AASHTO [15] which is simply a sectional approach utilizing an iterative process. The procedure can be used to compute the ultimate moment capacity of a section or the deflection of a structural component. The analysis assumes that plane sections remain plane, that stress and strain can be related through constitutive properties and that the shear stress is constant as shown in Fig 5.1.

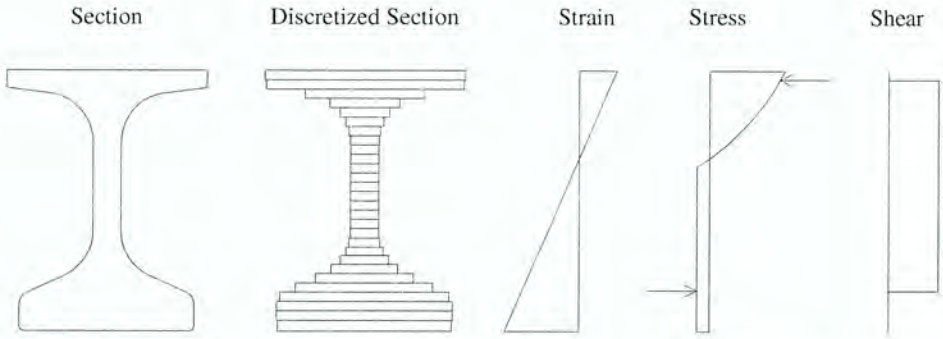

Figure 5.1. General strain, stress, and shear within a section.

5.2.1.1 Flexural Analysis

For a purely flexural analysis, the strain compatibility approach is used but the shear within a component is ignored. Therefore, this procedure should be used in situations where shear deformations are negligible.

For this procedure, computer processing has been used to facilitate the iterative calculations which basically solve two equations with two unknowns. The two "unknowns" are the curvature and strain at one location along the section height using the assumption of linear strain profile. The specific location of the unknown strain could be set at any location but has been arbitrarily chosen at the bottom flange. One of the "equations" results from force equilibrium (i.e., having a zero sum of forces in the horizontal direction at the sectional level). The other "equation" is satisfied by having the internal moment of the section equate to the external applied moment.

The external moment could be defined in one of two ways. First, the external moment could be the maximum possible applied moment or the moment capacity. In this case, Excel Solver was used to find the maximum value of the internal moment by iterating the strain and curvature and by satisfying force equilibrium. The second type of external moment is defined by the given loading conditions and is used for computing the deflection of a structural component. In this case the curvature and strain are iterated to equate the internal and external moment and satisfy force equilibrium. Deflection can then be computed by integrating the curvature twice over the length of the beam. In the case of this research with a non-uniform beam having harped strands, the procedure must be repeated for many locations along the length. If the structural component being analyzed is uniform, a simpler approach could be utilized by defining one equation for the moment-curvature relationship.

In order to compute a moment capacity, the following example can be followed. The following specifically describes the computation of the capacity of the large-scale test beam at its midspan. First, the constitutive properties of the materials being used must be established. The idealized stress vs. strain diagrams used for the UHPC and the prestressing strands are shown in Figs. 5.2 and 5.3 respectively. Next, the cross section of the beam is discretized into many rectangular segments that have a small height and the full width of the beam at each location as shown in Fig 5.1. With the assumption that plane sections remain plane, the strain profile must remain linear. Using an Excel spreadsheet, curvature and strain are iterated until a solution is found which satisfies the two previously described conditions. With this solution, the full strain profile can be determined as shown

in Fig. 5.4. Combining the known strains with the constitutive properties of concrete, the stress profile of the concrete is created in Fig. 5.5. The strains in the prestressing strands shown in Fig. 5.6 were determined by summing the prestressing strain with the strain induced by live loads. The stresses of the prestressing strands are shown in Fig. 5.7 and were determined by combining the strand strains with the constitutive strand properties. Next, a force resultant with its magnitude and position can be determined both in the compressive and tensile directions as shown in Fig. 5.8. The magnitudes of each must sum to zero for force equilibrium. Then the internal moment can be found by multiplying the distance between the two resultants by the magnitude of either one of the resultants. At this point iteration takes place to maximize the internal moment.

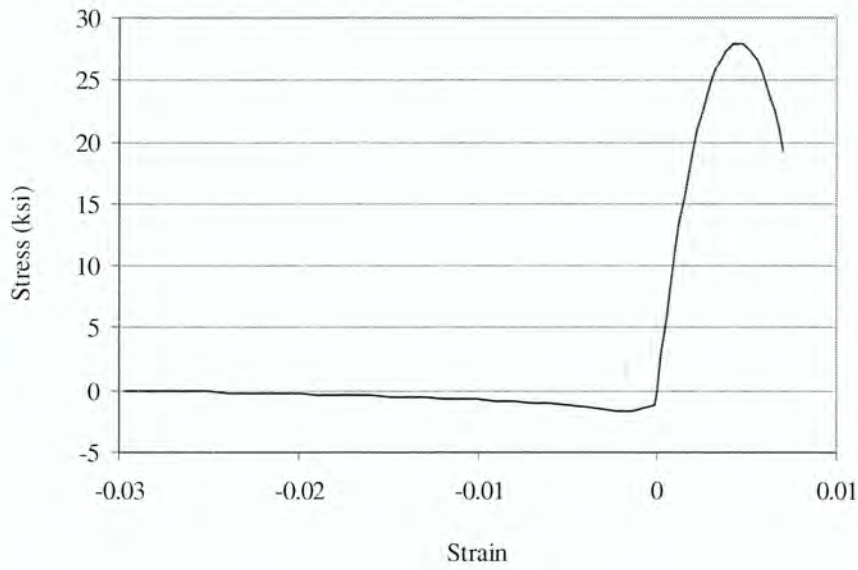

Figure 5.2. UHPC compressive and tensile constitutive properties.

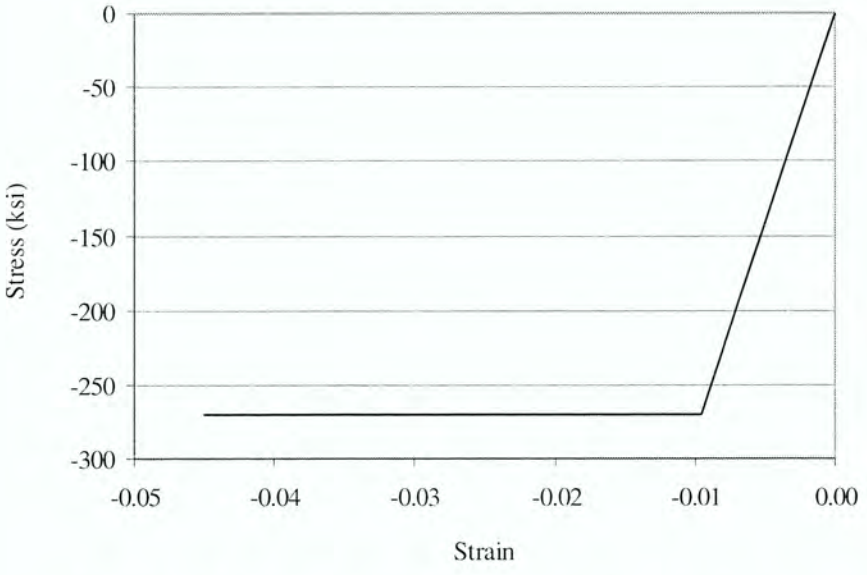

Figure 5.3. Prestressing strand tensile constitutive properties.

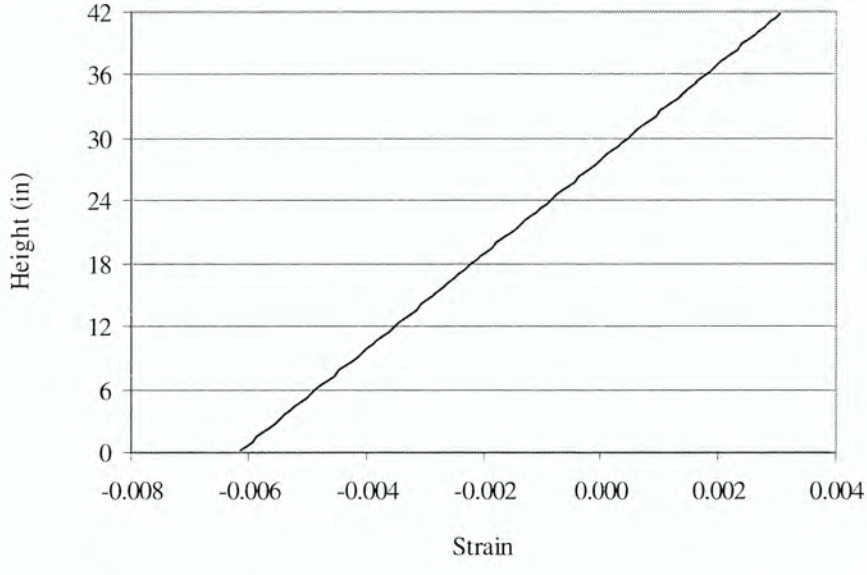

Figure 5.4. UHPC strain profile at midspan of large-scale flexure test beam at nominal moment strength.

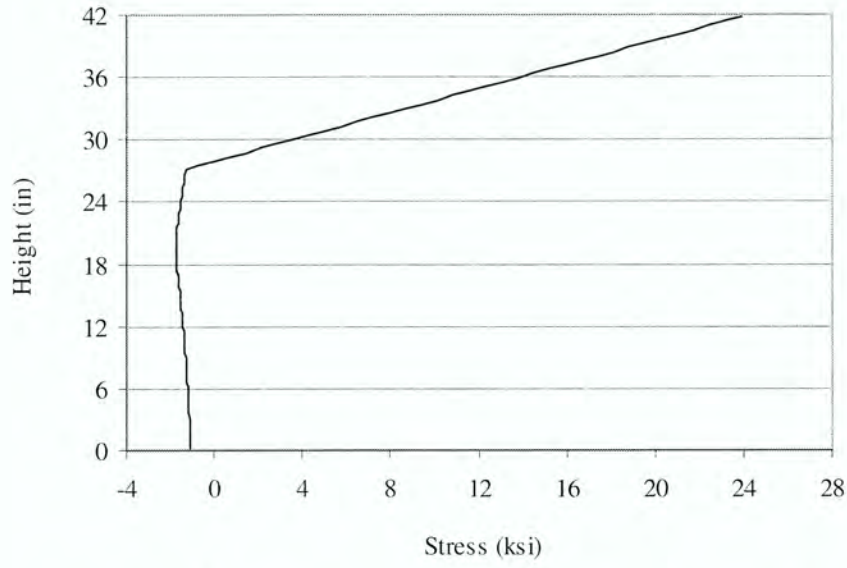

Figure 5.5. UHPC stress profile at midspan of large-scale flexure test beam at nominal moment strength.

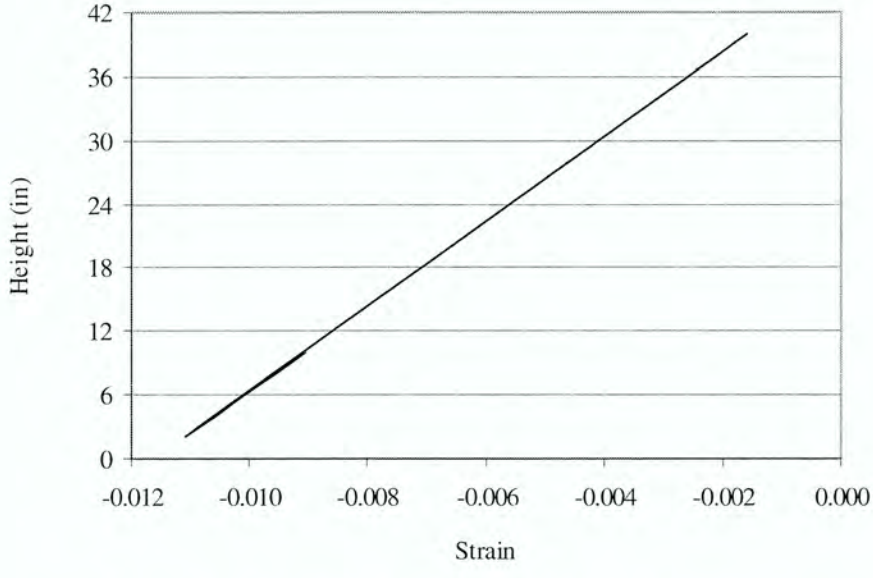

Figure 5.6. Strand strain profile at midspan of large-scale flexure test beam at nominal moment strength.

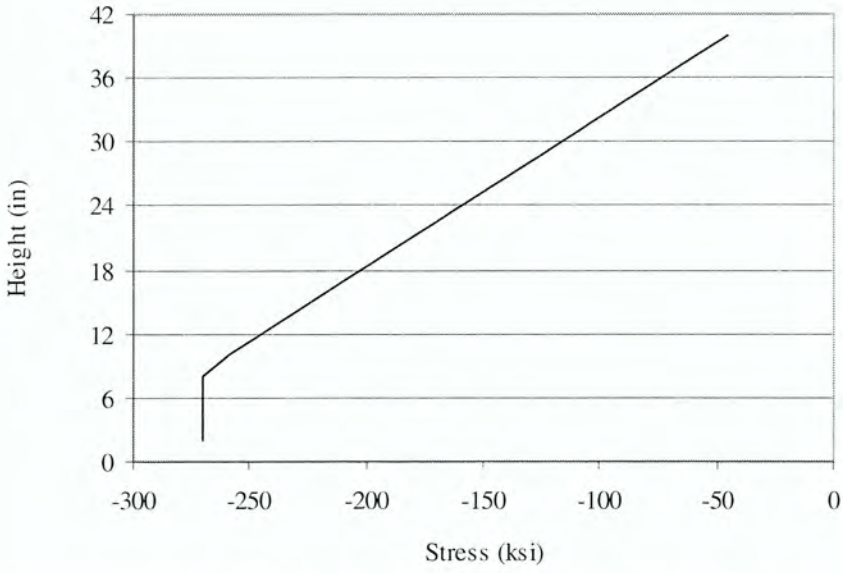

Figure 5.7. Strand stress profile at midspan of large-scale flexure test beam at nominal moment strength.

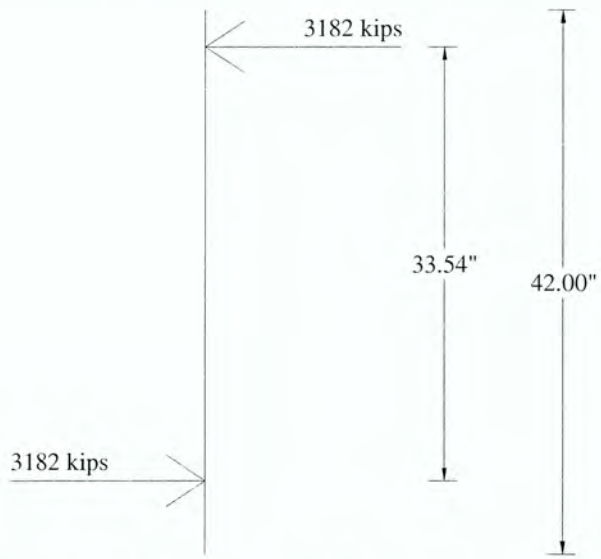

Figure 5.8. Force resultants at midspan of large-scale flexure test beam at nominal moment strength.

5.2.1.2 Flexure and Shear Analysis

For a combined flexure and shear analysis of a UHPC beam section, the purely flexural strain compatibility approach described in section 5.2.1.1 is combined with the shear analysis approach employing the Modified Compression Field Theory (MCFT) [11]. Some parameters of the MCFT approach have been calibrated for use with UHPC using test data from the current research. Future research is needed to verify and add to the accuracy of the empirical parameters and the proposed approach in its entirety. The basic idea of the MCFT is to combine equilibrium, compatibility, and constitutive properties of the materials into an analysis based on average strains and stresses. The MCFT states some warnings of using this approach for a member without shear reinforcement. A UHPC section does have shear reinforcement; although fibers and not stirrups are present. Since the fibers in UHPC are oriented randomly, the contribution of the fibers is included in the tensile constitutive properties and not as a separate variable as is done in the case with shear stirrups in the MCFT. The presence of fibers also affects the analysis procedure recommended herein. The MCFT suggests analyzing the full stress-strain state at only one location within a section where the full stress-strain state is known because both the Mohr's average stress and Mohr's average strain circle are fully defined.

When employing the MCFT for use with UHPC, it is suggested that the full stress-strain state at many discrete locations along a section height should be analyzed. The main reasoning for this modification is because UHPC exhibits residual tensile stress across a crack in the longitudinal direction which is generally ignored with conventional concrete. When a plane section analysis is employed as described in section 5.2.1.1, the stress profile can be predicted for conventional concrete by analyzing the full stress-strain state at only one location because the tensile strength of the concrete is essentially zero. In contrast, the stress profile is more accurately predicted for UHPC if many locations are used instead of just one. The directions of all the discussed stresses and strains are illustrated in Fig. 5.9 with stresses and strains occurring in the longitudinal, vertical, principal compressive, and principal tensile directions.

The MCFT as adopted in this research for combined flexure and shear analysis is described as follows. A plane section analysis will was used in conjunction with shear analysis. The curvature and the strain at the bottom of the section were first assumed for use with the plane section analysis as described in equations 5.12 and 5.13. These values were iterated until a solution was achieved and the strain was computed at every position along the section height as described by equation 5.14.

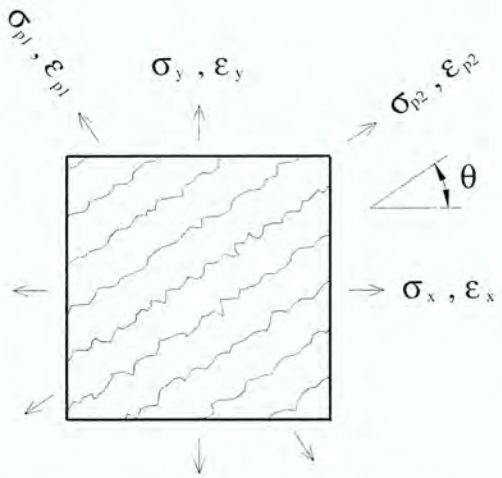

Figure 5.9. Directions of stresses and strains in a general UHPC element.

χ = *guess* curvature (1/in.) (5.12)

ε_{xb} = *guess* longitudinal strain at bottom of section (5.13)

$\varepsilon_x = \varepsilon_{xb} + \chi \cdot h$ longitudinal strain (5.14)

Where: h = distance above bottom of section (in.)

Next, an estimate of the longitudinal stress was made. This estimate is based solely on the stress-strain constitutive relationship of UHPC described in section 2.1 and by equations 5.15 through 5.19.

If $\varepsilon_x \geq 0$ then,

$$\sigma_{xc} = f`_c \cdot \left[ 2 \cdot \left( \frac{\varepsilon_x}{\varepsilon`_c} \right) - \left(\frac{\varepsilon_x}{\varepsilon`_c} \right)^2 \right]$$ longitudinal stress based on constitutive properties (ksi) (5.15)

If $0 \geq \varepsilon_x \geq \varepsilon_{cr}$ then,

$\sigma_{xc} = E_c \cdot \varepsilon_x$ longitudinal stress based on constitutive properties (ksi) (5.16)

If $\varepsilon_{cr} \geq \varepsilon_x \geq \varepsilon_{min}$ then,

$$\sigma_{xc} = f_{cr} + \frac{(\varepsilon_x - \varepsilon_{cr})}{(\varepsilon_{min} - \varepsilon_{cr})} \cdot (f_{max} - f_{cr})$$

longitudinal stress based on constitutive properties (ksi) (5.17)

If $\varepsilon_{min} \geq \varepsilon_x \geq \varepsilon_{max}$ then,

$\sigma_{xc} = f_{max}$ longitudinal stress based on constitutive properties (ksi) (5.18)

If $\varepsilon_x \leq \varepsilon_{max}$ then,

$$\sigma_{xc} = 0.672 \text{ ksi} \cdot \ln(-\varepsilon_x) + 2.362 \text{ ksi} \leq 0 \text{ ksi}$$

longitudinal stress based on constitutive properties (ksi) (5.19)

Where: f_{cr} = cracking tensile strength of concrete = -1.1 ksi

f_{max} = maximum tensile strength of concrete = -1.7 ksi

ε_{cr} = cracking tensile strain of concrete = -0.000141

ε_{max} = maximum magnitude of strain corresponding to f_{max} = -0.0024

ε_{min} = minimum magnitude of strain corresponding to f_{max} = -0.0014

However, due to a bilinear state of stress within a structural component, the constitutive property relationship which is based on uniaxial testing, is not fully valid. A material becomes weaker or "softer" in one direction when tension is applied in a perpendicular direction. The MCFT has developed equations relating the stress in the principal compressive direction to the strain in the principal tensile direction. In order to ease computation, for this approach, the "softening" relationship will be assumed to be applicable between the longitudinal stress and the vertical strain. In addition, the same softening affect will be assumed to take place for longitudinal tensile stresses due to vertical tensile strains. This relationship is not discussed by the MCFT because residual tensile stresses in the longitudinal direction are negligible in conventional concrete but not for UHPC. The following procedure up to equation 5.26 is performed in order to find the "softened" longitudinal stress.

Shear contributes to the "softening" of concrete. The MCFT assumes a shear stress distribution as being constant along the lever arm height "jd" and zero at other locations as shown in Fig. 5.1. The shear stress magnitude is described by equation 5.20. A shear stress distribution is assumed instead of being calculated because of the complexity of this approach. A dual-section analysis could be completed in order to more correctly calculate the shear stress. In this approach two sections within a beam which are quite close together are analyzed. The difference in the longitudinal stresses between the two sections requires shear stress in order to satisfy equilibrium. As has been discussed, shear contributes to the softening of concrete, thus altering the longitudinal stresses. As can be seen, the longitudinal and shear stresses are interdependent thus creating a difficult solution technique.

$$\tau_{xy} = \frac{V}{b_w \cdot j \cdot d} \quad \text{shear stress in the x-y plane (ksi)} \tag{5.20}$$

Where: V = applied shear (kips)

b_w = width of web (in.)

j = lever arm percentage of depth

d = depth (in.)

The lever arm height can be determined by a secondary iteration. An initial assumption is required provided by the MCFT which states that the lever arm "jd" need not be taken any smaller than 80% of the section height. Once the full computation of section 5.2.1 has been carried out, the distance between the compressive force resultant and the tensile force resultant can be compared to the initial assumption.

Next, the shear strain can be determined using the shear stress-strain relationship developed during research as shown subsequently in Fig. 6.8. The relationship is linear following the shear modulus until a stress of 2.3 ksi is reached. Then a parabolic relationship is used to a maximum stress of 3.5 ksi and strain of 0.01 as described in equations 5.21 and 5.22.

If $\tau_{xy} \leq \tau_{cr}$ then,

$$\gamma_{xy} = \frac{\tau_{xy}}{G} \quad \text{shear strain in the x-y plane (ksi)} \tag{5.21}$$

Where: G = shear modulus (ksi) = 3258 ksi

If $\tau_{xy} > \tau_{cr}$ then,

$$\gamma_{xy} = \gamma_{\max} - \sqrt{\frac{\left(\tau_{\max} - \tau_{xy}\right) \cdot \left(\gamma_{\max} - \frac{\tau_{cr}}{G}\right)^2}{\tau_{\max} - \tau_{cr}}} \quad \text{shear strain in the x-y plane} \tag{5.22}$$

Where: $\gamma_{\max}$ = maximum shear strain = 0.01

τ_{cr} = cracking shear stress = 2.3 ksi

$\tau_{\max}$ = maximum shear stress = 3.5 ksi

The MCFT theory has developed equation 5.23 to relate the "softening" effect on stress due to strain in the orthogonal direction. The left hand that is multiplied by σ_{xc} in equation 5.23 can be thought of as a softening factor. This term is always less than one because the concrete becomes weaker with an applied orthogonal strain. The MCFT uses a first softening coefficient of $\xi_1 = 0.8$, in which case if the vertical strain were zero, the entire softening term would be greater than one. Therefore the MCFT states that the entire term cannot be greater than one. However, within the procedure used herein, it is mathematically difficult to use this inequality statement. Therefore, the first softening coefficient has been set equal to one, so the entire softening term will never be greater than one. Based upon the experimental results discussed in Chapter 6, the second softening coefficient has been estimated as $\xi_2 = 3$. The MCFT had used a value of 0.34 for this term. This large discrepancy is due to the use of a different material with a larger maximum strain, a different solution procedure taking into account every location along the height of the member instead of only one location, and that the longitudinal and vertical directions are being related instead of the two principal directions.

All the basic information is now available to determine the "softened" longitudinal stress. There are six unknown values needed in order to fully define the stress-strain state at any one location of the beam. This is because in order to fully define Mohr's circle of average stresses, three values must be known. Three values must also be known to define Mohr's circle of average strains. As discussed, the shear stress, shear strain, and longitudinal strain are known. In addition, the vertical stress can be assumed to be zero. One assumption made by the MCFT and upheld herein is that the angle of principal compressive stress is equal to the angle of the principal compressive strain. This eliminates the need for one known value.

Now there are three unknowns, namely the longitudinal stress, principal compressive stress angle, and vertical strain. Equation 5.23 has been developed by the MCFT to define the longitudinal stress. Using Mohr's circle of average stresses and strains shown in Fig. 5.10 and 5.11, equations 5.24 and 5.25 can be derived describing the principal compressive stress angle and the vertical strain.

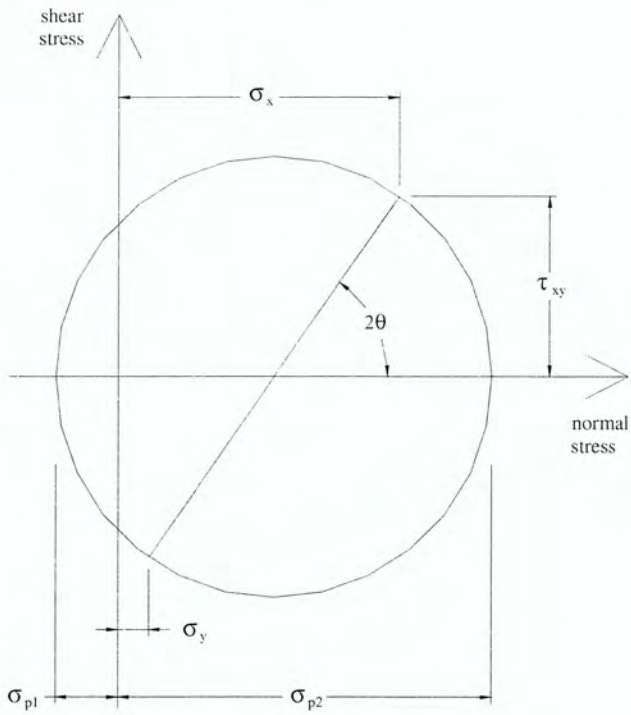

Figure 5.10. Mohr's circle of average concrete stresses in a general UHPC element [5].

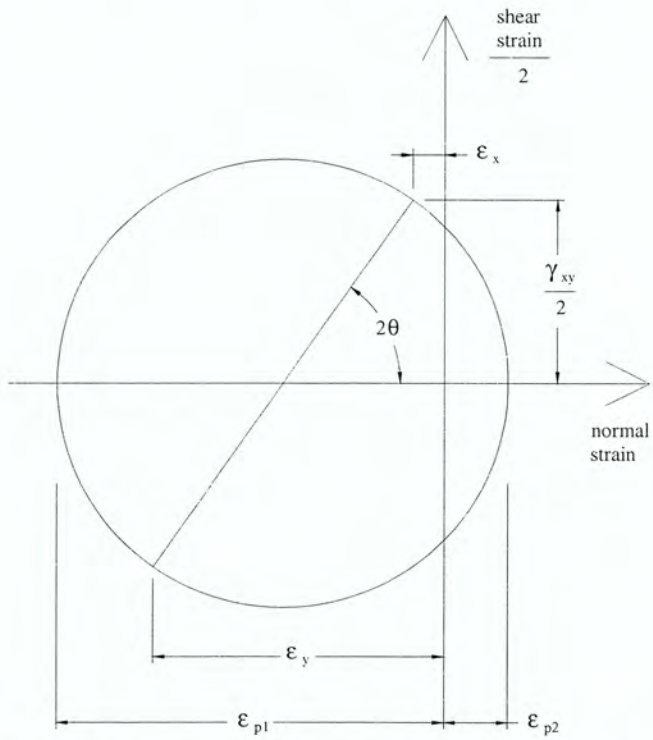

Figure 5.11. Mohr's circle of average concrete strains in a general UHPC element [5].

$$\sigma_x = \frac{1}{\xi_1 - \frac{\xi_2 \cdot \varepsilon_y}{\varepsilon`_c}} \cdot \sigma_{xc} \quad \text{longitudinal stress (ksi)} \tag{5.23}$$

Where: ξ_1 = first softening coefficient = 1

ξ_2 = second softening coefficient = 3

$\varepsilon`_c$ = strain associated with f`c

ε_y = vertical strain

$$\theta = \frac{1}{2} \cdot \tan^{-1} \cdot \left(\frac{2 \cdot \tau_{xy}}{|\sigma_x|} \right) \quad \text{principal compressive stress angle (degrees)} \tag{5.24}$$

$$\varepsilon_y = \varepsilon_x - \frac{\gamma_{xy}}{\tan(2 \cdot \theta)} \quad \text{vertical strain} \tag{5.25}$$

In order to develop a solution, a third order system of equations must be solved. (Equations 5.23 through 5.25) First, θ of equation 5.24 can be substituted into equation 5.25 resulting in equation 5.26. Then substituting ε_y from equation 5.26 into equation 5.23 results in equation 5.27. If equation 5.27 is rearranged, equation 5.28 is derived.

$$\varepsilon_y = \varepsilon_x - \frac{\gamma_{xy} \cdot |\sigma_x|}{2 \cdot \tau_{xy}} \quad \text{vertical strain} \tag{5.26}$$

$$\sigma_x = \frac{\varepsilon`_c \cdot \sigma_{xc}}{\xi_1 \cdot \varepsilon`_c - \xi_2 \cdot \left(\varepsilon_x - \frac{\gamma_{xy} \cdot |\sigma_x|}{2 \cdot \tau_{xy}} \right)} \quad \text{longitudinal stress (ksi)} \tag{5.27}$$

$$\left(\frac{\xi_2 \cdot \gamma_{xy}}{2 \cdot \tau_{xy}} \right) \cdot \sigma_x \cdot |\sigma_x| + \left(\xi_1 \cdot \varepsilon`_c - \xi_2 \cdot \varepsilon_x \right) \cdot \sigma_x - \varepsilon_c \cdot \sigma_{xc} = 0 \text{ ksi} \quad \text{quadratic equation} \tag{5.28}$$

The quadratic equation described by equations 5.29 through 5.33 is utilized as a solution technique for equation 5.28 resulting in the derivation of the "softened" longitudinal stress described by equation 5.34.

$$A_q \cdot \sigma_x^{\,2} + B_q \cdot \sigma_x + C_q = 0 \text{ ksi} \quad \text{quadratic equation} \tag{5.29}$$

If $\sigma_{xc} > 0$ ksi then,

$$A_q = \frac{\xi_2 \cdot \gamma_{xy}}{2 \cdot \tau_{xy}} \quad \text{second order quadratic equation coefficient (in.}^2\text{/kip)} \tag{5.30}$$

If $\sigma_{xc} < 0$ ksi then,

$$A_q = -\frac{\xi_2 \cdot \gamma_{xy}}{2 \cdot \tau_{xy}} \quad \text{second order quadratic equation coefficient (in.}^2\text{/kip)} \tag{5.31}$$

$$B_q = \xi_1 \cdot \varepsilon`_c - \xi_2 \cdot \varepsilon_x \quad \text{first order quadratic equation coefficient} \tag{5.32}$$

$$C_q = -\varepsilon`_c \cdot \sigma_{xc} \quad \text{constant quadratic equation coefficient (ksi)} \tag{5.33}$$

$$\sigma_x = \frac{-B_q + \sqrt{B_q^{\,2} - 4 \cdot A_q \cdot C_q}}{2 \cdot A_q} \quad \text{longitudinal stress (ksi)} \tag{5.34}$$

This process will cause a mathematically erroneous answer for portions of the section with zero shear stress due to division by zero. Therefore, it has been assumed that the softening coefficient is constant across the section height set at the value computed at the beginning of the moment arm region.

Once the longitudinal stress is known, the plane section nonlinear flexural model described in section 5.2.1.1 is used. In that case, strain and curvature where solved based on moment and axial load. Now, in addition to those quantities, if the shear force is given, the shear stress distribution can also be determined which, in turn, impacts the other quantities. Utilizing a computer algorithm and/or an Excel spreadsheet with solver, the iterative calculations can be completed. The solution process is similar to solving three equations with three unknowns. Excel solver has a feature which allows the maximum value of shear force to be determined. Therefore, not only can this procedure be used with a given shear force but it can also be used to determine shear strength.

To illustrate an example of the previous description several figures are shown. Figures 5.12 through 5.16 show the unsoftened longitudinal stress, vertical strain, principal compressive stress angle, softening coefficient, and the softened longitudinal stress analyzed at load application point L4 at a total load of 600 kips during the flexure-shear test.

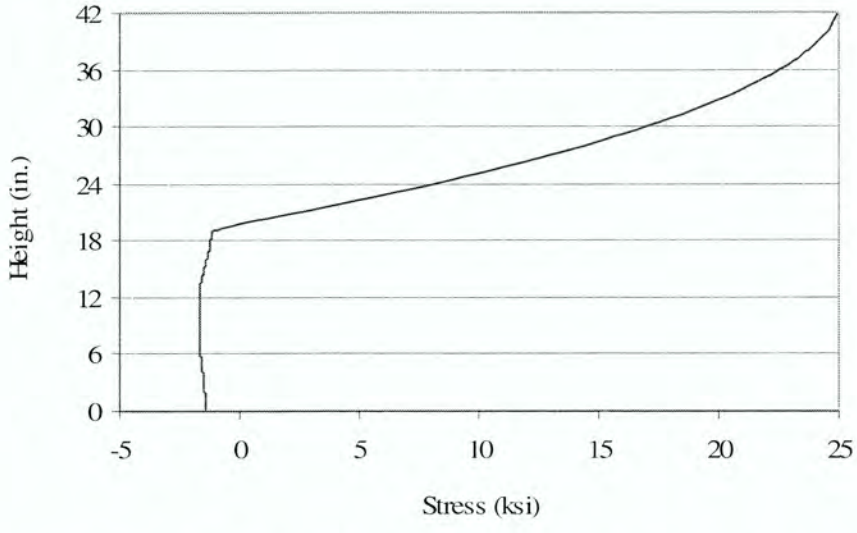

Figure 5.12. Unsoftened longitudinal stress of large-scale flexure-shear test beam at load application point L4 while undergoing a total load of 600 kips.

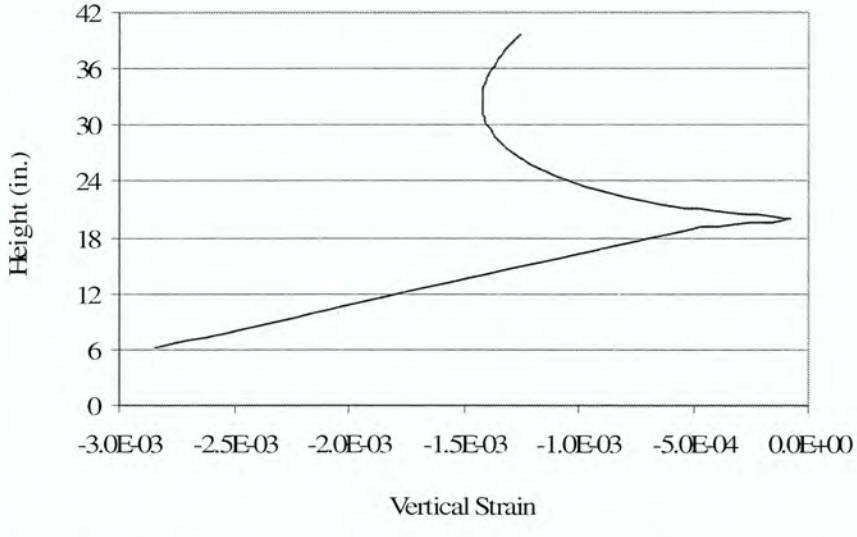

Figure 5.13. Vertical strain of large-scale flexure-shear test beam at load application point L4 while undergoing a total load of 600 kips.

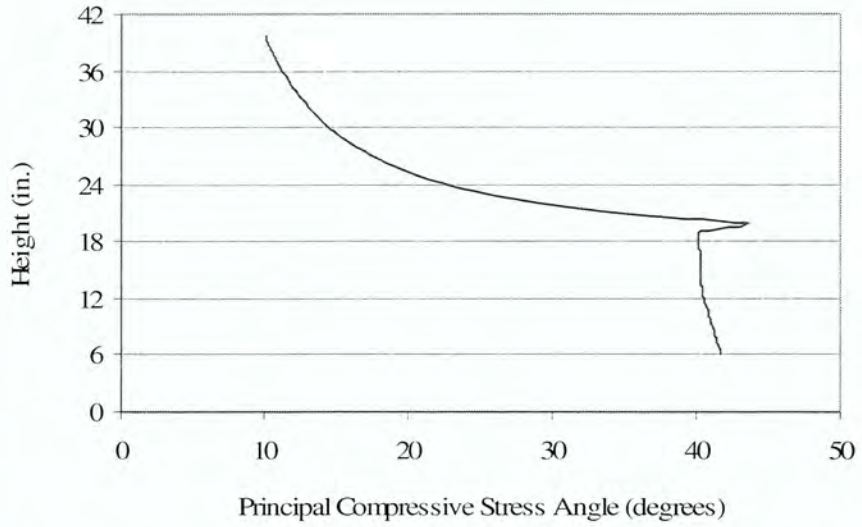

Figure 5.14. Principal compressive stress angle of large-scale flexure-shear test beam at load application point L4 while undergoing a total load of 600 kips.

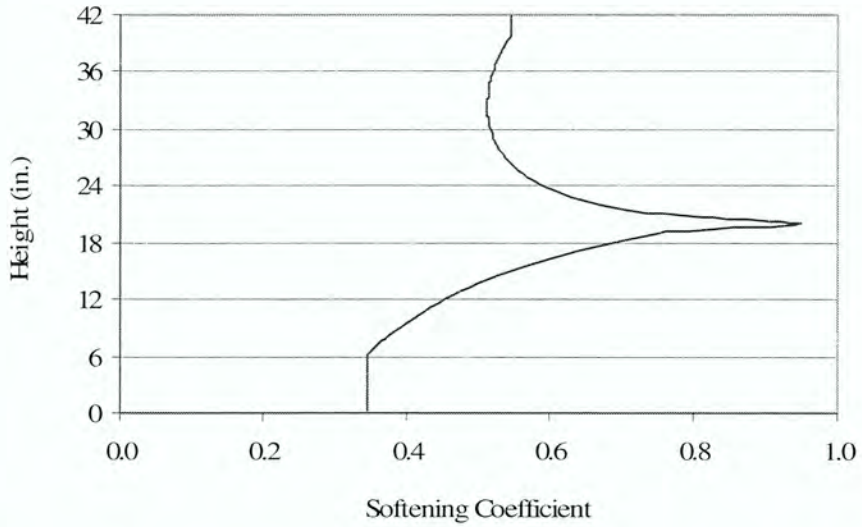

Figure 5.15. Softening coefficient of large-scale flexure-shear test beam at load application point L4 while undergoing a total load of 600 kips.

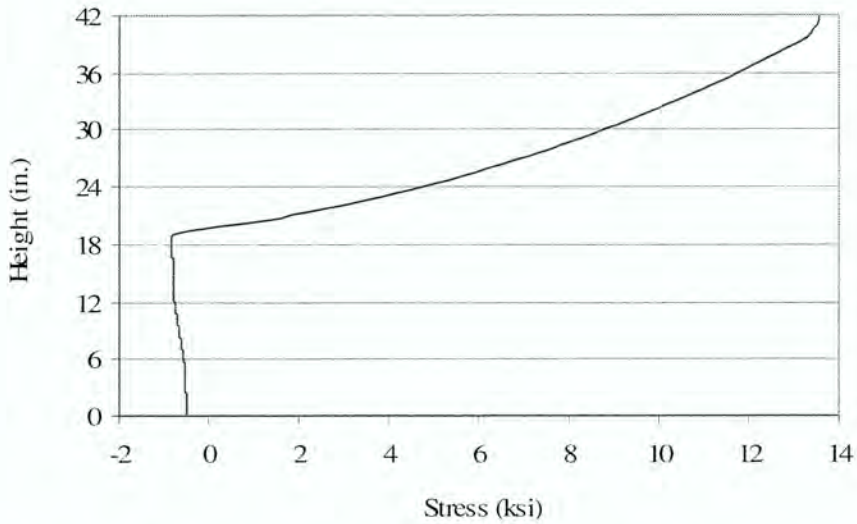

Figure 5.16. Softened longitudinal stress of large-scale flexure-shear test beam at load application point L4 while undergoing a total load of 600 kips.

In order to determine the maximum value of shear, different failure modes should be analyzed. The modes that have been identified for this research are flexural tension failure, flexural compression failure, flexural tension failure of strands, compression failure of a web strut caused by shear, and tension failure of the web caused by shear. When flexural tension failure of the UHPC flange occurs, the longitudinal tension strain within the flange becomes large enough for the concrete to lose strength as described by its constitutive properties in section 2.1. The same is true for compression failure of the UHPC flange but large compression strains are developed instead of tension. Flexural tension failure of the strands occurs when the tensile strain in the strands exceeds the strain capacity. Shear compression failure of the web strut occurs when the principal compressive stress equates to the compressive strength of UHPC which can be determined with cylinder testing and a "softening" analysis. Shear tension failure of the web occurs when the principal tensile strain of UHPC becomes too large. This value can be obtained by multiplying the crack spacing by the maximum inclined crack width in the UHPC beam. Both of these parameters will need further research to fully define.

5.2.2 Deflection Analysis

The following describes a procedure for determining beam deflections in the elastic or post-elastic range after cracking. The beam is first discretized into many small portions along its length. Given a particular loading condition, the external moments corresponding to each location along the beam length can be found and set equal to the internal moments at each location. When this process is

completed, the curvature at the discrete locations along the length of the beam can be determined. Next, two integrations of the curvature over the length of the beam are preformed. It is not practical to express the curvature in closed form for a cracked beam because a very complicated equation would be required. Therefore, numerical integration is used. In the case of this research, the trapezoidal rule has been used and would be recommended although any numerical integration technique is acceptable. By integrating the curvature over the beam length, the slope can be found. However, an initial value for the slope must be determined in an iterative process. Integrating the slope numerically will determine the value of the deflection as shown in equation 5.35. The initial deflection at both ends of the beam must be equated to the boundary conditions which in most cases is zero. The solution is found by iteratively solving for the initial slope of the beam which can be done using Excel Solver as was done in this research.

$$\Delta = \int_0^x \left(\int_0^x \chi \cdot dx \right) \cdot dx \qquad \text{deflection due to moment and shear (in.)} \tag{5.35}$$

Where: χ = curvature (1/in.)

x = position along length of beam (in.)

Deflections computed using this procedure have been attempted to be verified by comparing them to experimental deflections obtained during the FHWA structural testing described in section 2.4. Using the procedure of section 5.2.1.1, Fig. 5.17 shows that for the FHWA Flexure Test the experimental and analytical deflections correlate fairly well. Also, FHWA Shear Test #2 was analyzed using the procedure of section 5.2.1.2. The results did not match well. It should be noted that Chuang and Ulm [12] completed analysis on this test which closely match the analysis done in this work. The experimental deflection is shown in Fig. 5.18 to be approximately a constant 1.4 times larger than the analytical deflection. Possible reasons for this discrepancy are previous damage to the beam, underestimation of shear deformation, errors in the experimental data, or strand slip. Some previous damage did occur in the beam because the broken portion of the FHWA Flexure Test beam was used for the FHWA Shear Test #2. Analytically, shear deformation accounted for approximately 9% of the total deflection of the FHWA Shear Test #2 within the linear range.

5.2.3 Strut and Tie Analysis

Strut and tie analysis has been carried out according to section 2.3 and the provisions of ACI [9]. The computations show that the concrete is sufficiently strong in compression in order not to fail the struts

when a strut factor of 0.85 is used. Therefore, the applied load is iterated until the tension in the tie reaches its ultimate capacity or until the angle between the strut and tie reaches 25 degrees as dictated by the strut and tie method. In section A.3, an example of the strut and tie method is given for the small-scale beams of this research.

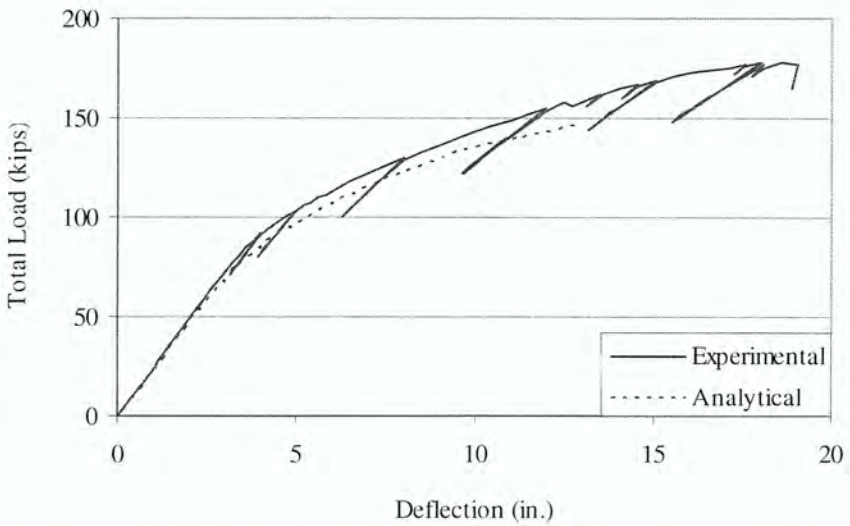

Figure 5.17. Deflection of FHWA flexure test beam at midspan.

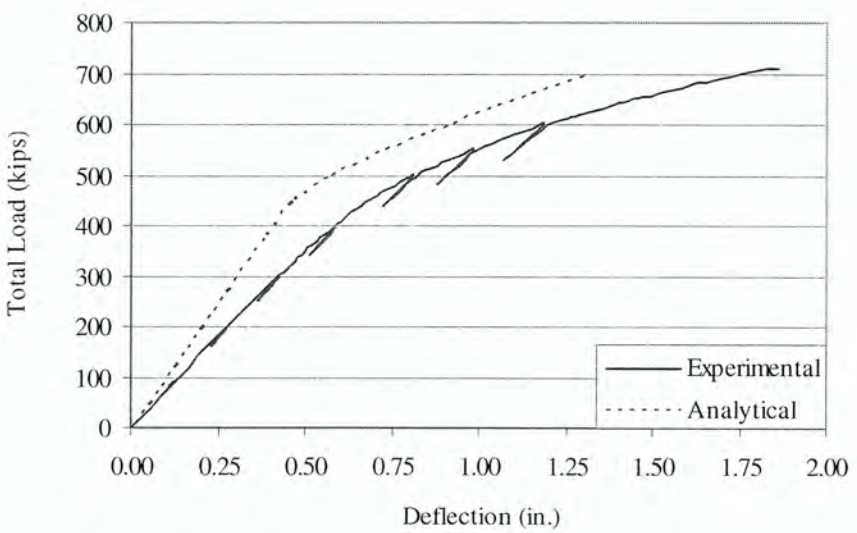

Figure 5.18. Deflection of FHWA shear test #2 beam at the load application point.

CHAPTER 6: EXPERIMENTAL AND ANALYTICAL RESULTS

This chapter describes the experimental and analytical results for this research. Where appropriate, results include qualitative observations, quantitative data and interpretations of the data. The test specimen descriptions, test configurations and test procedures are presented in Chapter 4. The analysis methods used herein are discussed in Chapter 5.

6.1 MATERIAL TESTING

6.1.1 Uniaxial Compression Testing

Uniaxial compression strengths were determined using the previously described procedure in section 5.1.1. The average and standard deviation strength values are summarized in Table 6.1 for three different groups of samples; those cured at 194°F in a controlled chamber, those cured with the product, and those cured at room temperature. As a whole, the samples had slightly lower strength than the anticipated strength of 28 ksi mentioned previously. It is apparent that curing the samples in a controlled chamber at 194°F resulted in the highest compressive strength, while curing with the product was slightly lower but with greater consistency and curing at room temperature resulted in the lowest strengths.

Table 6.1. Uniaxial compressive strength of UHPC cubes.

Curing Method	Average (ksi)	Standard Deviation (ksi)
194°F	25.12	4.32
With Product	24.56	2.91
Room Temperature	21.5	3.98

6.1.2 Prism Flexural Testing

In general, flexural testing of the prism specimens caused them to first crack in the central constant moment region as expected. After cracking, the prisms held additional load until failing in that same region. For this work, the load at which the load vs. table displacement became non-linear was defined as the flexural cracking load as is illustrated in Fig. 6.1 at a load of about 0.9 kips. Using equation 5.7 (which is not valid after cracking), the cracking tensile stress can be calculated. The resulting flexural tensile cracking strength statistics are summarized in Table 6.2 for the three different curing conditions. Curing at 194°F resulted in the highest strengths, while curing at room temperature resulted in the lowest strengths. In general, the flexural tensile cracking strength results relate well to previously published test results [1], [2], [3], [4].

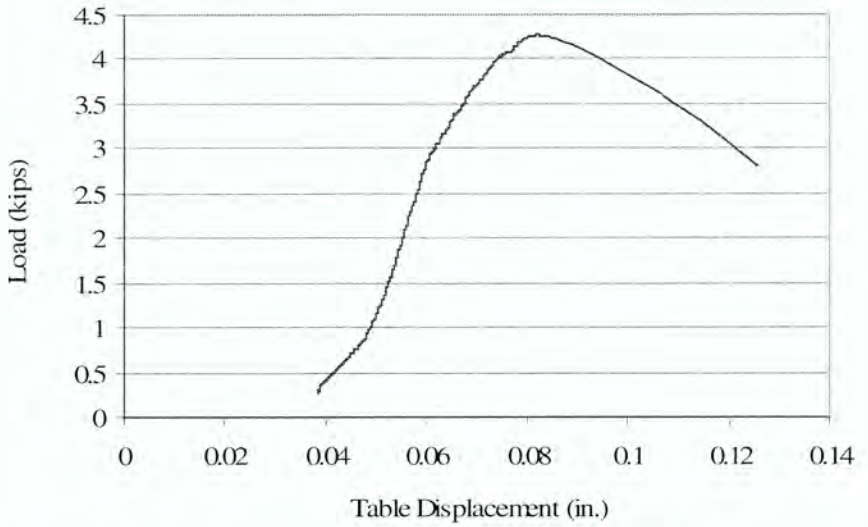

Figure 6.1. Load vs. table displacement during a typical prism flexure test.

Table 6.2. Flexural cracking tensile strength of UHPC prisms.

Curing Method	Average (ksi)	Standard Deviation (ksi)
194°F	-1.16	0.21
With Product	-1.04	0.12
Room Temperature	-0.93	0.12

6.2 LARGE-SCALE LABORATORY TESTING

6.2.1 Flexural Testing

6.2.1.1 Test Observations

During testing, the beam was inspected for cracks three times. The first inspection occurring at a total load level of approximately 237.4 kips revealed one very small hairline crack near the beam midspan which was subsequently identified to be a crack during the second sequence of loading. The second inspection took place at a total load level of approximately 256 kips during the second sequence of loading when 13 hairline cracks spaced at about 6 in. were discovered on the bottom flange of the beam within the constant moment region. The third and final inspection took place at the end of the second sequence of loading at a total load level of approximately 265 kips. At this point, the previously identified cracks had extended. Also, one new crack was found nearly at the midspan of the beam. This flexural crack extended up to the web region of the beam on the north side (higher than any of the other cracks) and extended about 3 in. up from the bottom flange on the south side (lower than any of the other cracks). All 14 cracks ran transversely across the entire bottom flange of the beam. The cracks on the north face ended within the tapered portion of the bottom flange. While

the cracks on the south side ended near the beginning of the tapered portion of the bottom flange. Generally, the cracks could be classified as "hairline". The cracks were marked with typical examples shown in a close up view on the bottom flange of the north face of the beam in Figure 6.2. On the east end of the beam, the concrete around one strand had several cracks extending in the radial direction around the strand perimeter. On the west end of the beam, horizontal and vertical cracks extended to both the side and bottom of the beam at each of the two bottom corner strands.

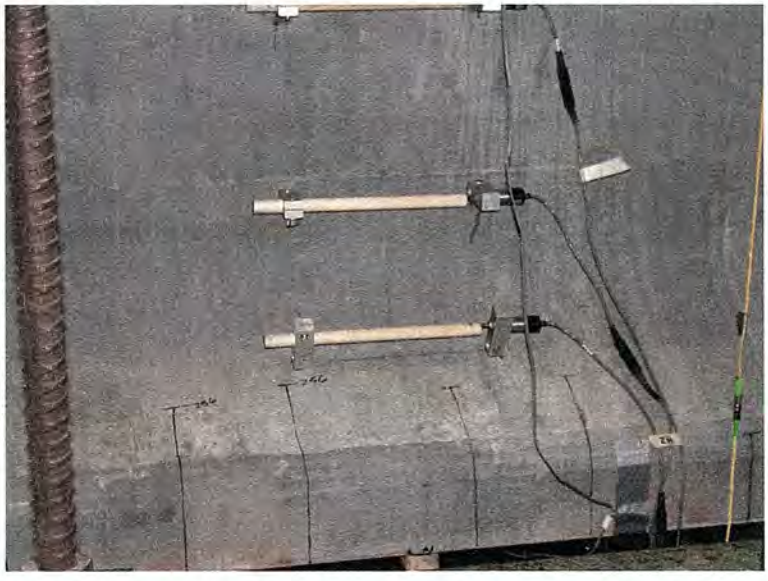

Figure 6.2. Flexural cracks on north bottom flange at midspan at peak load of large-scale flexure test.

6.2.1.2 Test Results

The primary purpose of the flexure test was to provide reassurance to the design engineer that the beam had sufficient capacity for implementation in the first United States UHPC bridge in Wapello County, Iowa. This was achieved by reaching a load level above the expected service loads before cracking occurred. The service level is determined by a simple summation of external moments required to be resisted by the bridge beam including from the bridge deck, future overlay, barriers, and the live load as required by code. Using the effective width of the bridge deck according to AASHTO [15], the bridge beams have a larger section than the test beam and therefore can resist more moment. As can be seen in Fig. 6.3, the total load when non-linearity occurs at cracking was 237.4 kips which corresponds to a moment of 3,730 ft-k, not including the beam self-weight. Using this information and the additional effective width of the slab, a service moment capacity of the bridge beam can be determined which should be larger than the applied service moment as shown in Table 6.3. The same type of process is carried out for the ultimate limit state, although test data for

this beam did not reach this level, and therefore the quantities shown in Table 6.3 are based off of analysis rather than testing.

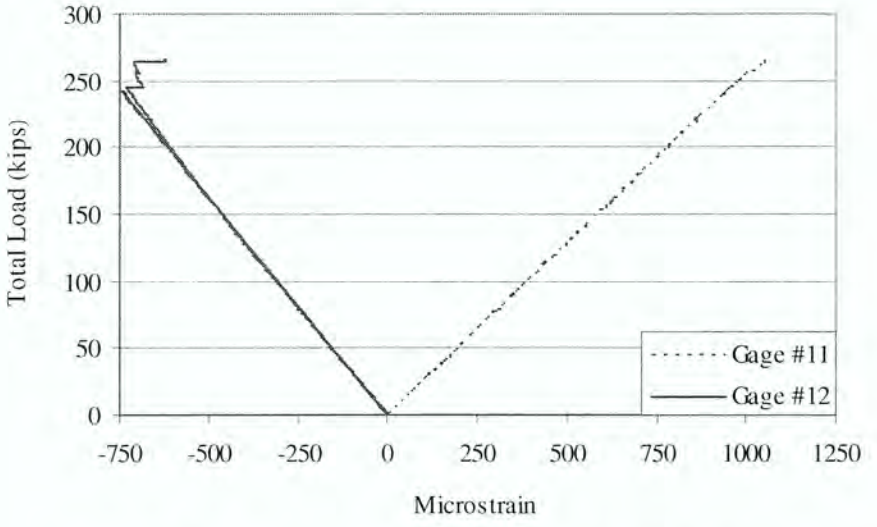

Figure 6.3. Strain at midspan during large-scale flexure test.

Table 6.3. Comparison of large-scale flexure test capacities to applied bridge moments.

Limit State	Experimental Moment Capacity of Test Beam (ft-kips)	Analytical Moment Capacity of Bridge Beam (ft-kips)	Applied Moment on Bridge Beam (ft-kips)
Service Level	3,730	4,760	4,624
Ultimate Level	N/A	7,620	7,350

In addition, the flexure test was useful for estimating the amount of prestressing in the test beam. By using the applied moment at which cracking occurred, the prestressing force was estimated to be 1517 kips (27.2% loss) experimentally using a simple linear stress analysis. The amount of prestressing determined experimentally was also compared with traditional calculations made during initial design. The losses that were accounted for are the initial relaxation, elastic shortening, shrinkage, creep, and secondary relaxation. These loss calculations are described by AASHTO [15] and are documented in Appendix A using the material properties presented previously. The calculated analytical prestressing force after losses is 1450 kips (30.4% loss) which correlates fairly well with the experimental results.

Several instruments recorded data during the test to ensure that the beam was behaving as expected. The deflection at several locations could be accurately calculated within the linear range when using

the unit load method. (Any number of simple elastic models could also be used.) Figure 6.4 shows the midspan experimental and analytical deflection. As well, the stresses within the beam could be predicted accurately. For instance, in Fig. 6.5 the stresses at midspan under a total load of 237 kips are shown to be accurate and uphold the assumption that plane sections remain plane. In addition, three strands were monitored for slip. One gage indicated a rapid increase in slip to 0.005 in. at the maximum load as shown in Fig. 6.6.

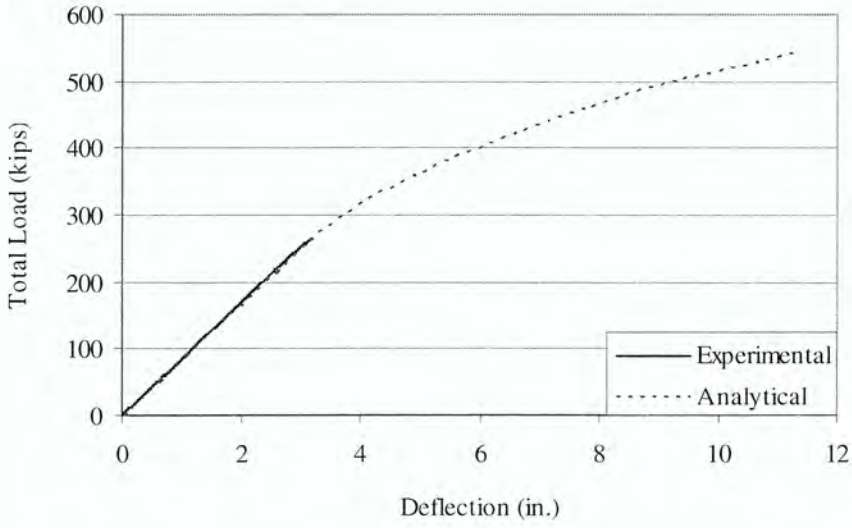

Figure 6.4. Deflection at midspan during large-scale flexure test.

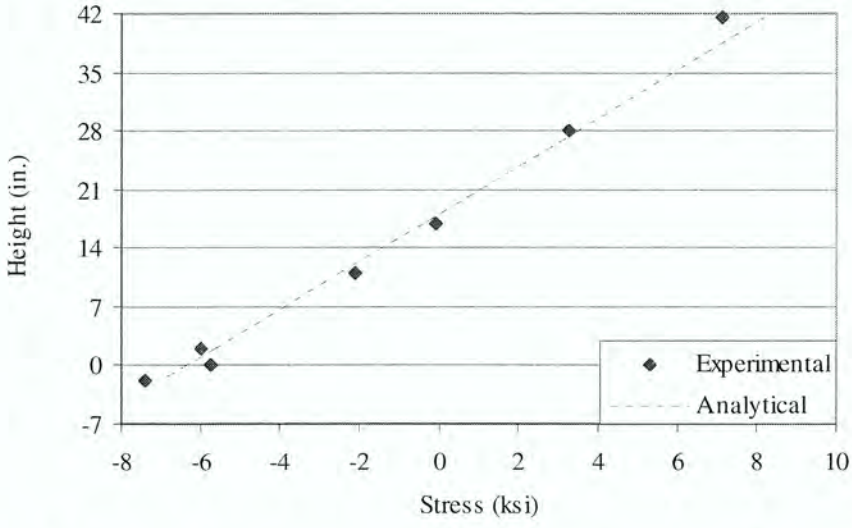

Figure 6.5. Longitudinal live load stresses at cracking of large-scale flexure test beam.

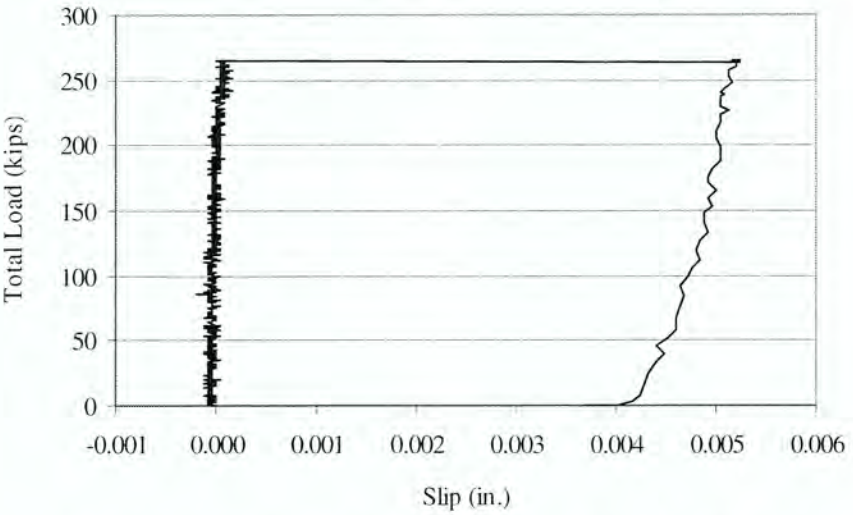

Figure 6.6. Strand slip at gage S1 during large-scale flexure test.

6.2.2 Shear Testing

6.2.2.1 Test Observations

Periodically throughout the test, the beam was inspected and cracks were marked. At a total load of 369.8 kips, shear cracking first occured in the end region of the beam. As shown in Fig. 6.7, crack #1 extended at an approximately 25 degree angle from the top of the web approximately one foot from the first applied load to the bottom of the web and approximately two feet away from the abutment. Using equation 5.9, the crack angle can be computed as 25.3 degrees at the bottom of the web and 23.3 degrees at the top of the web. As loading resumed several more inclined shear cracks developed. At a total load of 397.6 kips, flexural cracks occured under the east-most applied load, extending about 2 inches up from the bottom flange. This region was not cracked in the previous flexure test. At this time it was also observed that some, but not all, of the transverse cracks caused by the flexural test on May 11th had extended a short distance. Also, new longitudinal cracks were observed at the top of the bottom flange near the bottom of the web, possibly due to bursting of the concrete around the bottom flange strands.

When the beam failed at a total load of 594.0 kips, crack #2 not crack #1 was the most prominent within the failure region as shown in Fig. 6.7. After failure and additional subsequent loading crack #2 was about one inch wide. Crack #2 extended from the top of the web near the second applied load (L2) to the bottom of the web at the location of a lifting loop. This lifting loop is assumed to have shifted the failure critical region of the beam and to have added slightly to the ultimate load.

Additional unexpected cracking was found at the end of the beam. The beam was sitting on two independent neoprene pads that separated horizontally during the test. This may have caused half of the beam to move with each pad and created a vertical cracked plane from the bottom of the beam up to the harped strands as shown in Fig. 6.8. The additional diagonal cracks that can be seen on the side of the beam web did not occur until the beam was loaded well past failure.

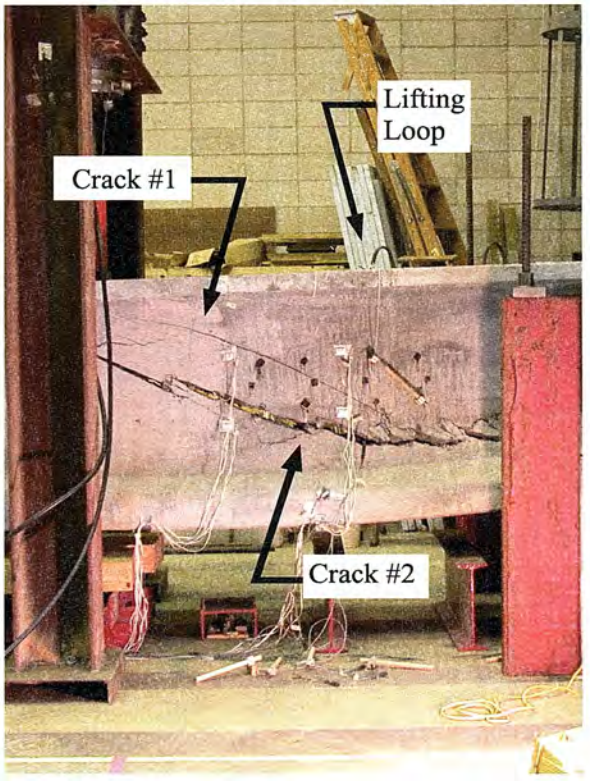

Figure 6.7. Shear crack at west end of large-scale shear test beam after failure.

Figure 6.8. Vertical crack in web at west end of large-scale shear test beam after failure.

6.2.2.2 Test Results

The primary purpose of the shear testing was to asses the shear behavior of UHPC in a full scale specimen and to collect data useful for the calibration of a prediction model that could be used as the basis for developing a shear design procedure. In addition, the shear strength of the beam was of interest to insure sufficient capacity of the UHPC girders designed for the Wapello County bridge. Applied total loads and shear loads are given in Table 6.4 at which three different events occurred: shear cracking, flexure cracking, and failure.

Table 6.4. Live load applied at three events during the large-scale shear test.

Event	Total Load (kips)	Shear Force (kips)
Shear Crack	369.8	306.5
Flexure Crack	397.6	329.5
Failure	594.0	492.0

The service and ultimate capacities of the test beams are determined as shown in Table 6.5 by including dead load and prestressing with the tested cracking and failure shear forces. The bridge beams are assumed to have the same capacities. As shown, the shear capacities are greater than the applied shear forces, making an acceptable design.

Table 6.5. Comparison of large-scale shear test capacities to applied bridge shears.

Limit State	Experimental Shear Capacity of Test Beam (kips)	Analytical Shear Capacity of Bridge Beam (kips)	Applied Shear on Bridge Beam (kips)
Service Level	312	312	210
Ultimate Level	497	497	301

The load at which shear cracking occurred is determined as the point when measured strains measured using a rosette are no longer linear as shown in Fig. 6.9. Gage "a" refers to horizontal strain, "b" to strain at a positive 45 degree angle and "c" to strain at a negative 45 degree angle. The load at flexural cracking was determined using the point of non-linearity in Fig. 6.10. Both the shear cracking and flexural cracking load levels corresponded to slight discontinuities in the deflection data, thus verifying the loads at cracking. The load at failure was simply determined as the maximum load applied during testing as shown in Fig. 6.11.

Figure 6.11 shows the analytical deflection calculated using the procedure described in section 5.2.1.2. The softening coefficients mentioned in Chapter 5 have been back-calculated as was previously discussed to best match the analytical and experimental deflections. Shear deformation accounts for 4% of the deflection in this instance. This procedure can be compared to that described in section 5.2.1.1 where the impact of shear on deflection is ignored resulting in the analysis shown in Fig. 6.12.

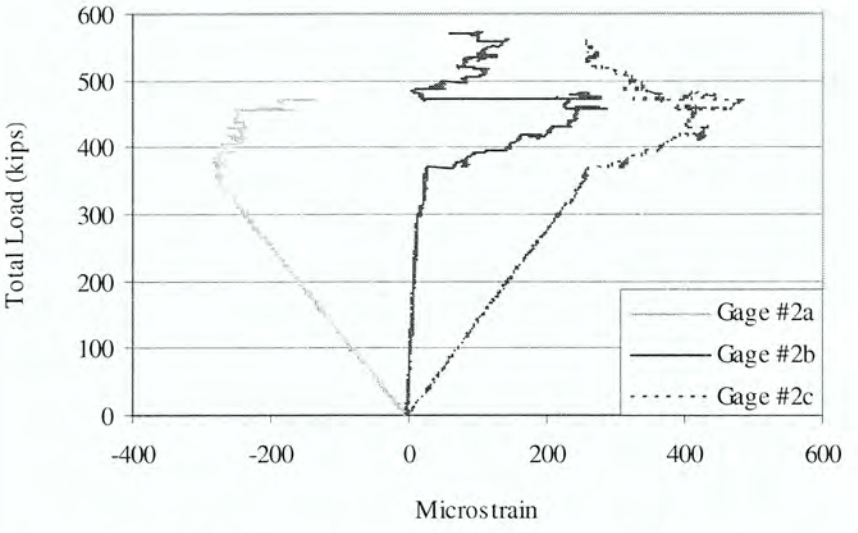

Figure 6.9. Strain at gage #2 during large-scale shear test.

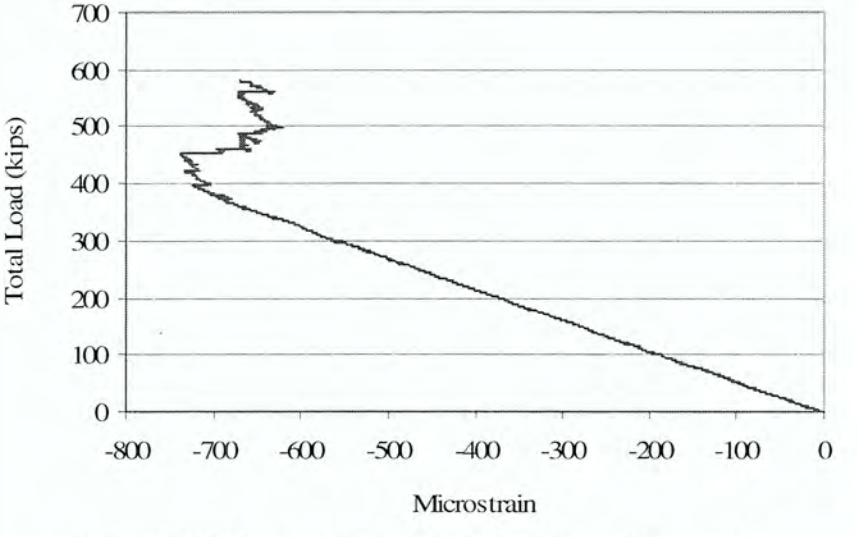

Figure 6.10. Strain at gage #10 during large-scale shear test.

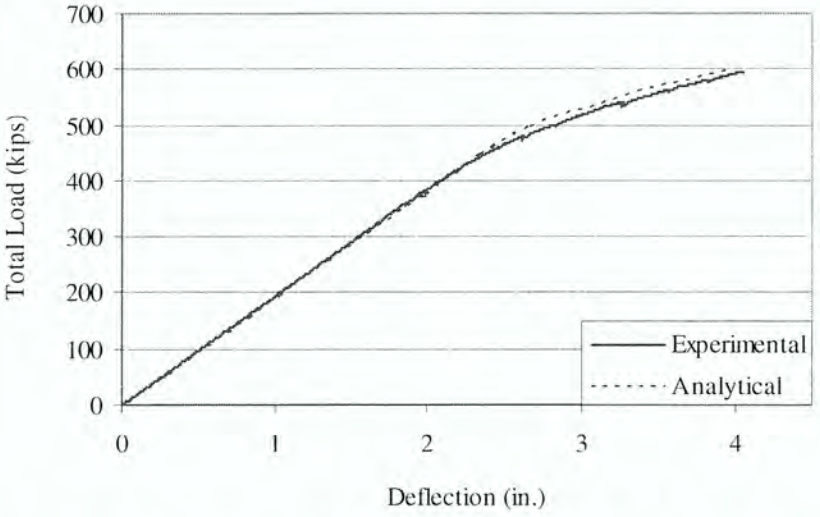

Figure 6.11. Deflection including shear analysis at gage D3 during large-scale shear test.

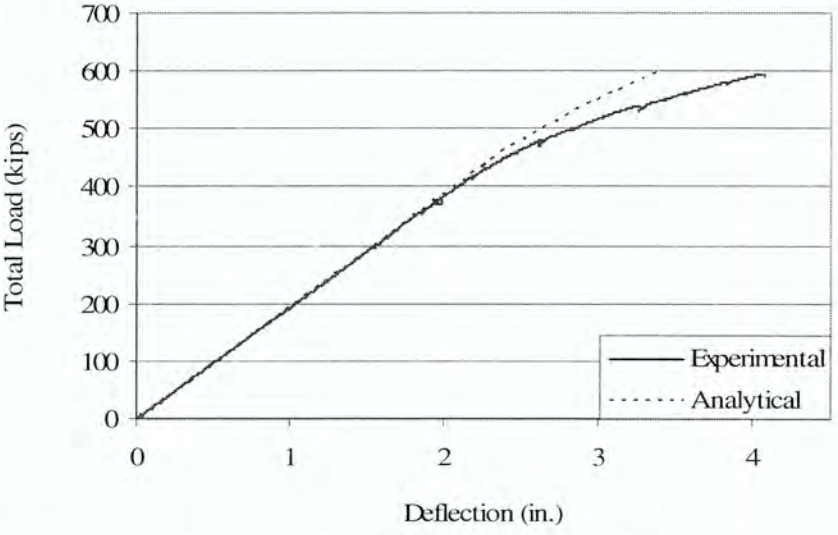

Figure 6.12. Deflection excluding shear analysis at gage D3 during large-scale shear test.

Analytical capacities were computed for comparison to experimental values. Following the procedure described in section 5.1.1, the service shear and flexural strengths were determined. The service shear strength was estimated as 303 kips while the corresponding measured value was 312 kips, showing that cracking could be accurately predicted. The flexural cracking was also accurately predicted at a total load of 405 kips as compared to the measured load of 397.6 kips. For the ultimate limit state, the failure mode was observed to be shear tensile failure of the UHPC web. At the experimental failure load, the principal tensile strain was determined analytically to be 0.00125.

Multiplying the principal tensile strain at failure by the crack spacing results in a crack width at failure. Further research should be conducted to accurately predict the crack spacing of UHPC under shear loading and to determine a crack width that will induce failure. During this research microcracks were observed at approximately two in. crack spacings. However, the crack spacing of localized cracks should be used. This value was not available during testing because essentially one primary localized crack formed. A secondary crack was observed but it is thought to have occurred due to the shifting of the primary crack which crossed a vertical prestressing strands used as a lifting loop.

Throughout the shear test strand slip was measured on three different strands. Slip did not occur on two of the strands. Some strand slip did occur in one of the three strands that were investigated as shown in Fig. 6.13. Other strands may have slipped as well.

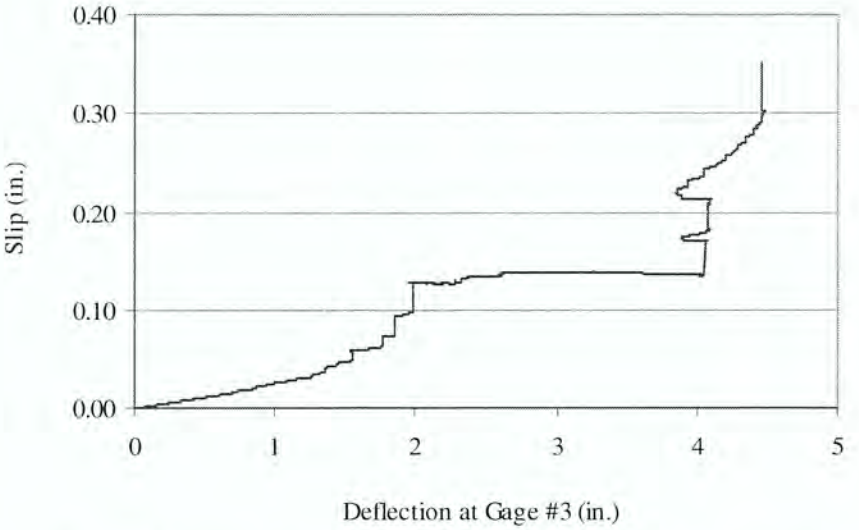

Figure 6.13. Strand slip at gage S3 during large-scale shear test.

The live load principal stresses in the beam could be calculated and compared to experimental data up to the point of shear cracking as shown in Fig. 6.14. After shear cracking, the experimental strain data are difficult to interpret due to discontinuities caused by shear cracking. All of the gages showed fairly good correlation between the analytical and experimental values showing that the elastic behavior of the beam was being captured. There is some discrepancy between the experimental and analytical values which could be caused by misalignment of the strain gage rosettes or by arching action in the end of the beam. The total principal stresses shown in Fig. 6.15 included prestressing,

dead load, and live load so that the results are no longer linear as with live load alone. The total principal stresses began to show discontinuos behavior after exceeding the shear cracking load of 369.8 kips. Generally, all the gages showed total principal stresses at the cracking stress of approximately -1.1 ksi as expected.

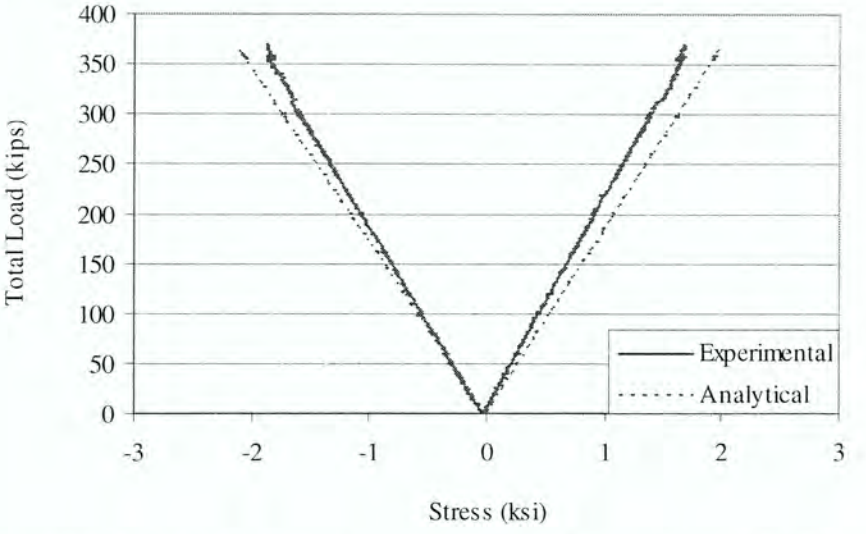

Figure 6.14. Live load principal stresses at gage #2 during large-scale shear test.

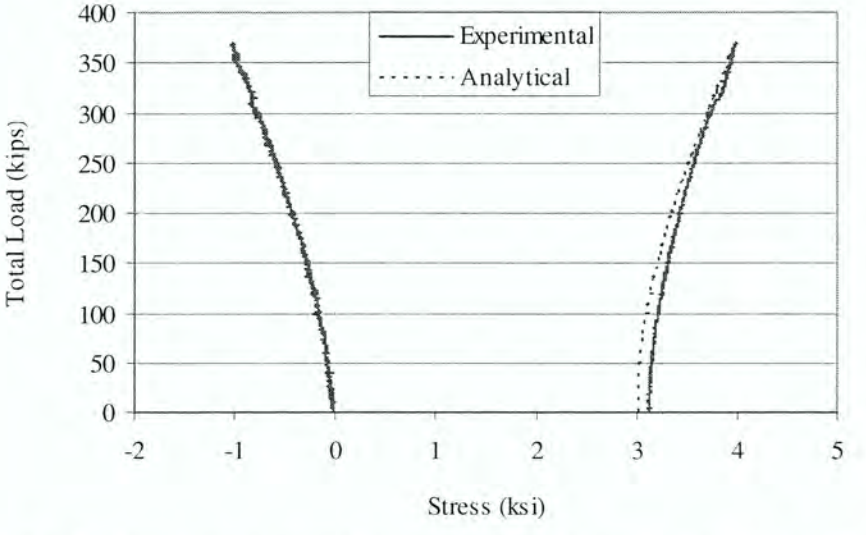

Figure 6.15. Total load principal stresses at gage #2 during large-scale shear test.

6.2.3 Flexure-Shear Testing

6.2.3.1 Test Observations

Periodically throughout the test, the beam was inspected and cracks were marked. The first cracks to be observed were flexural cracks occurring at a total load of 366.9 kips. These were vertical cracks located near load application point L2. No shear cracks were found in this region throughout testing. At this point and thereafter the beam could be heard to be cracking repeatedly.

As loading continued, shear cracking occurred at a total load of 481.8 kips. Diagonal shear cracks were found in the end region of the beam between the support and load point L4 as shown in Fig. 6.16. After additional loading, flexure cracks began to occur in this region. The shear cracks were seen to bend from the diagonal direction within the web toward the vertical direction within the bottom flange. During additional loading, longitudinal cracks near the original midspan of the flexure test were observed. Furthermore, a vertical-longitudinal splitting crack could be seen at the east end of the beam going through the center of the beam, where no strands were present. This crack was much smaller than a similar crack which occurred at the opposite end of the beam during the shear test shown in Fig. 6.8. Eventually, little additional load was being applied to the beam and the beam continued to deflect to a maximum of 8.5 in. at the easternmost load point when testing was ended at a total load of 658.1 kips.

Figure 6.16. Flexure and shear cracking near gage R1 at a total load of 482 kips during the large-scale flexure-shear test.

6.2.3.2 Test Results

The purpose of the flexure-shear testing was to determine the behavior of UHPC under combined flexure and shear loading. Loads are given in Table 6.6 at which three different events occurred: flexure cracking, shear cracking, and the maximum applied load which is determined to be near the failure load. The total load at flexure cracking is shown in Fig. 6.17 when the strain becomes non-linear. The total load due to shear cracking was determined at the point when strains have a discontinuity as shown in Fig. 6.18. The maximum applied load can be seen in Fig. 6.19.

Table 6.6. Live load applied at three events during the large-scale flexure-shear test.

Event	Total Load (kips)	Shear Force (kips)
Flexure Crack	366.9	226.1
Shear Crack	481.8	296.1
Maximum	658.1	404.2

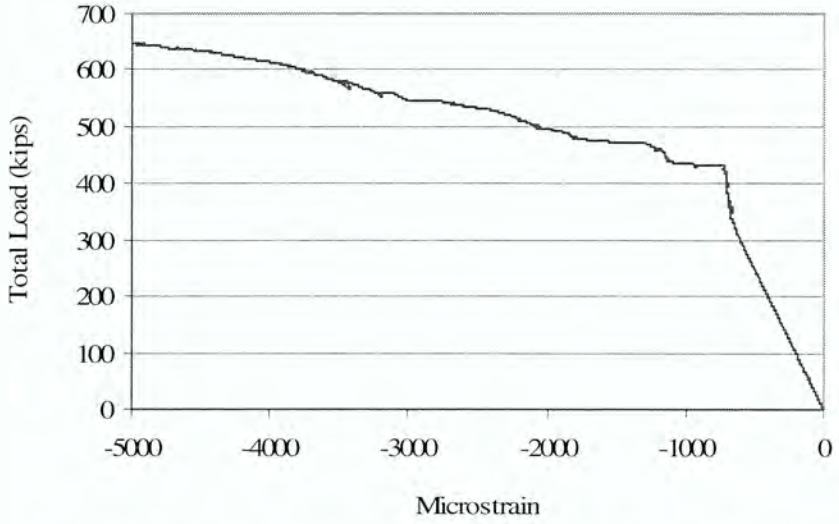

Figure 6.17. Strain at gage F5 during large-scale flexure-shear test.

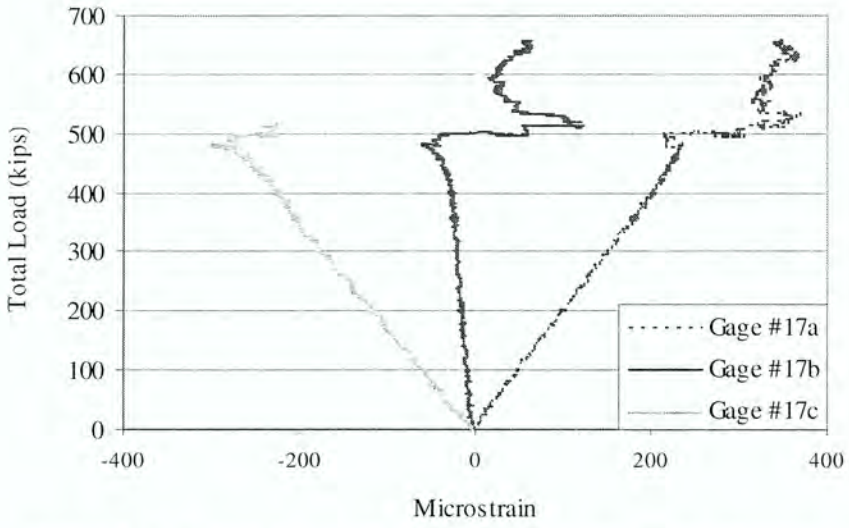

Figure 6.18. Strain at gage #17 during large-scale flexure-shear test.

The large scale flexure-shear test resulted in nearly maximizing the load that could safely be applied. No actual failure took place which is normally described by a drop in applied load. However, it appears by the flattening of the load vs. deflection curve that a load near failure was achieved although additional deflection would have occurred. The beam was analyzed using the procedure outlined in section 5.2.1.2. The maximum total load applied during the test was 658 kips with an analytically predicted failure load of 649 kips which corresponds to 404 kips and 399 kips of shear force respectively. In addition, the deflection values correlate well as shown in Fig. 6.19 where 4% of the deflection is due to shear deformation.

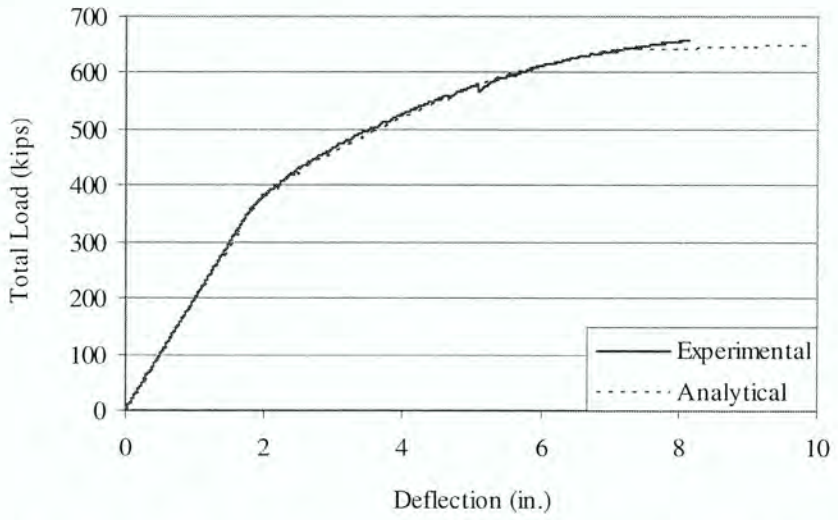

Figure 6.19. Deflection at gage D5 during large-scale flexure-shear test.

The live load principal stresses were measured within the web with a strain rosette and are shown in Fig. 6.20. The analytical and experimental results generally correlate. In general, the gages show that an approximate total principal stress of -1.1 ksi is reached at cracking within the failure region as shown in Fig. 6.21 at a total load of 481.8 kips. This agrees with the tested cracking strength reported for the material properties in section 2.2. Strand slip was measured at three strands at the end of the beam closest to the applied loads. No significant slip to these three strands was observed throughout the test.

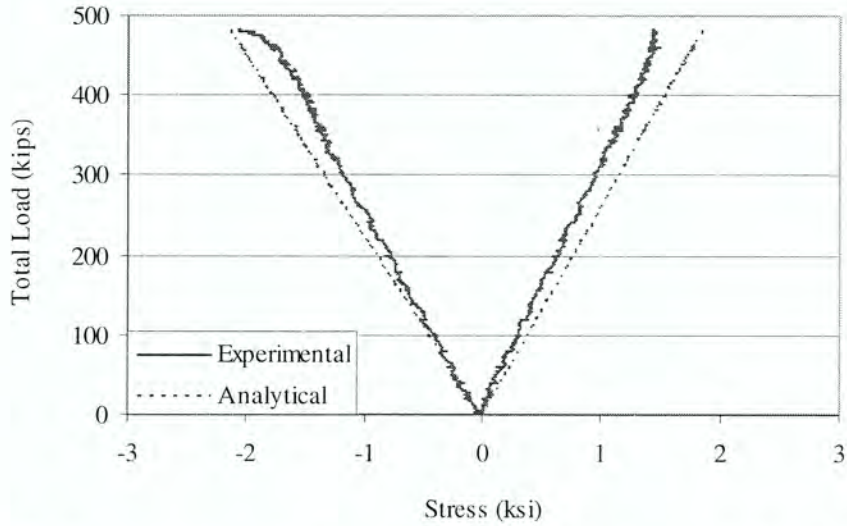

Figure 6.20. Live load principal stresses at gage #17 during large-scale flexure-shear test.

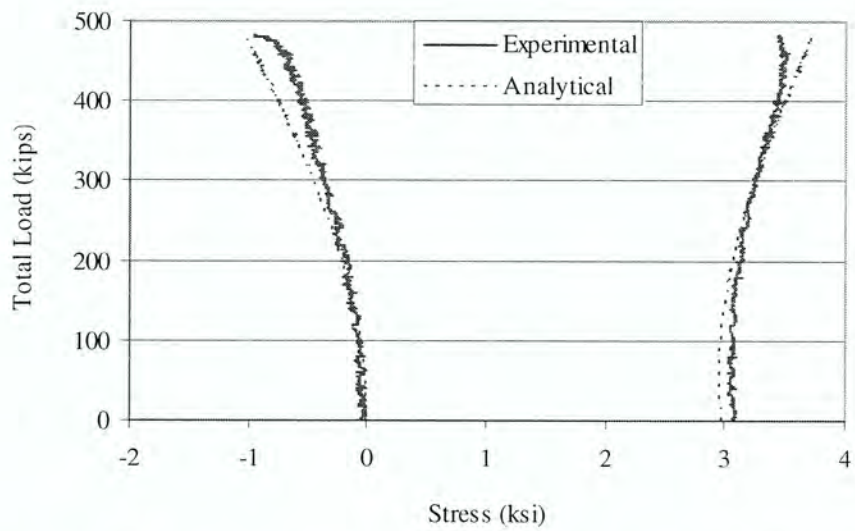

Figure 6.21. Total load principal stresses at gage #17 during large-scale flexure-shear test.

Using data from the shear test and the flexure-shear test, an idealized shear stress-strain relationship can be formulated. The idealized relationship is expressed mathematically in Chapter 5 as being linear until a stress of 2.3 ksi is reached, at which point the stress-strain relationship follows a parabolic relationship. Figure 6.22 shows data for two different tests, with the idealized relationship representing roughly an average of the two experimental data sets. This data was collected with the large wooden dowel strain gage rosettes shown in Figs. 4.11 and 4.16. These gages helped to overcome the effects of localized cracking because their gage lengths were 10 in. which is much longer than a typical strain rosette. However, the gages did fall off during testing when cracks were formed at the locations that the gages were glued to the beam. Drilling such gages into the beam would probably result in better data.

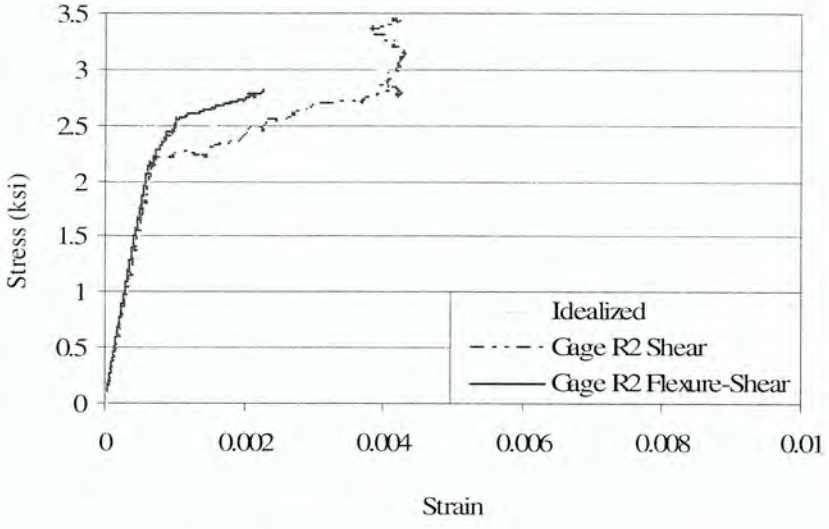

Figure 6.22. Shear constitutive properties of UHPC.

6.3 SMALL-SCALE LABORATORY TESTING

6.3.1 Test Observations

During testing of the small-scale beams observations were recorded throughout testing without pauses in the loading. In each of the beams cracking occurred either due to flexure or shear at a load level ranging from 47 kips to 82 kips as shown in Table 6.7. As loading continued to a peak load ranging from 116 kips to 164 kips as shown in Table 6.7, strand slip occurred in each of the beams and localized flexure or shear cracks formed.

The failure mode of the beams seemed to be that of a bond failure. It was apparent by instrumentation that the stands were slipping which eventually contributed to the beam failure. In addition, the localized cracking occurring during failure was dependent on the span lengths. Specifically, the longer spans showed localized flexural cracks in the bottom flange, while the shorter spans showed localized shear cracks in the web. These failures are listed in Table 6.8.

The B beams were tested first, being the most likely to fail in flexure with the larger web width and lower amount of reinforcement. The first beam to be tested, beam B1, had a long span length causing a flexural failure. For the next two beams B2 and B3 the span length was reduced, resulting in localized shear cracking. Next, for beam C1, the span length was increased, causing localized flexure and shear cracks to develop almost simultaneously. The beams C2, C3, A1, A2, A3, E1, E2, E3, D2, and D3 once again had the reduced span length resulting in localized shear cracking. The beam D1 had the same span but resulted in localized flexural cracking. Photographs of each of the failed beams are shown in Fig. 6.23. The flexure cracks and shear cracks are shown, with the shear cracks possibly occurring on either end of the beam. Straight vertical lines have been marked on the beams indicating where the load was applied or where the support was located.

In all of the beams strands slip could be visually observed on both sides of the beam. In the case of beams A2, A3, and D2, strand slip caused shear failure on the opposite side of the beam than was expected. The expectation was to see this occur on the side of the beam with its support closest to the applied load. Instead, the strand slip and shear failure occurred on the side of the beam with its support furthest from the applied load. With the occurrence of strand slip causing some concern, beam B1 was dismantled to examine the strands. The inspection of beam B1 showed that one of the seven wires of one strand was fractured as shown in Fig. 6.23.e.

Table 6.7. Live load and shear force applied at cracking and failure of the small-scale test beams.

Beam	Total Cracking Load (k)	Cracking Shear (k)	Total Failure Load (k)	Failure Shear (k)
A1	60.7	33.1	145.4	79.3
A2	70.8	38.6	156.9	85.6
A3	82.0	44.7	139.5	76.1
B1	47.4	26.8	116.6	65.9
B2	60.1	32.8	146.9	80.1
B3	61.8	33.7	153.6	83.8
C1	53.8	28.5	154.5	81.8
C2	51.5	28.1	149.4	81.5
C3	56.1	30.6	152.9	83.4
D1	70.0	38.2	164.3	89.6
D2	66.0	36.0	159.1	86.8
D3	46.0	25.1	152.5	83.2
E1	60.9	33.2	150.0	81.8
E2	41.8	22.8	118.4	64.6
E3	49.7	27.1	142.3	77.6

Table 6.8. Failure modes of small-scale test beams.

Beam	Failure Mode
A1	Bond / Shear
A2	Bond / Shear (Long Side)
A3	Bond / Shear (Long Side)
B1	Bond / Flexure
B2	Bond / Shear
B3	Bond / Shear
C1	Bond / Flexure-Shear
C2	Bond / Shear
C3	Bond / Shear
D1	Bond / Flexure
D2	Bond / Shear (Long Side)
D3	Bond / Shear
E1	Bond / Shear
E2	Bond / Shear
E3	Bond Shear

a. Beam A1.

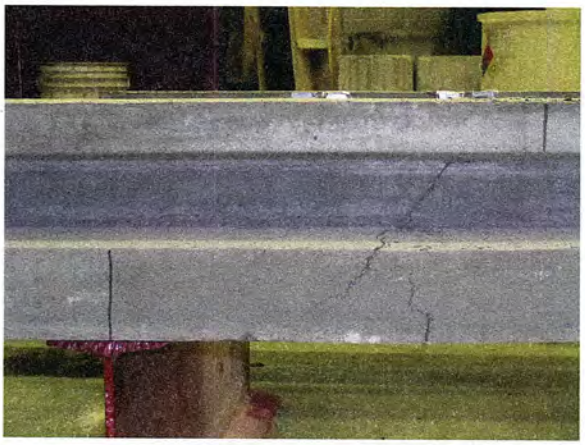

b. Beam A2.

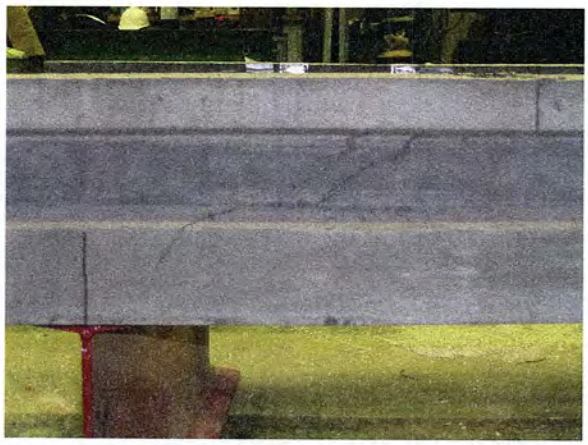

c. Beam A3.

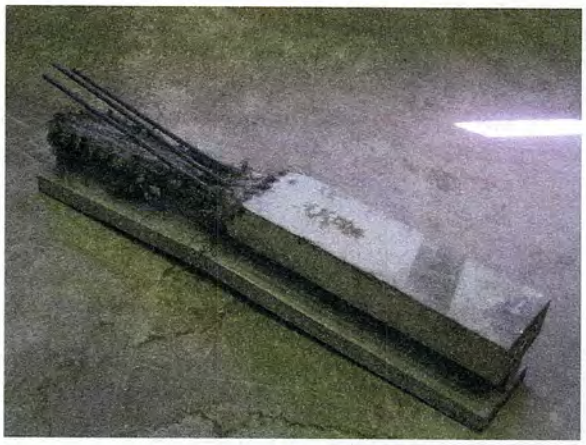

d. Beam B1 overall.

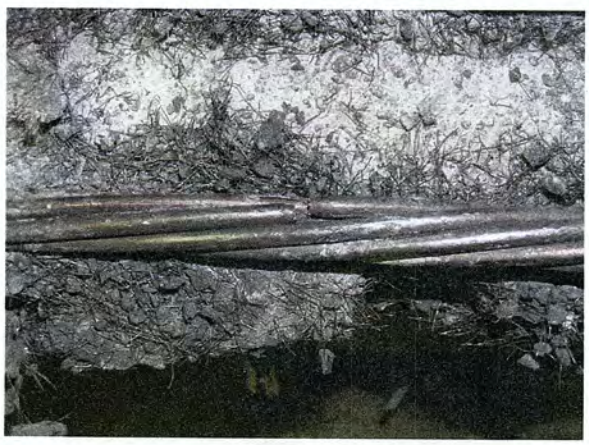

e. Beam B1 strand.

f. Beam B2.

Figure 6.23. Cracking of small-scale test beams after failure.

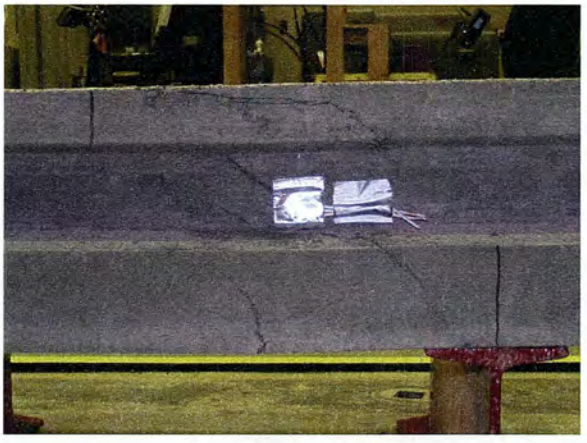

g. Beam B3.

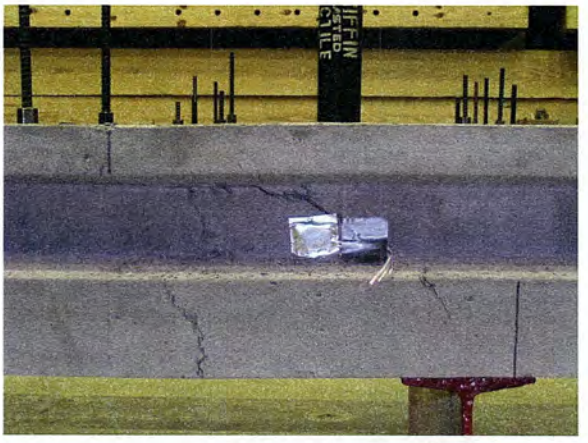

h. Beam C1.

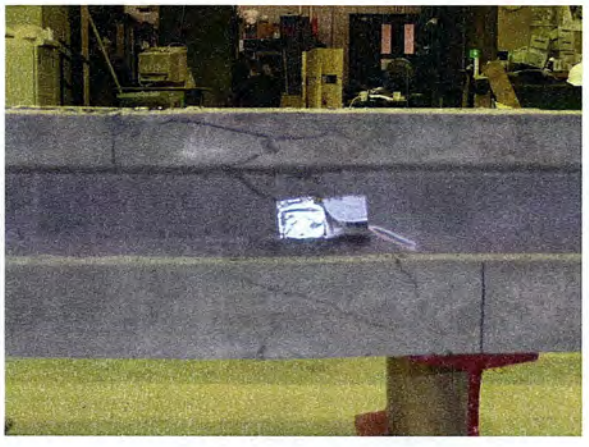

i. Beam C2.

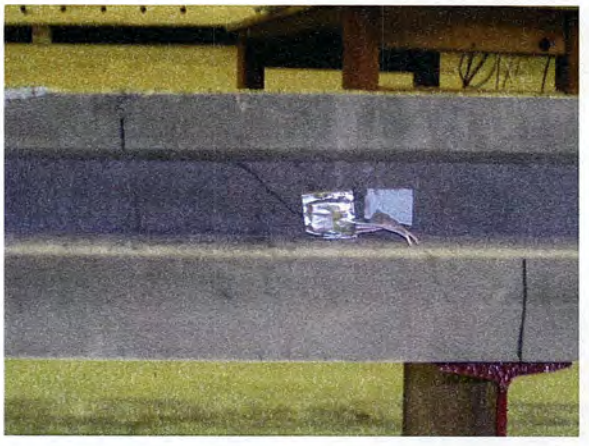

j. Beam C3.

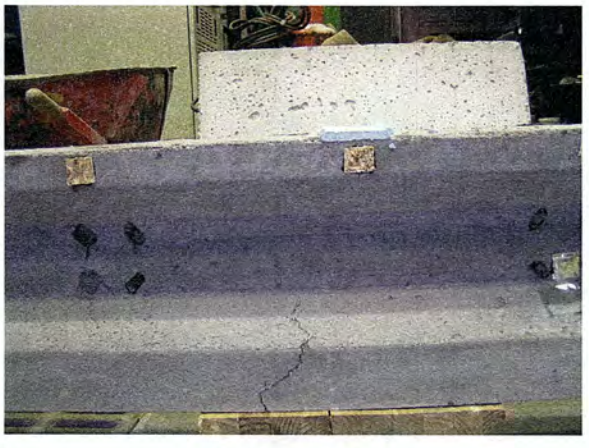

k. Beam D1.

l. Beam D2.

Figure 6.23. Cracking of small-scale test beams after failure (continued).

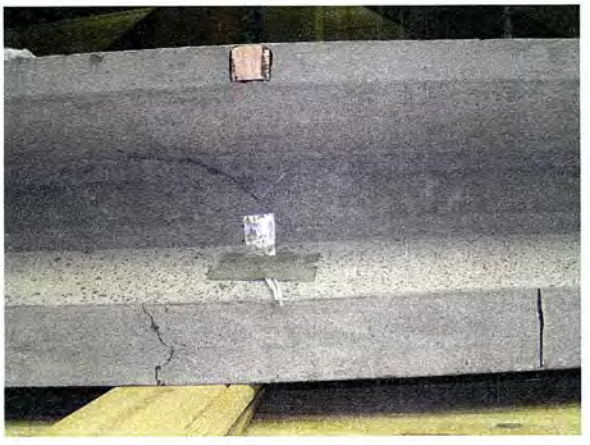

m. Beam D3.

n. Beam E1.

o. Beam E2.

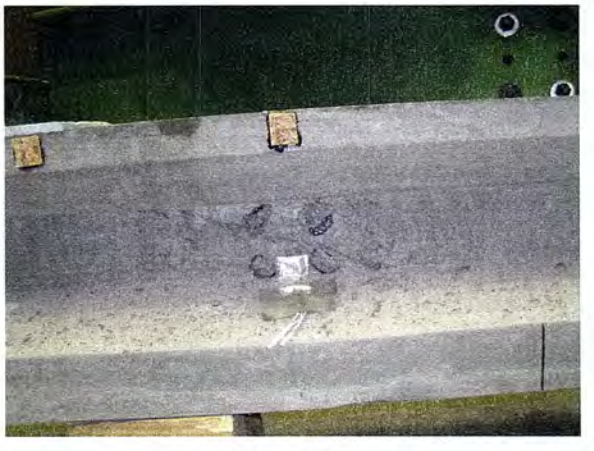

p. Beam E3.

Figure 6.23. Cracking of small-scale test beams after failure (continued).

6.3.2 Test Results

The small-scale testing did not provide extensive information about the shear behavior of UHPC. The failures that occurred in the beams were not generally considered to be a pure shear failure. Instead bond failure was quite predominant. The bond failure mode was unexpected as previous research [13] had indicated significantly higher bond strength than was found in this study. Additionally, because of arching action, the shear capacity was larger than expected. Arching action occurs in short spans where a compression strut develops between the load application and the support. This is different than the load being carried by traditional beam theory shear and moment forces. Due to the use of short spans, some of the sectional analysis described in Chapter 5 is less applicable in the regions close to concentrated loads according to St. Venant's principle. In the case

of the small-scale beams, these regions end up encompassing nearly the entire beam. However, information about the deflection and stresses are still interesting and are described herein.

Analytical cracking loads were calculated as shown in Table 6.9 using the previously described procedure from section 5.1.1. The calculated load at cracking was consistently underestimated due to arching action caused by the short span to depth ratio. Analytical failure loads were also predicted using the strut and tie model described in sections 2.3, 5.2.3 and A.3. This analysis indicated a total failure load of 205 kips for beam section A and 135 kips for beam sections B, C, D, and E as shown in Table 6.9. The analysis was based on the failure of the tension tie, because the strut and tie model showed that the concrete would not fail in compression. Therefore, sections with similar span to depth ratios and amount of reinforcement had similar calculated total failure loads. The strut and tie model does not address the prediction of when the strut will split which did occur in some tests. The strut and tie model instead prescribes a certain amount of reinforcement to ensure that the strut will not split. Therefore it is difficult to produce an accurate analysis based on the splitting of the tie or on the bond failure of the strand which is not addressed by the strut and tie method.

Table 6.9. Comparison of experimental and analytical live loads required to cause cracking and failure of the small-scale test beams.

Beam	Total Cracking Load (k)	Error (%)	Total Failure Load (k)	Error (%)
A1	39.0	36	205.0	41
A2	39.0	45	205.0	31
A3	39.0	52	205.0	47
B1	-	-	-	-
B2	40.5	33	135.0	8
B3	40.5	34	135.0	12
C1	34.0	37	135.0	13
C2	33.3	35	135.0	10
C3	33.3	41	135.0	12
D1	34.6	51	135.0	18
D2	34.6	48	135.0	15
D3	34.6	25	135.0	11
E1	32.1	47	135.0	10
E2	32.1	23	135.0	14
E3	32.1	35	135.0	5

General results of the small-scale beam testing will be illustrated with beam C2 which is used to represent all beams. The deflection of the beam can be seen in Fig. 6.24 with the analytical deflection calculated using section 5.2.2. It is interesting to note that for this specimen the shear deflection accounts for about 60% of the total deflection. The calculated deflection is lower than the

experimental values due, in part, to support settlement. Also it was found that measuring the deflection on the bottom of the beam resulted in larger deflections than if measured on the top of the beam due to vertical strain. These problems were corrected in the twelve inch beams. In addition, slip of the strands may have resulted in larger deflections than expected.

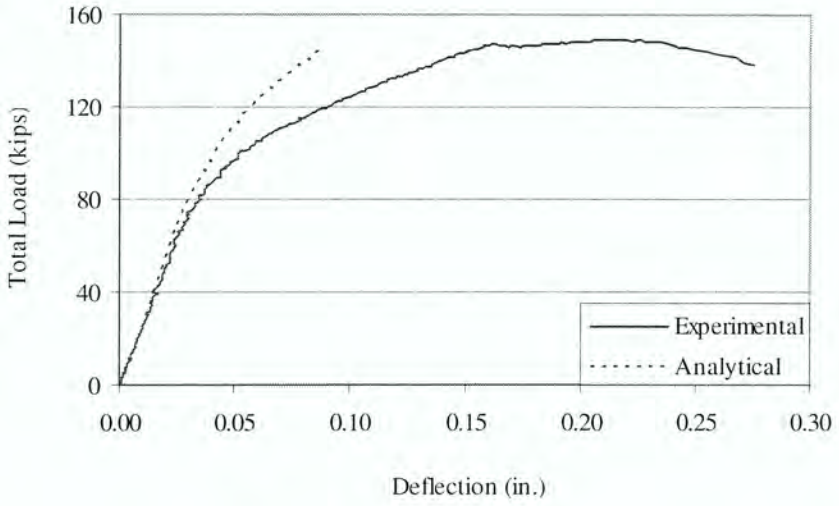

Figure 6.24. Deflection at gage D1 of small-scale test beam C2.

Analytical and experimental stresses within the beams can be compared as shown in Fig. 6.25. Without any experimental data for the release stresses, the experimental release stresses at zero load are equated to the analytical stresses. Since the beam is on a short span, arching action is taking place causing less tensile stress than predicted.

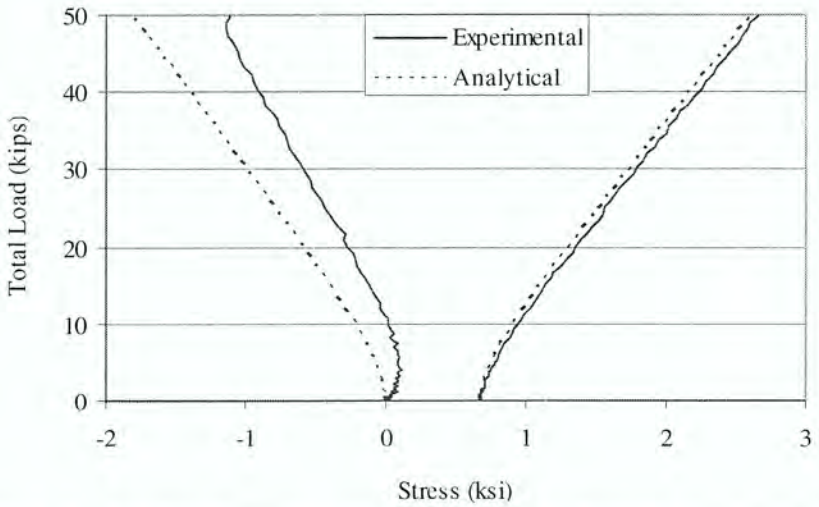

Figure 6.25. Total load principal stresses at gage #7 of small-scale test beam C2.

After observing that some of the deflection results could not accurately be predicted for the ten inch beams, deflections were measured from the compression flange instead of the tension flange and support settlement was measured in the twelve inch beams. Beam E1 will be used to represent the twelve inch beams. As shown in Fig. 6.26, the deflection at gage D3 was closely predicted as was gage D1 both located near the quarter spans of the beam. However, the deflection at gage D2 located at the load application is even further off than with the ten inch beams as shown in Fig. 6.27. The cause of this difference is not well understood. Analytical deflections were once again calculated following the procedure described in section 5.2.2. Stresses were again found to compare similarly as with the ten inch beams. The tensile stresses were again overestimated analytically.

Typical strand slip for all the beams is shown in Fig. 6.28 and 6.29 at one end of the beam. Slip at the opposite end of beam E1 was much smaller, up to about 0.007 in. which is also typical for the other beams. A spike as shown in Fig. 6.28 occurred in all the strand slips of all the beams at the point when the beam behavior becomes non-linear. The large amount of strand slip shown in Fig. 6.29 is beginning to occur at the maximum applied load. The large amounts of strand slip are occurring after the maximum load has been applied.

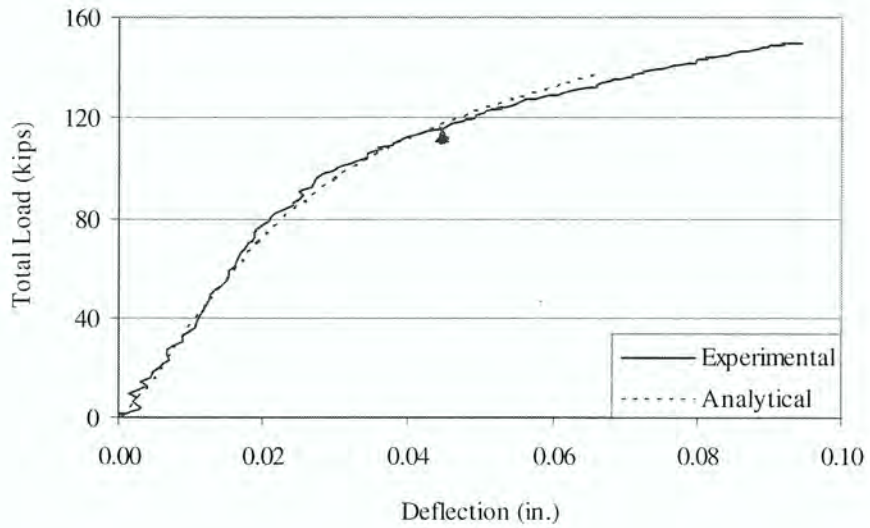

Figure 6.26. Deflection at gage D3 of small-scale test beam E1.

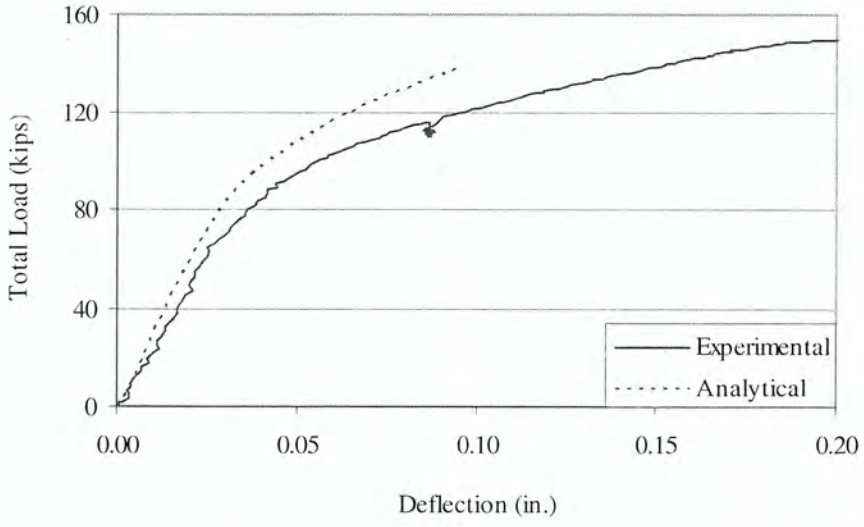

Figure 6.27. Deflection at gage D2 of small-scale test beam E1.

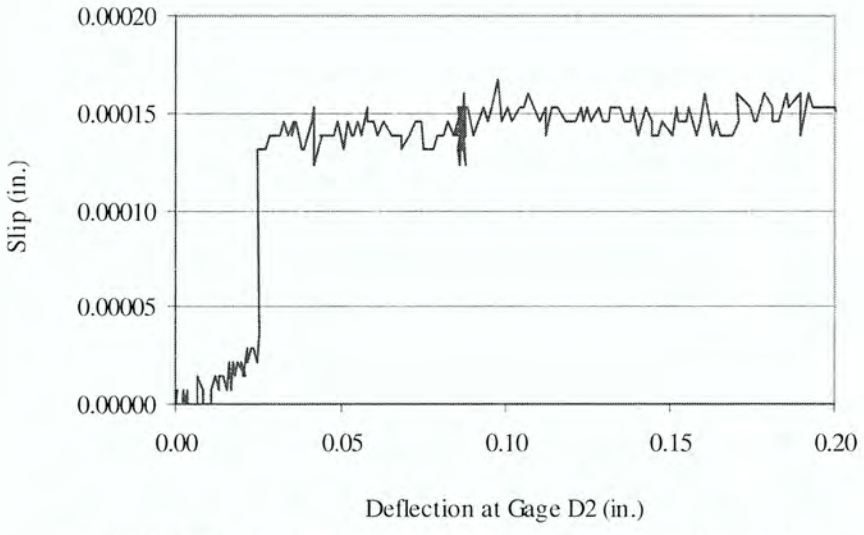

Figure 6.28. Strand slip at gage S1 of small-scale test beam E1.

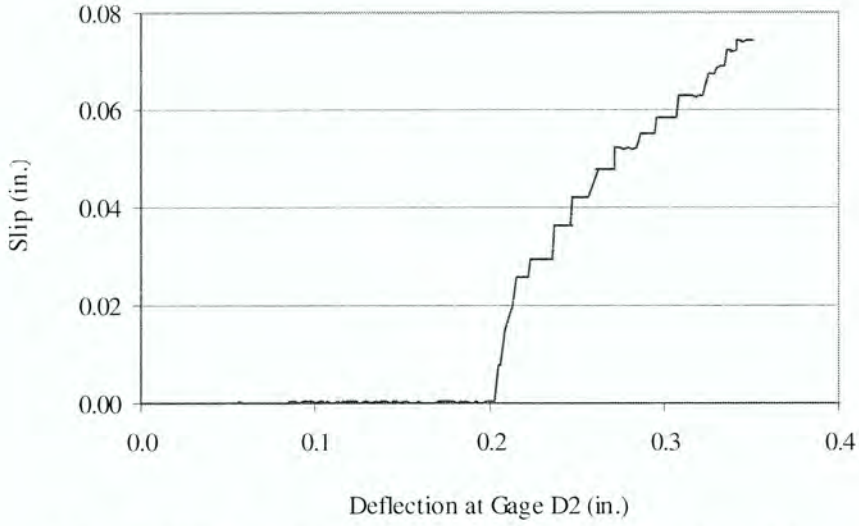

Figure 6.29. Strand slip at gage S3 of small-scale test beam E1.

6.4 FIELD TESTING

6.4.1 Release Testing

During strand release of the test beam and one bridge beam the strain in the fiber optic strain gages were monitored. Figure 6.30 shows the change in strain with time for the test beam. Pauses can be seen as the strain remains constant when no strands were being cut. The total change in strain can be related to the initial release stress assuming a constant temperature without shrinkage or creep.

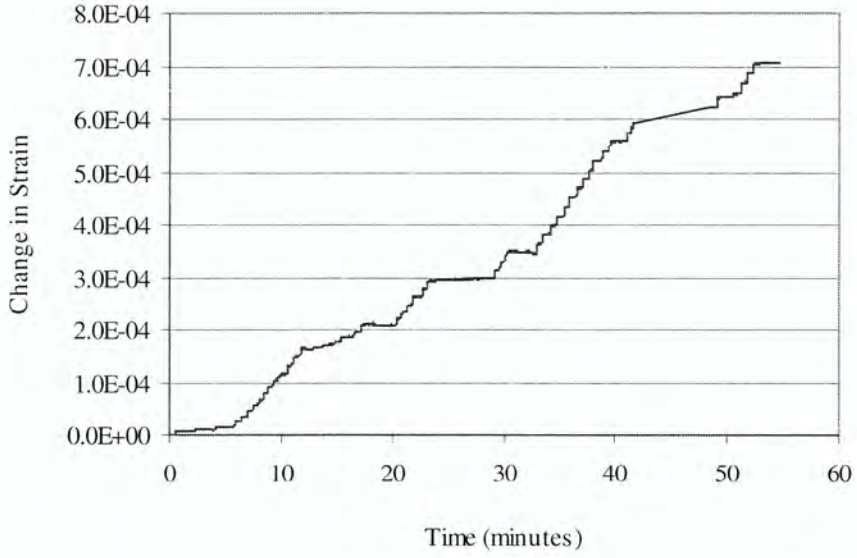

Figure 6.30. Strains at gage F3 of large-scale test beam during strand release.

The initial experimental and analytical release stresses are shown in Tables 6.10 and 6.11. The table compares the experimental and analytical results using the initial prestress force instead of the final prestress force. These results are based on the UHPC having an initial elastic modulus of 5700 ksi and an 1484 kips of estimated prestress after losses. Notice that the analytical stresses overestimate the experimental release stresses. This was expected because the initial prestress force assumes that the strands were released instantaneously without elastic shortening losses. Final release stresses are also shown in Tables 6.10 and 6.11. These stresses are more difficult to decipher from the experimental data. The difficulty was caused because the strains were becoming more compressive due to shrinkage and creep while the stresses were becoming less compressive due to loss of prestress. Final release stresses were not recorded for the bridge beam until after deck rebar was placed which changed the strain readings due to the additional load.

Table 6.10. Stresses in large-scale test beam after strand release.

a. Initial stresses

Gage	Experimental (ksi)	Analytical (ksi)
F1	3.87	5.57
F2	4.50	5.57
F3	4.43	5.60
F4	4.02	5.72
F5	4.32	5.60

b. Final stresses

Gage	Experimental (ksi)	Analytical (ksi)
F1	---	4.66
F2	2.03	4.64
F3	4.61	4.65
F4	5.73	4.72
F5	0.93	4.65

Table 6.11. Stresses in bridge beam after strand release.

a. Initial stresses

Gage	Experimental (ksi)	Analytical (ksi)
F1	---	---
F2	3.78	5.03
F3	1.99	1.52
F4	3.52	5.05
F5	3.75	5.03

b. Final stresses

Gage	Experimental (ksi)	Analytical (ksi)
F1	---	---
F2	---	4.11
F3	---	1.57
F4	---	4.07
F5	---	4.11

6.4.2 Dead Load Testing

Fiber optic instrumentation was monitored during the deck placement of the Wappello County bridge. The purpose of the monitoring was to insure that the dead load stresses acting on the bridge matched analytical design values. Gage F5 at the quarter span had a reading taken at the beginning and end of the placement which will show the total change in strain. Gages F3 and F4 at the midspan had continuous readings throughout the deck pour. It was evident that as concrete was pumped onto the

bridge, the strain readings increased. Figure 6.31 shows the recorded strains. It can be seen that the strains had a reversal of sign assumed to be due to temperature change at the bridge site. The total change in strain was related to the dead load stress created by the deck placement when corrections are made for the change in temperature.

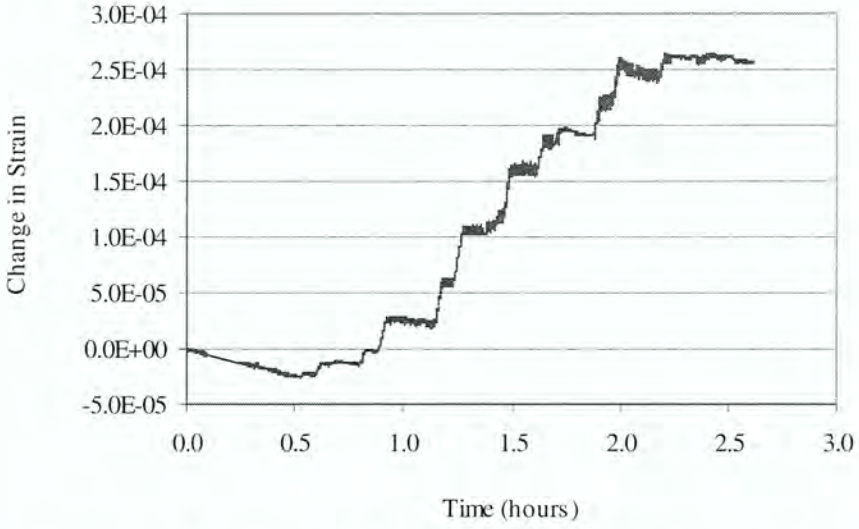

Figure 6.31. Strains at gage F3 of bridge beam during deck pour.

Dead load stress values can be easily estimated using the load applied on the bridge beam from the wet deck concrete. The beam monitored was an exterior beam. Assuming that half of the slab width between beams was applied to the exterior beam, changes in stresses of 2.77 ksi, -1.97 ksi, and -1.50 ksi for gages F3, F4 and F5 respectively were determined.

The fiber optic instrumentation indicated that tension was occurring in the top of the beam during the early stages of the deck pour. This is not logical for tension to occur in the top of a simply supported beam under positive moment. It was noted that during the pour, the temperature rose by about 15 degrees Fahrenheit. This rise in temperature likely caused the strain in the fiber optic gages to change and accounts for the stress reversal.

The temperature corrected stress readings can be seen in Figs. 6.32 and 6.33. The figures were corrected using the assumption that the temperature changed linearly with time. The stress reversal is nearly eliminated and the magnitudes of the stresses generally matched the analytical values.

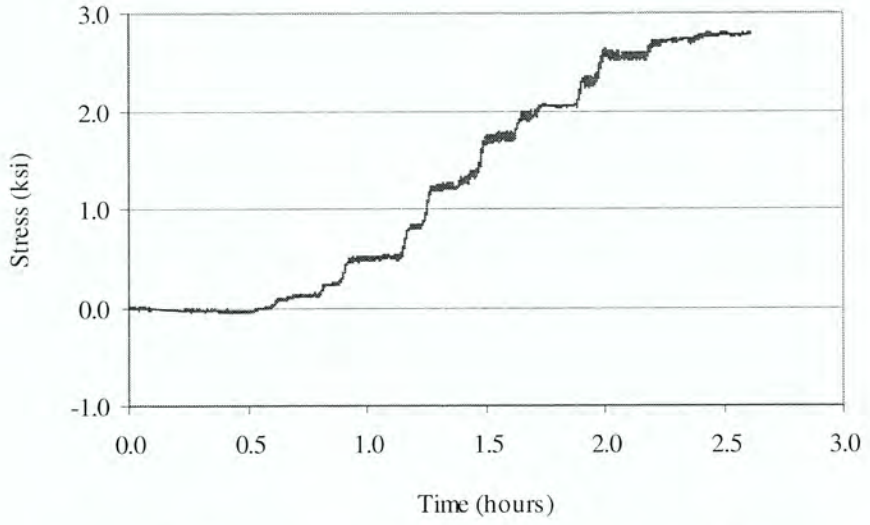

Figure 6.32. Stresses at gage F3 of bridge beam during deck pour.

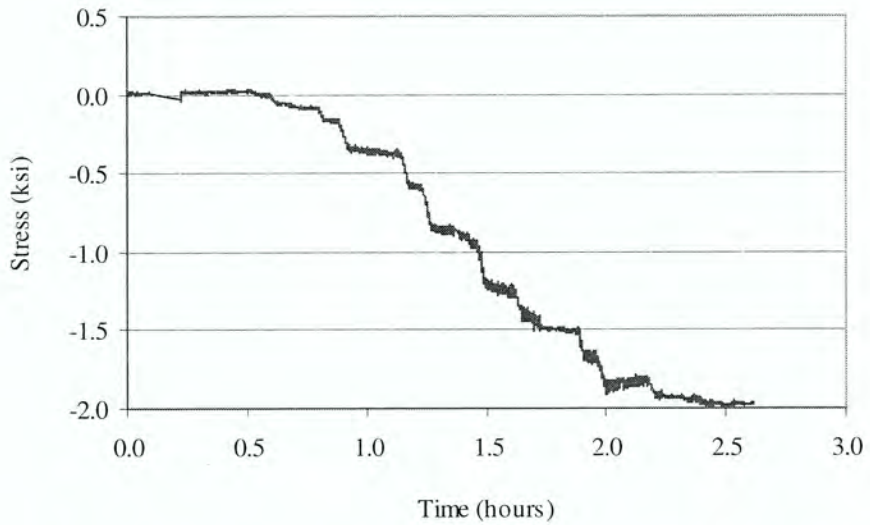

Figure 6.33. Stresses at gage F4 of bridge beam during deck pour.

6.4.3 Live Load Testing

Live load testing of the Wappello County UHPC bridge should be conducted in the future by Iowa State University and the Center for Transportation Research and Education.

CHAPTER 7: RECCOMMENDED SHEAR DESIGN PROCEDURE

Recommendations will be made for the design of UHPC components in shear for both the service limit state and the ultimate limit state. These recommendations make use of some of the current AASHTO [15] code provisions for bridge design.

7.1 SERVICE LIMIT STATE

The recommended service limit state design procedure is based upon a mechanics of materials, linear stress analysis. The design is carried out to ensure that the principal tensile stress at any location within a component due to service loading is smaller in magnitude than the material's cracking tensile strength. The procedure has been compared to structural testing to ensure conservatism. A design example following this procedure is given in section A.2.

7.1.1 Procedure Description

The recommended service limit state design procedure is a sectional approach. At any location within a member, the following equations 7.1 to 7.3 describe the applied stresses. Equation 7.4 should hold true for all locations within a member. Some judgement can be used to determine a few discrete points for completing calculations. The following guidelines can be used in the case of traditional prestressed beam shapes. The stresses should be checked near the centroid of the section. Also, if positive moment is being applied to the beam, stresses should be checked at the bottom of the web. If negative moment is being applied, stresses should be checked at the top of the web.

$$\sigma_x = \frac{P_f}{A} + \frac{P_f \cdot e \cdot c}{I} + \frac{M_t \cdot c_t}{I_t} + \frac{M_c \cdot c_c}{I_c} \qquad \text{longitudinal stress (ksi)} \qquad (7.1)$$

Where: P_f = prestressing force final (kips)

A = gross cross-sectional area (in.^{2})

e = eccentricity of axial force (in.)

c = distance from centroid (in.)

c_t = distance from transformed centroid (in.)

c_c = distance from composite centroid (in.)

I = moment of inertia (in.^{4})

I_t = transformed moment of inertia (in.^{4})

I_c = composite moment of inertia (in.^{4})

M_t = moment applied to transformed section (in.- kips)

M_c = moment applied to composite section (in.- kips)

$$\tau_{xy} = \frac{V_t \cdot Q_t}{I_t \cdot b} + \frac{V_c \cdot Q_c}{I_c \cdot b} \quad \text{shear stress in the x-y plane (ksi)} \tag{7.2}$$

Where: V_t = shear applied to transformed section (kips)

V_c = shear applied to composite section (kips)

Q_t = transformed second moment of area (in.^{3})

Q_c = composite second moment of area (in.^{3})

b = width of section (in)

$$\sigma_{p1} = \frac{\sigma_x}{2} - \sqrt{\left(\frac{\sigma_x}{2}\right)^2 + \tau_{xy}^{\ 2}} \quad \text{principal tensile stress (ksi)} \tag{7.3}$$

$$f_{cr} < \sigma_{p1} \quad \text{cracking tensile strength of concrete (ksi)} \tag{7.4}$$

This procedure should be repeated at several sections along the length of the beam with the associated and appropriate shear and moment conditions. The first section for this procedure to be applied is half the beam height away from the support. Other sections should be spaced close enough so that a crack cannot occur between locations. Assuming that the crack angle is conservatively 45 degrees, the locations can be spaced at the height of the beam. For each of these sections, if using the HS-20 design truck specified by AASHTO [15], place the heaviest wheel load at the predetermined location with the remaining wheel loads positioned away from the support as shown in Figure 7.1.

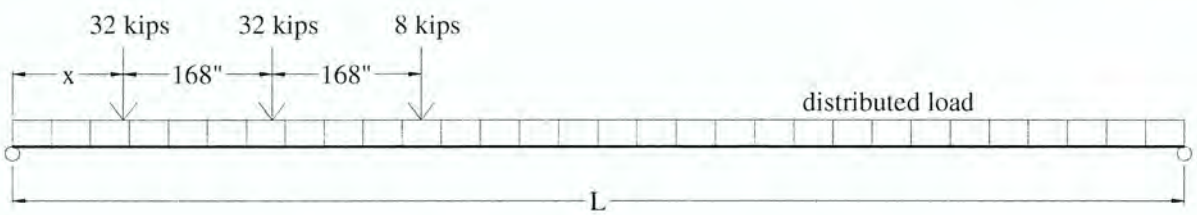

Figure 7.1. Bridge loading required by AASHTO.

7.1.2 Conservatism of Procedure

In order to demonstrate the conservatism of the recommended shear design procedure, analytical results will be compared with experimental results. The procedure that has been outlined is somewhat limited in that it is difficult to predict the actual load that will cause cracking in an experiment. Instead, based on a given load, the procedure will determine the stress caused and whether that stress is above or below the cracking stress. Therefore, the experimental cracking load is used to find an analytical stress at that load. This has been carried out for each of the experiments with the resulting analytical stresses shown in Table 7.1. This table shows that the procedure calculates an analytical stress at the point of experimental cracking that is above the material strength of 1.1 ksi for all cases.

Table 7.1. Analytical cracking stress calculated at experimental cracking load for all beam tests.

Beam	Principal Stress (ksi)
Shear	-1.21
Flexure-Shear	-1.44
A1	-2.01
A2	-2.39
A3	-2.82
B1	-1.54
B2	-1.95
B3	-2.02
C1	-1.91
C2	-1.88
C3	-2.08
D1	-2.13
D2	-1.99
D3	-1.30
E1	-2.15
E2	-1.38
E3	-1.70

7.2 ULTIMATE LIMIT STATE

The recommended ultimate limit state design procedure is based on the Modified Compression Field Theory (MCFT). This theory has been emplyed for use with UHPC. When using this procedure with UHPC, the substantion tensile capacity of UHPC after cracking should be incorporated in the analysis. This is normally disregarded with conventional concrete. Simplifications have been adopted in order to eliminate the need for solution iteration. In addition, using empirical data, high bounds have been placed on the nominal shear strength. This procedure has been demonstrated to be

conservative by comparison with structural testing. A design example has also been provided in section A.2.

7.2.1 Procedure Description

The nominal shear strength can be determined assuming that the maximum tensile stress of UHPC is applied across a failure surface inclined at an angle over the height of the moment arm. This stress distribution is illustrated in Fig. 7.2 and described in equation 7.5. Assuming that for shear design, the section properties have already been selected, the only unknown in equation 7.5 is the angle θ. (Note that the lever arm percentage of depth can be found from a moment analysis.) The variable θ can be thought of as the minimum angle that results in the longitudinal strain, described by equation 7.9, being more compressive than the allowable longitudinal strain. As discussed in Chapter 5, the longitudinal strain can be determined along the section height through iteration. In order to simplify the procedure, a closed form formula will be used to estimate the longitudinal strain at only one location along the section height. Since longitudinal tension causes a decrease in shear capacity, it is conservative to use a large tensile strain at the level of the bottom reinforcement. The forces shown applied to the sections are illustrated in Fig. 7.3. Collins [11] described a similar equation to 7.9 for the longitudinal strain but it does not including the tensile capacity present with UHPC. The term F_{bf} shown in equation 7.7 and 7.8 has been added to the basic MCFT because for UHPC tensile stresses are retained within the cracked concrete. Testing has illustrated that the tensile stresses stay nearly constant at a level equal to the cracking strength within the section of the beam that is below the neutral axis when loading beyond cracking has been applied. The neutral axis can be conservatively estimated to be at the centroid of the section after cracking although it will actually rise at higher load levels. Therefore, the area over which the tensile stress acts can be determined as in equation 7.6. The area varies linearly dependant on the applied moment. The area is conservatively assumed to be zero at an applied moment equal to the cracking moment and it increases to the area below the centroid of the section at an applied moment equal to the nominal moment strength of the section. The allowable longitudinal strain ε_{xa} is described in equation 7.10.

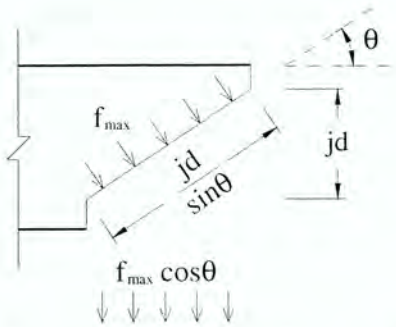

Figure 7.2. Tensile stresses within a general beam at the ultimate loading condition according to the MCFT.

$$V_{n1} = \left| f_{\max} \cdot b_w \cdot j \cdot d \cdot \cot\theta \right| \quad \text{nominal shear strength (kips)} \tag{7.5}$$

Where: $f_{\max}$ = maximum tensile strength of concrete (ksi) = -1.7 ksi

b_w = width of web (in.)

j = lever arm percentage of depth

d = depth (in.)

θ = principal compressive stress angle (degrees)

$$A_e = A_b \cdot \frac{M_u - M_{cr}}{M_n - M_{cr}} \quad \text{effective area (in.}^2\text{)} \tag{7.6}$$

Where: A_b = area below centroid (in.^{2})

M_u = factored ultimate moment (in.- kips)

M_{cr} = cracking moment (in.- kips)

M_n = nominal moment strength (in.- kips)

The cracking moment is the live load moment that causes the longitudinal stress of equation 7.1 to equate to the cracking tensile stress of concrete. The nominal moment strength can be calculated using section 5.2.1.1 or section 2.2.

If $M_u < M_{cr}$ then,

$$F_{bf} = 0 \text{ ksi} \quad \text{tensile force resultant in bottom flange (kips)} \tag{7.7}$$

If $M_u > M_{cr}$ then,

$$F_{bf} = f_{cr} \cdot A_e \quad \text{tensile force resultant in bottom flange (kips)} \tag{7.8}$$

Where: f_{cr} = cracking tensile strength of concrete (ksi)

$$\varepsilon_x = \frac{P_f - \frac{M_u}{j \cdot d} - F_{bf} - 0.5 \cdot V_u \cdot \cot\theta + 0.5 \cdot N_u}{A_{sbf} \cdot E_s + A_{pbf} \cdot E_p} \quad \text{longitudinal strain} \qquad (7.9)$$

Where: P_f = prestressing force final (kips)

V_u = factored ultimate shear force (kips)

N_u = factored ultimate axial force (kips)

A_{sbf} = area of mild reinforcement in bottom flange (in.^{2})

A_{pbf} = area of strands in bottom flange (in.^{2})

E_s = modulus of mild reinforcement (ksi)

E_p = modulus of strand (ksi)

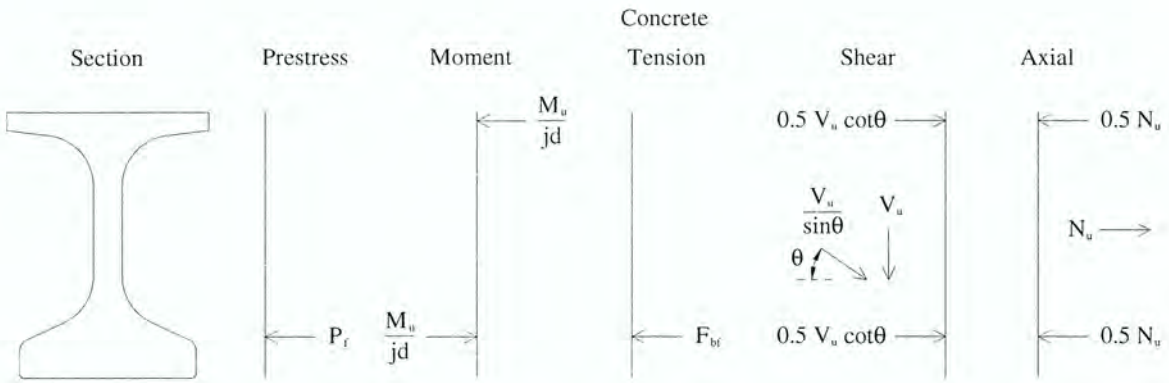

Figure 7.3. Applied forces within the longitudinal reinforcement of a general beam at the ultimate loading condition according to the MCFT.

$$\varepsilon_{xa} = \frac{\varepsilon_{max} \cdot E_c + \left(\cot\theta + \cot^3\theta\right) \cdot \frac{V_u}{b_w \cdot j \cdot d} + f_{max}}{E_c \cdot \left(1 + \cot^2\theta\right)} \quad \text{allowable longitudinal strain} \qquad (7.10)$$

Where: ε_{max} = maximum magnitude of strain corresponding to f_{max} = -0.0024

E_c = modulus of concrete (ksi) = 7820 ksi

Equation 7.10 is derived assuming that the shear stress distribution is constant as given in equation 7.11. The stress and strain at failure are set at values found during testing as shown in equations 7.12 and 7.13. Also, using Wagner's approach to reinforced concrete where it is conservatively assumed that the cracked concrete does not carry tension and that the shear is carried by a field of diagonal compression, equation 7.14 is given. Next, using Mohr's circle of average stresses, equation 7.15 is derived. Also, the modulus of elasticity can be used to define the relationship between the principal compressive stress and strain as in equation 7.16. This is an estimate, ignoring the softening of the concrete as discussed in Chapter 5. Finally, with some mathematical manipulation, equation 7.10 is derived.

$$\tau_{xy} = \frac{V_u}{b_w \cdot j \cdot d} \quad \text{shear stress in the x-y plane (ksi)} \tag{7.11}$$

$$\varepsilon_{p1} = \varepsilon_{\max} \quad \text{principal tensile strain} \tag{7.12}$$

$$\sigma_{p1} = f_{\max} \quad \text{principal tensile stress (ksi)} \tag{7.13}$$

$$\tan^2(\theta) = \frac{\varepsilon_x - \varepsilon_{p2}}{\varepsilon_{p1} - \varepsilon_x} \quad \text{Wagner's equation} \tag{7.14}$$

Where: ε_{p2} = principal compressive strain

$$\sigma_{p2} = (\tan\theta + \cot\theta) \cdot \tau_{xy} + \sigma_{p1} \quad \text{principal compressive stress (ksi)} \tag{7.15}$$

$$\sigma_{p2} = \varepsilon_{p2} \cdot E_c \quad \text{principal compressive stress (ksi)} \tag{7.16}$$

As mentioned previously, the recommended shear design procedure is a sectional approach employing the MCFT. Since a sectional analysis is used, the section of the beam to be analyzed must be chosen. The MCFT states that the most accurate way to choose the controlling section is at the center of the "cut" portion of the beam where the "cut" takes place on a diagonal line at the angle of the principal compressive stress. However, to ease computation and to ensure conservatism, it is recommended to use the section at which the highest combination of shear and moment are applied. These locations are shown in Fig. 7.4 for the flexure-shear test conducted and described herein. This controlling location along the length of the beam is the same as that described in section 7.1.1 for the service limit state design.

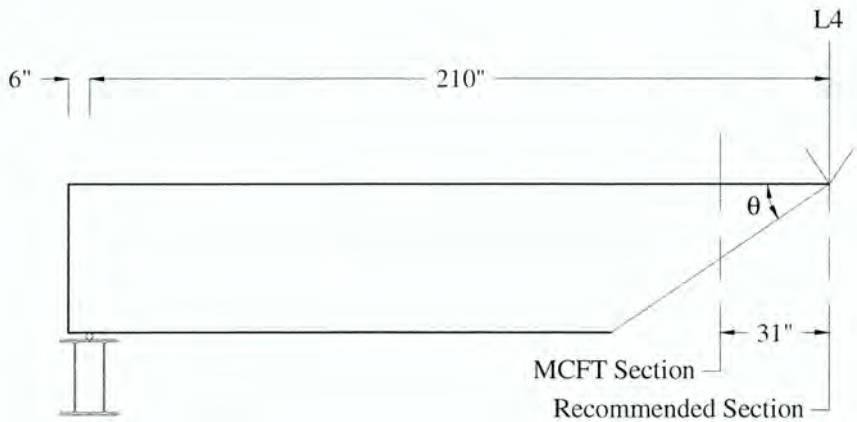

Figure 7.4. Recommended and MCFT Sections at which to perform analysis.

When this procedure is used with a truck load, the analysis section can be chosen under the wheel load nearest to the support. Also, when using a truck load, the loads are not stationary but instead the loads move. The standard procedure of AASHTO [15] can be used where the wheel load does not need to be placed any closer to the support than half the height of the beam. In addition, other load points should be investigated for flexure-shear interaction at intervals equal to the beam height as described in section 7.1.1. In situations where the loads are applied close to the support, the controlling section would also be close to the support. However, the MCFT procedure will not provide accurate results close to the support due to St. Venant's Principle that the strain is no longer linear. Therefore in this situation, a procedure has been developed describing the pure shear strength of an UHPC component.

The pure shear strength of UHPC has been determined by Chuang and Ulm [7] and the AFGC [3] as described in section 2.3 and repeated here in equations 7.17 through 7.19. Refer to equation 5.9 for computation of the crack angle.

$$V_c = 1.7 \cdot b_w \cdot d \sqrt{f`_c} \quad \text{concrete shear contribution (kips)} \tag{7.17}$$

$$V_f = \frac{0.9 \cdot b_w \cdot d \cdot |f_{\max}|}{\gamma_{bf} \cdot \tan \beta} \quad \text{fiber shear contribution (kips)} \tag{7.18}$$

Where: γ_{bf} = partial safety factor = 1.3

β = crack angle (degrees)

$$V_{n2} = V_c + V_f \quad \text{nominal shear strength (kips)} \tag{7.19}$$

The design is satisfactory if the design shear strength is larger than the ultimate applied shear at all locations along the beam length. This is shown in equation 7.20.

$$\phi \cdot \min(V_{n1}, V_{n2}) \geq V_u \quad \text{design shear strength (kips)} \tag{7.20}$$

Where: ϕ = strength reduction factor

7.2.2 Conservatism of Procedure

In order to show that the above described shear design procedure is conservative, this section will ignore all of the load factors and strength reduction factors. This means that instead of using ultimate moments and shears, actual applied moments and shears will be used instead.

This work has proposed to use the limiting shear strength defined by equations 7.11 through 7.13. These equations are meant to cap the shear strength for an essentially pure shear loading without moment. The small-scale test beams underwent predominantly pure shear loading. Therefore, the shear strength calculated using equations 7.11 through 7.13 should be smaller than the tested shear strengths. This is shown to be the case in Table 7.2. For the calculations in this table, the assumption is used that the crack angle is 45 degrees. This is conservative because for prestressed concrete the crack angle will always be below 45 degrees.

For loading conditions other than pure shear, showing that the shear design procedure is conservative is not as easy as ensuring that the experimental shear strength is greater than the analytical shear strength. This is because the shear strength is also dependent on applied moment. In a design situation this applied moment is known because the load is given. However, in an experimental situation, the load is continuously changing. Therefore, the experimentally measured load at failure serves as a substitute for a given design load.

The following approach will be used to verify conservatism. The experimentally measured shear at failure will be set equal to the nominal shear strength in equation 7.5 and the ultimate shear in equations 7.9 and 7.10. The experimentally measured moment at failure will be set equal to the ultimate moment in equations 7.6, 7.9, and 7.10. The compressive stress angle can then be computed from equation 7.5. All the variables of equations 7.9 and 7.10 are now known. The longitudinal strain and the allowable longitudinal strain can be calculated. To ensure conservatism, the longitudinal strain should be more tensile than the allowable longitudinal strain. This is reversed from the comparison of the strains in the design procedure because in the design, failure is not

desired. However, to show conservatism failure of the model is desired before the actual failure occurs. The comparison of the strain values in Table 7.3 verifies conservatism.

Table 7.2. Experimental and analytical ultimate shear strength of small-scale test beams.

Beam	Experimental (kips)	Analytical (kips)	Analytical without Partial Safety Factor (kips)
A1	79.3	45.6	57.9
A2	85.6	45.6	57.9
A3	76.1	45.6	57.9
B1	65.9	45.6	57.9
B2	80.1	45.6	57.9
B3	83.8	45.6	57.9
C1	81.8	39.9	50.7
C2	81.5	39.9	50.7
C3	83.4	39.9	50.7
D1	89.6	49.9	63.4
D2	86.8	49.9	63.4
D3	83.2	49.9	63.4
E1	81.8	42.8	54.3
E2	64.6	42.8	54.3
E3	77.6	42.8	54.3

Table 7.3. Comparison of calculated and allowable longitudinal strains at failure of the large-scale shear and flexure-shear tests.

Test	Longitudinal Strain	Allowable Longitudinal Strain
Shear	-0.0010	0.0002
Flexure-Shear	-0.0046	-0.0002

CHAPTER 8: CONCLUSIONS

Several conclusions have been made during the current research program. The following conclusions apply to the use of UHPC in general.

- The compressive strength of UHPC is approximately 24 ksi to 28 ksi.
- The tensile cracking strength of UHPC is approximately -1.1 ksi.
- Prestress losses are determined using the procedure given in section A.2.
- Ultimate flexural capacity is determined using the procedure given in section 2.2 or 5.1.1.
- Ultimate shear capacity is determined using the procedure given in section 5.1.2 or 7.2.
- Use of the MCFT can capture the shear behavior of UHPC.

Additional conclusions have been made pertaining to the adequacy of the Wapello County bridge as follows:

- The service level and ultimate level flexural capacity are adequate for the Wapello County bridge as shown in Table 6.3
- The service level and ultimate level shear capacity are adequate for the Wapello County bridge as shown in Table 6.3, Table 6.5, Fig. A.1, and Fig. A.2.

8.1 SUMMARY OF RESEARCH

Research has shown that UHPC has superior material characteristics as compared to other types of concretes. Both its tensile and compressive strengths are much higher than for conventional concrete. Quantifying these properties by defining the full stress vs. strain diagram has been possible by gathering information from a variety of sources as described in section 2.1. This constitutive property information has then been used to analyze the global structural behavior of components in flexure and shear. A simplified flexural design procedure has been described in section 2.2 based on previous research. Also, a more extensive iterative strain compatibility procedure has been described in section 5.2.1. This procedure can be used for both analysis and design for flexure. A complex shear model used for analysis and design has been described in section 5.2.1. This is an iterative procedure based on the Modified Compression Field Theory and employed for use with UHPC. These flexural and shear models have been shown to be accurate representations of structural behavior as described in Chapter 6. However, a simplified shear model is still desired for design in a code-type format. Therefore, using the same theory as the more complex model, a simplified shear design procedure has been developed in Chapter 7.

8.2 PERFORMANCE EVALUATION

Evaluation of the Wapello County bridge beam design for shear strength was required to ensure that the bridge had adequate strength. Evaluation was carried out initially by comparing the experimentally obtained shear strengths to the applied design shear forces. The service shear strength and ultimate shear strength determined during the shear test were shown to be greater than the service shear force and ultimate shear force demands, respectively. Additionally, the shear strength of the test beam under combined flexure-shear testing was determined to be sufficient for the type of loading demands of the bridge. After approval of the bridge design using these initial findings, additional calculations were also carried out. These calculations show that the analytical shear strength is greater than the code-required strength at every location along the length of the beam. These calculations are shown in section A.2 and Figs. A.2.16 and A.2.17.

8.3 FUTURE RESEARCH OF UHPC

Further research would be helpful in fully defining the shear strength characteristics of UHPC. There are three areas that have not been fully developed for applying the MCFT to UHPC. First, a method for prediction of the crack spacing should be developed so that multiplying this value by the principal tensile strain results in a crack width. A limiting shear stress on the crack interface had been determined for the MCFT but is not applicable for UHPC. Developing a maximum crack width under shear loading in the web has been attempted herein but should be further examined. Research has been completed in these areas for conventional concrete. Vecchio and Collins [16] completed testing on conventional concrete loaded in pure shear in order to asses the previously described properties. This type of experiment may prove useful for research with UHPC as well.

In addition, this research has raised some concerns related to the bond of prestressed strands in UHPC. Slipping of the strands was observed in several small-scale beam tests and to a lesser extent in a large-scale beam test which could cause premature structural failures. Further investigation into this area may be warranted.

The most reliable structural shear testing of UHPC has now taken place on the FHWA AASHTO type II girder and on the test beam described in the this report. Subsequent structural testing would be helpful in creating a more statistically relevant data pool with which the reported design procedure could be further validated and calibrated.

REFERENCES

1. B. A. Graybeal and J. L. Hartmann. *Strength and Durability of Ultra-High Performance Concrete*. Report to the 2003 Concrete Bridge Conference, 2003.
2. E. Chuang, H. Park, and F.-J. Ulm. *Structural Effect of UHPC Ductility*. Report to the 2003 ISHPC, 2003.
3. Association Francaise de Genie Civil (AFGC) (The French Association of Civil Engineering). *Ultra High Performance Fibre-Reinforced Concretes*. January 2002.
4. Bristow, B. and S. Sritharan. Uniaxial and Cyclic Behavior of Ultra-High Performance Concrete, *To be submitted to the ACI Materials Journal*.
5. N. Gowripalan and R. I. Gilbert. *Design Guidelines for RPC Prestressed Concrete Beams*. The University of New South Wales, 2000.
6. H. Park, E. Chuang, and F.-J. Ulm. *Model-Based Optimization of Ultra High Performance Concrete Highway Bridge Girders*. Publication No. R03-01, Department of Civil and Environmental Engineering, Massachusetts Institute of Technology, 2003.
7. F.-J. Ulm and E. Chuang. *UHPC Design Issues*. Presentation to the Iowa Department of Transportation, 2003.
8. S. K. Padmarajaiah, and Ananth Ramaswamy. *Behavior of Fiber-Reinforced Prestressed and Reinforced High-Strength Concrete Beams Subjected to Shear*. ACI Structural Journal, V. 98, No. 5, September-October 2001, pp. 752-761.
9. American Concrete Institute (ACI) Committee 318, *Building Code Requirements for Structural Concrete (ACI 318-02) and Commentary (ACI 318R-02)*. American Concrete Institute, Farmington Hills, Michigan.
10. Thomas T.C. Hsu. *Unified Theory of Reinforced Concrete*. CRC Press. 1993.
11. Michael P. Collins and Denis Mitchell. *Prestressed Concrete Structures*. Prentice Hall. 1991.
12. A. Lubbers. *Bond Performance between Ultra-High Performance Concrete and Prestressing Strands*. Department of Civil Engineering, Ohio University, August 2003.
13. ASTM, *ASTM – Volume 04.02 Concrete and Aggregates, 2004*. ASTM, Washington, D.C.
14. S. Sritharan. *Structural Effects of Creep and Shrinkage on Concrete Structures*. University of Auckland, 1989.
15. American Association of State Highway and Transportation Officials (AASHTO), *AASHTO LRFD Bridge Design Specifications, 1998*. American Association of State Highway and Transportation Officials, Washington, D.C.

16. IABSE Colloquium. *Vecchio F and Collins Stress-Strain Characteristics of Reinforced Concrete in Pure Shear. Advanced Mechanics of Reinforced Concrete*, V. 34, 1981, pp. 211-225.

APPENDIX: DESIGN CALCULATIONS

A.1 LARGE-SCALE TEST BEAM

A.1.1 Design Parameters

Concrete

$f_{ci} := 12.0\text{ksi}$	initial comp. strength
$f_c := 28.0\text{ksi}$	final comp. strength
$f_{cr} := -1.1\text{ksi}$	tensile strength
$E_{ci} := 5700\text{ksi}$	initial modulus of elasticity
$E_c := 7820\text{ksi}$	final modulus of elasticity
$u := 156\text{pcf}$	unit weight of concrete
$\varepsilon_{sh} := 5.5 \cdot 10^{-4}$	shrinkage strain
$H_u := 70$	average humidity
$K := 0.3$	creep coefficient with heat treatment
$\alpha := 0.0000655$	thermal expansion coef.

Beam

$L := 70\text{ft}$	bearing length
$A := 512.3\text{in}^2$	gross cross sectional area
$y := 18.72\text{in}$	gross nuetral axis
$I := 123654\text{in}^4$	gross moment of inertia
$H := 42\text{in}$	height
$b_t := 32\text{in}$	top flange width

Strands

$d_{bx} := 0.6\text{in}$	diameter of strand
$A_p := 0.217\text{in}^2$	area of strand
$E_p := 28500\text{ksi}$	modulus of elasticity
$f_{pu} := 270\text{ksi}$	design stress
$f_{\%} := 72.6\%$	initial prestress
$n_s := 49$	number of strands
$h_d := 0.1 \cdot L$	hold down length
$t := 5.0$ days	stressing to transfer time
$f_{py} := 0.9 \cdot f_{pu}$	yield stress
$f_{pj} := 0.75 \cdot f_{pu}$	maximum jacking stress
$f_{pe} := 0.8 \cdot f_{py}$	max stress after losses

A.1.2 Gross Section Properties

Centerline (or Hold Down) of Beam

$$y_s := \frac{13 \cdot 2in + 13 \cdot 4in + 11 \cdot 6in + 7 \cdot 8in + 3 \cdot 10in + 2 \cdot 40in}{n_s}$$

$y_s = 6.33in$ strand centroid

$e := y_s - y$ $e = -12.39in$ strand eccentricity

$c_t := H - y$ $c_t = 23.28in$ top fiber

$c_b := -y$ $c_b = -18.72in$ bottom fiber

End of Bonded Strands

$$c_h := 34in - \frac{6.5ft}{\frac{L}{2} + 0.5ft - h_d} \cdot 28in$$

$c_h = 27.61in$ centroid of harped strands

$$y_{se} := \frac{8 \cdot 2in + 8 \cdot 4in + 8 \cdot 6in + 4 \cdot 8in + 2 \cdot 10in + 5 \cdot c_h + 2 \cdot 40in}{n_s}$$

$y_{se} = 7.47in$ strand centroid

$e_e := y_{se} - y$ $e_e = -11.25in$ strand eccentricity

A.1.3 Initial Transformed Section Properties

$n_i := \frac{E_p}{E_{ci}}$ $\quad n_i = 5.00$ modular ratio

$AP_i := n_s \cdot A_p \cdot (n_i - 1)$ $\quad AP_i = 42.5in^2$ transformed strand area

$A_{ti} := A + AP_i$ $\quad A_{ti} = 554.83in^2$ transformed area

Centerline (or Hold Down) of Beam

$y_{ti} := \frac{A \cdot y + AP_i \cdot y_s}{A_{ti}}$ $\quad y_{ti} = 17.77in$ transformed centroid

$I_{ti} := I + A \cdot (y - y_{ti})^2 + AP_i \cdot (y_{ti} - y_s)^2$ $\quad I_{ti} = 129686in^4$ transformed moment of inertia

$e_{ti} := y_s - y_{ti}$ $\quad e_{ti} = -11.44in$ strand eccentricity

$c_{tti} := H - y_{ti}$ $\quad c_{tti} = 24.23in$ top fiber

$c_{bti} := -y_{ti}$ $\quad c_{bti} = -17.77in$ bottom fiber

End of Bonded Strands

$y_{tei} := \frac{A \cdot y + AP_i \cdot y_{se}}{A_{ti}}$ $\quad y_{tei} = 17.86in$ transformed centroid

$I_{tei} := I + A \cdot (y - y_{tei})^2 + AP_i \cdot (y_{tei} - y_{se})^2$ $\quad I_{tei} = 128624in^4$ transformed moment of inertia

$e_{tei} := y_{se} - y_{tei}$ $\quad e_{tei} = -10.39in$ strand eccentricity

$c_{ttei} := H - y_{tei}$ $\quad c_{ttei} = 24.14in$ top fiber

$c_{btei} := -y_{tei}$ $\quad c_{btei} = -17.86in$ bottom fiber

A.1.4 Final Transformed Section Properties

$n_f := \frac{E_p}{E_c}$ $n_f = 3.64$ modular ratio

$AP := n_s \cdot A_p \cdot (n_f - 1)$ $AP = 28.1 in^2$ transformed strand area

$A_t := A + AP$ $A_t = 540.42 in^2$ transformed area

Centerline (or Hold Down) of Beam

$y_t := \frac{A \cdot y + AP \cdot y_s}{A_t}$ $y_t = 18.08in$ transformed centroid

$I_t := I + A \cdot (y - y_t)^2 + AP \cdot (y_t - y_s)^2$ $I_t = 127748 in^4$ transformed moment of inertia

$e_t := y_s - y_t$ $e_t = -11.75in$ strand eccentricity

$c_{tt} := H - y_t$ $c_{tt} = 23.92in$ top fiber

$c_{bt} := -y_t$ $c_{bt} = -18.08in$ bottom fiber

End of Bonded Strands

$y_{te} := \frac{A \cdot y + AP \cdot y_{se}}{A_t}$ $y_{te} = 18.13in$ transformed centroid

$I_{te} := I + A \cdot (y - y_{te})^2 + AP \cdot (y_{te} - y_{se})^2$ $I_{te} = 127027 in^4$ transformed moment of inertia

$e_{te} := y_{se} - y_{te}$ $e_{te} = -10.66in$ strand eccentricity

$c_{tte} := H - y_{te}$ $c_{tte} = 23.87in$ top fiber

$c_{bte} := -y_{te}$ $c_{bte} = -18.13in$ bottom fiber

A.1.5 Composite Section Properties

There is no slab for the test beam and therefore no composite setion properties.

A.1.6 Dead Load Moments

Moment at Centerline

$$M_{bm} := \frac{u \cdot A \cdot L^2}{8} \qquad M_{bm} = 340\,ft \cdot k$$ moment due to beam

Moment at Hold Down

$$M_{bmh} := \frac{u \cdot A \cdot L}{2} \cdot \left(\frac{L}{2} - h_d \right) - \frac{u \cdot A}{2} \cdot \left(\frac{L}{2} - h_d \right)^2 \qquad M_{bmh} = 326\,ft \cdot k$$ moment due to beam

Moment at End of Bonded Strands

$$M_{bme} := \frac{u \cdot A \cdot L}{2} \cdot 6ft - \frac{u \cdot A}{2} \cdot (6ft)^2 \qquad M_{bme} = 107\,ft \cdot k$$ moment due to beam

A.1.7 Prestress Losses

{LRFD 5.9.5}

Calculate Losses

$$\Delta F_{pr1} := \frac{\log(24 \cdot t)}{40} \cdot \left(\frac{f_{pj}}{f_{py}} - 0.55 \right) \cdot f_{pj}$$ $\Delta F_{pr1} = 2.98\text{ksi}$ initial relaxation loss

$$P := n_s \cdot A_p \cdot \left(f\% \cdot f_{pu} - \Delta F_{pr1} \right)$$ $P = 2053\text{k}$ prestress after relaxation

$$F_{cgp} := \frac{P}{A} + \frac{P \cdot e^2}{I} + \frac{M_{bm} \cdot e_t}{I_t}$$ $F_{cgp} = 6.18\text{ksi}$ release stress

$$\Delta F_{pes} := \frac{E_p}{E_{ci}} \cdot F_{cgp}$$ $\Delta F_{pes} = 30.9\text{ksi}$ elastic shortening loss

$$\Delta F_{psr} := \varepsilon_{sh} \cdot E_p$$ $\Delta F_{psr} = 15.68\text{ksi}$ shrinkage loss

$$\Delta F_{pcr} := K \cdot \Delta F_{pes}$$ $\Delta F_{pcr} = 9.27\text{ksi}$ creep loss

$$\Delta F_{pr2} := 0.3 \cdot \left[20.0\text{ksi} - 0.4 \cdot \Delta F_{pes} - 0.2 \cdot \left(\Delta F_{psr} + \Delta F_{pcr} \right) \right]$$ $\Delta F_{pr2} = 0.79\text{ksi}$ relaxation loss

$$\Delta F_{pi} := \Delta F_{pr1} + \Delta F_{pes}$$ $\Delta F_{pi} = 33.89\text{ksi}$ initial losses

$$\Delta F_{pf} := \Delta F_{pr1} + \Delta F_{pes} + \Delta F_{psr} + \Delta F_{pcr} + \Delta F_{pr2}$$ $\Delta F_{pf} = 59.6\text{ksi}$ final losses

$$P_i := n_s \cdot A_p \cdot \left(f\% \cdot f_{pu} - \Delta F_{pi} \right)$$ $P_i = 1724\text{k}$ initial prestress

$$P_f := n_s \cdot A_p \cdot \left(f\% \cdot f_{pu} - \Delta F_{pf} \right)$$ $P_f = 1450\text{k}$ final prestress

Strain Based on Fiber Optic Gage Readings and Mean Stress Method [16]

$\Delta T := 14.5$

$$\sigma_i := \frac{P_i}{A} + \frac{P_i \cdot e \cdot (c_b + 2 \cdot in)}{I} + \frac{M_{bm} \cdot (c_{bti} + 2in)}{I_{ti}} \qquad \sigma_i = 5.76ksi$$

initial stress at fiber optic

$$\sigma_f := \frac{P_f}{A} + \frac{P_f \cdot e \cdot (c_b + 2 \cdot in)}{I} + \frac{M_{bm} \cdot (c_{bti} + 2in)}{I_{ti}} \qquad \sigma_f = 4.77ksi$$

final stress at fiber optic

$$\varepsilon := \frac{\sigma_i}{E_{ci}} + \frac{\sigma_i + \sigma_f}{2 \cdot E_c} \cdot K + \frac{\sigma_f - \sigma_i}{2} \cdot \left(\frac{1}{E_c} + \frac{1}{E_{ci}} \right) \qquad \varepsilon = 1.06 \times 10^{-3}$$

initial and creep strain at fiber optic

$$\varepsilon_t := \varepsilon + \varepsilon_{sh} + \alpha \cdot \Delta T \qquad \varepsilon_t = 2.56 \times 10^{-3}$$

total calculated strain at fiber optic

$$\varepsilon_t := 0.00268 \qquad \varepsilon_t = 2.68 \times 10^{-3}$$

total measured strain from fiber optic

Losses Based on Fiber Optic Strain Gage Readings and Mean Stress Method [16]

$$\varepsilon := \varepsilon_t - \varepsilon_{sh} - \alpha \cdot \Delta T \qquad \varepsilon = 1.18 \times 10^{-3}$$

initial and creep stain at fiber optic

$$\sigma_f := \frac{\varepsilon + \sigma_i \cdot \left(\frac{1}{2 \cdot E_c} - \frac{K}{2 \cdot E_{ci}} - \frac{1}{2 \cdot E_{ci}} \right)}{\frac{1}{2 \cdot E_c} + \frac{K}{2 \cdot E_c} + \frac{1}{2 \cdot E_{ci}}} \qquad \sigma_f = 5.22ksi$$

final stress at fiber optic

$$P_f := \frac{\sigma_f - \frac{M_{bm} \cdot (c_{bti} + 2in)}{I_{ti}}}{\frac{1}{A} + \frac{e \cdot c_b}{I}} \qquad P_f = 1493k$$

final prestress

Losses Based on Tested Cracking Load

$F := 237.4k$

total live load at cracking

$$M_{ll} := \frac{F}{2} \cdot \frac{L}{2} - \frac{F}{4} \cdot 32in - \frac{F}{4} \cdot 54in \qquad M_{ll} = 3729ft \cdot k$$

live load moment

$$\frac{P_f}{A} + \frac{P_f \cdot e \cdot c_b}{I} + \frac{M_{bm} \cdot c_{bt}}{I_t} + \frac{M_{ll} \cdot c_{bt}}{I_t} = f_{cr}$$

equate stresses

$$P_f := \frac{f_{cr} - \frac{M_{bm} \cdot c_{bt}}{I_t} - \frac{M_{ll} \cdot c_{bt}}{I_t}}{\frac{1}{A} + \frac{e \cdot c_b}{I}} \qquad P_f = 1517k$$

final prestress

A.1.8 Release Stresses

Allowable Release Stresses {LRFD 5.9.4}

$f_{ac} := 0.6 f_{ci}$ $f_{ac} = 7.20\text{ksi}$ allowable comp.

$f_{at} := -1.0\text{ksi}$ allowable ten.

Stresses at Centerline

$$f_{ct} := \frac{P_i}{A} + \frac{P_i \cdot e \cdot c_t}{I} + \frac{M_{bm} \cdot c_{tt}}{I_t}$$ $f_{ct} = 0.11\text{ksi}$ top stress

$$f_{cb} := \frac{P_i}{A} + \frac{P_i \cdot e \cdot c_b}{I} + \frac{M_{bm} \cdot c_{bt}}{I_t}$$ $f_{cb} = 6.02\text{ksi}$ bottom stress

Stresses at Hold Down

$$f_{ht} := \frac{P_i}{A} + \frac{P_i \cdot e \cdot c_t}{I} + \frac{M_{bmh} \cdot c_{tt}}{I_t}$$ $f_{ht} = 0.08\text{ksi}$ top stress

$$f_{hb} := \frac{P_i}{A} + \frac{P_i \cdot e \cdot c_b}{I} + \frac{M_{bmh} \cdot c_{bt}}{I_t}$$ $f_{hb} = 6.05\text{ksi}$ bottom stress

Stresses at End of Bonded Strands

$$f_{tt} := \frac{P_i}{A} + \frac{P_i \cdot e_e \cdot c_t}{I} + \frac{M_{bme} \cdot c_{tte}}{I_{te}}$$ $f_{tt} = -0.05\text{ksi}$ top stress

$$f_{tb} := \frac{P_i}{A} + \frac{P_i \cdot e_e \cdot c_b}{I} + \frac{M_{bme} \cdot c_{bte}}{I_{te}}$$ $f_{tb} = 6.12\text{ksi}$ bottom stress

A.2 BRIDGE BEAMS

A.2.1 Design Parameters

Bridge Orientation

$L := 110ft$	bearing length
$n_b := 3$	number of beams
$S := 115in$	beam spacing
$W := 24ft$	roadway width
$O := 4ft$	overhang
$t_n := 8.0in$	slab thickness
$t_s := 7.5in$	design slab thickness
$b_a := 316.7plf$	barrier weight
$f_{ws} := 0.02ksf$	future wearing surface
$h := 1.5in$	design haunch
$H_u := 70$	average humidity

Slab Concrete

$f_{cs} := 4.5ksi$	compressive strength
$E_{sl} := 3861ksi$	modulus of elasticity
$u_s := 145pcf$	unit wieght of slab

Beam Concrete

$f_{ci} := 12.0ksi$	initial comp. strength
$f_c := 28.0ksi$	final comp. strength
$E_{ci} := 5700ksi$	initial modulus of elasticity
$E_c := 7820ksi$	final modulus of elasticity
$u := 156pcf$	unit wieght of concrete
$\varepsilon_{sh} := 5.5 \cdot 10^{-4}$	shrinkage strain
$K := 0.3$	creep coefficient with heat treatment

Strands

$d_{bx} := 0.6in$	diameter of strand
$A_p := 0.217in^2$	area of strand
$E_p := 28500ksi$	modulus of elasticity
$f_{pu} := 270ksi$	design stress
$f_{\%} := 72.6\%$	initial prestress
$n_s := 49$	number of strands
$h_d := 0.1 \cdot L$	hold down length
$t := 5.0 \ days$	stressing to release time
$f_{py} := 0.9 \cdot f_{pu}$	yield stress
$f_{pj} := 0.75 \cdot f_{pu}$	maximum jacking stress
$f_{pe} := 0.8 \cdot f_{py}$	max stress after losses

Beams

$A := 512.3in^2$	gross cross sectional area
$y := 18.72in$	gross nuetral axis
$I := 123654in^4$	gross moment of inertia
$H := 42in$	height
$b_t := 32in$	top flange width
$b_w := 4.5in$	web thickness

A.2.2 Gross Section Properties

Centerline (or Hold Down) of Beam

$$y_s := \frac{13 \cdot 2in + 13 \cdot 4in + 11 \cdot 6in + 7 \cdot 8in + 3 \cdot 10in + 2 \cdot 40in}{n_s}$$

$y_s = 6.33in$ strand centroid

$e := y_s - y$ $e = -12.39in$ strand eccentricity

$c_t := H - y$ $c_t = 23.28in$ top fiber

$c_b := -y$ $c_b = -18.72in$ bottom fiber

End of Bonded Strands

$$c_{he} := 34in - \frac{6.5ft}{\frac{L}{2} + 0.5ft - h_d} \cdot 28in$$

$c_{he} = 29.91in$ centroid of harped strands

$$y_{se} := \frac{12 \cdot 2in + 12 \cdot 4in + 10 \cdot 6in + 6 \cdot 8in + 2 \cdot 10in + 5 \cdot c_{he} + 2 \cdot 40in}{n_s}$$

$y_{se} = 8.77in$ strand centroid

$e_e := y_{se} - y$ $e_e = -9.95in$ strand eccentricity

Quarter Span

$$c_{hq} := 34in - \frac{\frac{L}{4} + 0.5ft}{\frac{L}{2} + 0.5ft - h_d} \cdot 28in$$

$c_{hq} = 16.38in$ centroid of harped strands

$$y_{sq} := \frac{12 \cdot 2in + 12 \cdot 4in + 10 \cdot 6in + 6 \cdot 8in + 2 \cdot 10in + 5 \cdot c_{hq} + 2 \cdot 40in}{n_s}$$

$y_{sq} = 7.39in$ strand centroid

A.2.3 Initial Transformed Section Properties

Initial transformed section properties are not required for bridge design. They were used for the test beam for research purposes.

A.2.4. Final Transformed Section Properties

$n_f := \frac{E_p}{E_c}$ $\quad n_f = 4$ modular ratio

$AP := n_s \cdot A_p \cdot (n_f - 1)$ $\quad AP = 28.12in^2$ transformed area of strands

$A_t := A + AP$ $\quad A_t = 540.42in^2$ transformed area

Centerline (or Hold Down) of Beam

$y_t := \frac{A \cdot y + AP \cdot y_s}{A_t}$ $\quad y_t = 18.08in$ transformed centroid

$I_t := I + A \cdot (y - y_t)^2 + AP \cdot (y_t - y_s)^2$ $\quad I_t = 127748in^4$ transformed moment of inertia

$e_t := y_s - y_t$ $\quad e_t = -11.75in$ strand eccentricity

$c_{tt} := H - y_t$ $\quad c_{tt} = 23.92in$ top fiber

$c_{bt} := -y_t$ $\quad c_{bt} = -18.08in$ bottom fiber

End of Bonded Strands

$y_{te} := \frac{A \cdot y + AP \cdot y_{se}}{A_t}$ $\quad y_{te} = 18.20in$ transformed centroid

$I_{te} := I + A \cdot (y - y_{te})^2 + AP \cdot (y_{te} - y_{se})^2$ $\quad I_{te} = 126295in^4$ transformed moment of inertia

$e_{te} := y_{se} - y_{te}$ $\quad e_{te} = -9.44in$ strand eccentricity

$c_{tte} := H - y_{te}$ $\quad c_{tte} = 23.80in$ top fiber

$c_{bte} := -y_{te}$ $\quad c_{bte} = -18.20in$ bottom fiber

Quarter Span

$y_{tq} := \frac{A \cdot y + AP \cdot y_{sq}}{A_t}$ $\quad y_{tq} = 18.13in$ transformed centroid

$I_{tq} := I + A \cdot (y - y_{tq})^2 + AP \cdot (y_{tq} - y_{sq})^2$ $\quad I_{tq} = 127078in^4$ transformed moment of inertia

$e_{tq} := y_{sq} - y_{tq}$ $\quad e_{tq} = -10.74in$ strand eccentricity

$c_{ttq} := H - y_{tq}$ $\quad c_{ttq} = 23.87in$ top fiber

$c_{btq} := -y_{tq}$ $\quad c_{btq} = -18.13in$ bottom fiber

A.2.5 Composite Beam Properties

$n_c := \frac{E_{sl}}{E_c}$ $n_c = 0.49$ modular ratio

$y_{sl} := H + 0.5 \cdot t_s$ $y_{sl} = 45.75\text{in}$ slab centroid

Interior Beam

$b_e := \min\left(\frac{L}{4}, 12 \cdot t_n + \max\left(b_w, \frac{b_t}{2}\right), S\right)$ $b_e = 112.00\text{in}$ effective flange width {LRFD 4.6.2.6}

$A_{sl} := b_e \cdot t_s \cdot n_c$ $A_{sl} = 414.74\text{in}^2$ effective area of slab

$A_c := A_t + A_{sl}$ $A_c = 955.16\text{in}^2$ composite area

$y_c := \frac{A_t \cdot y_t + A_{sl} \cdot y_{sl}}{A_c}$ $y_c = 30.09\text{in}$ composite centroid

$I_c := I_t + A_t \cdot (y_c - y_t)^2 + \frac{b_e \cdot t_s^3}{12} \cdot n_c + A_{sl} \cdot (y_{sl} - y_c)^2$

$I_c = 309414\text{in}^4$ composite moment of inertia

$e_c := y_s - y_c$ $e_c = -23.77\text{in}$ composite eccentricity

$c_{1c} := H + t_s - y_c$ $c_{1c} = 19.41\text{in}$ top fiber of slab

$c_{2c} := H - y_c$ $c_{2c} = 11.91\text{in}$ top fiber of beam

$c_{bc} := -y_c$ $c_{bc} = -30.09\text{in}$ bottom fiber

Exterior Beam

$b_{e2} := \min\left(\frac{L}{8}, 6 \cdot t_n + \max\left(\frac{b_w}{2}, \frac{b_t}{4}\right), O\right)$ $b_{e2} = 48.00\text{in}$ effective flange width {LRFD 4.6.2.6}

$A_{sl2} := b_{e2} \cdot t_s \cdot n_c$ $A_{sl2} = 177.74\text{in}^2$ effective area of slab

$A_{c2} := A_t + A_{sl2}$ $A_{c2} = 718.16\text{in}^2$ composite area

$y_{c2} := \frac{A_t \cdot y_t + A_{sl2} \cdot y_{sl}}{A_{c2}}$ $y_{c2} = 24.92\text{in}$ composite centroid

$I_{c2} := I_t + A_t \cdot (y_{c2} - y_t)^2 + \frac{b_{e2} \cdot t_s^3}{12} \cdot n_c + A_{sl2} \cdot (y_{sl} - y_{c2})^2$

$I_{c2} = 231022\text{in}^4$ composite moment of inertia

$e_{c2} := y_{c2} - y_s$ $e_{c2} = 18.60\text{in}$ composite eccentricity

A.2.6 Dead Load Moments

Moments at Centerline

$$M_{bm} := \frac{u \cdot A \cdot L^2}{8} \qquad M_{bm} = 839\,ft\cdot k$$ moment due to beam

$$M_{sl} := \frac{u_s \cdot (S \cdot t_n + h \cdot b_t) \cdot L^2}{8} \qquad M_{sl} = 1474\,ft\cdot k$$ moment due to slab

$$M_b := \frac{2 \cdot b_a \cdot L^2}{n_b \cdot 8} \qquad M_b = 319\,ft\cdot k$$ moment due to barrier

$$M_o := \frac{f_{ws} \cdot W \cdot L^2}{n_b \cdot 8} \qquad M_o = 242\,ft\cdot k$$ moment due to overlay

Moment at Hold Down

$$M_{bmh} := \frac{u \cdot A \cdot L}{2} \cdot \left(\frac{L}{2} - h_d\right) - \frac{u \cdot A}{2} \cdot \left(\frac{L}{2} - h_d\right)^2 \qquad M_{bmh} = 806\,ft\cdot k$$ moment due to beam

Moment at End of Bonded Strands

$$M_{bme} := \frac{u \cdot A \cdot L}{2} \cdot 6ft - \frac{u \cdot A}{2} \cdot (6ft)^2 \qquad M_{bme} = 173\,ft\cdot k$$ moment due to beam

A.2.7 Prestress Losses

{LRFD 5.9.5}

$$\Delta F_{pr1} := \frac{\log(24 \cdot t)}{40} \cdot \left(\frac{f_{pj}}{f_{py}} - 0.55 \right) \cdot f_{pj}$$ $\Delta F_{pr1} = 2.98\text{ksi}$ initial relaxation loss

$$P := n_s \cdot A_p \cdot \left(f_{\%} \cdot f_{pu} - \Delta F_{pr1} \right)$$ $P = 2053\text{k}$ prestress after relaxation

$$F_{cgp} := \frac{P}{A} + \frac{P \cdot e^2}{I} + \frac{M_{bm} \cdot e_t}{I_t}$$ $F_{cgp} = 5.63\text{ksi}$ release stress

$$\Delta F_{pes} := \frac{E_p}{E_{ci}} \cdot F_{cgp}$$ $\Delta F_{pes} = 28.15\text{ksi}$ elastic shortening loss

$$\Delta F_{psr} := \varepsilon_{sh} \cdot E_p$$ $\Delta F_{psr} = 15.68\text{ksi}$ shrinkage loss

$$\Delta F_{pcr} := K \cdot \Delta F_{pes}$$ $\Delta F_{pcr} = 8.44\text{ksi}$ creep loss

$$\Delta F_{pr2} := 0.3 \cdot \left[20.0\text{ksi} - 0.4 \cdot \Delta F_{pes} - 0.2 \cdot \left(\Delta F_{psr} + \Delta F_{pcr} \right) \right]$$ $\Delta F_{pr2} = 1.17\text{ksi}$ relaxation loss

$$\Delta F_{pi} := \Delta F_{pr1} + \Delta F_{pes}$$ $\Delta F_{pi} = 31.13\text{ksi}$ initial losses

$$\Delta F_{pf} := \Delta F_{pr1} + \Delta F_{pes} + \Delta F_{psr} + \Delta F_{pcr} + \Delta F_{pr2}$$ $\Delta F_{pf} = 56.43\text{ksi}$ final losses

$$P_i := n_s \cdot A_p \cdot \left(f_{\%} \cdot f_{pu} - \Delta F_{pi} \right)$$ $P_i = 1753\text{k}$ initial prestress

$$P_f := n_s \cdot A_p \cdot \left(f_{\%} \cdot f_{pu} - \Delta F_{pf} \right)$$ $P_f = 1484\text{k}$ final prestress

A.2.8 Release Stresses

Allowable Release Stresses {LRFD 5.9.4}

$f_{ac} := 0.6 f_{ci}$ $f_{ac} = 7.20\text{ksi}$ compression

$f_{at} := -1.0\text{ksi}$ tension

Stresses at Centerline

$$f_{ct} := \frac{P_i}{A} + \frac{P_i \cdot e \cdot c_t}{I} + \frac{M_{bm} \cdot c_{tt}}{I_t}$$ $f_{ct} = 1.218\text{ksi}$ top stress

$$f_{cb} := \frac{P_i}{A} + \frac{P_i \cdot e \cdot c_b}{I} + \frac{M_{bm} \cdot c_{bt}}{I_t}$$ $f_{cb} = 5.29\text{ksi}$ bottom stress

Stresses at Hold Down

$$f_{ht} := \frac{P_i}{A} + \frac{P_i \cdot e \cdot c_t}{I} + \frac{M_{bmh} \cdot c_{tt}}{I_t}$$ $f_{ht} = 1.14\text{ksi}$ top stress

$$f_{hb} := \frac{P_i}{A} + \frac{P_i \cdot e \cdot c_b}{I} + \frac{M_{bmh} \cdot c_{bt}}{I_t}$$ $f_{hb} = 5.34\text{ksi}$ bottom stress

Stresses at End of Bonded Strands

$$f_{tt} := \frac{P_i}{A} + \frac{P_i \cdot e_e \cdot c_t}{I} + \frac{M_{bme} \cdot c_{tte}}{I_{te}}$$ $f_{tt} = 0.53\text{ksi}$ top stress

$$f_{tb} := \frac{P_i}{A} + \frac{P_i \cdot e_e \cdot c_b}{I} + \frac{M_{bme} \cdot c_{bte}}{I_{te}}$$ $f_{tb} = 5.76\text{ksi}$ bottom stress

A.2.9 Load Factor Reduction

{1.3.2}

$\eta_d := 0.95$ high ductility

$\eta_r := 1.0$ normal redundancy

$\eta_l := 0.95$ low importance

$\eta_i := \max(\eta_d \cdot \eta_r \cdot \eta_l, 0.95)$ $\eta_i = 0.95$ ultimate load modifier

$$\eta_{is} := \min\left(\frac{1}{\eta_d \cdot \eta_r \cdot \eta_l}, 1\right)$$ $\eta_{is} = 1.00$ service load modifier

A.2.10 Distribution Factors

$$2 \cdot \frac{0.5 \cdot (S - 8 \cdot ft) + 0.5 \cdot (S - 2 \cdot ft)}{S} = 0.96$$ moment distribution factor lever rule, interior beam

0.692 moment distribution factor by STAAD, interior beam

$DF_{mi} := 0.75$ design moment distribution factor, interior

$$1.2 \cdot \frac{0.5 \cdot (S + 0.67ft) + 0.5 \cdot 4.25ft}{S} = 0.91$$ moment distribution factor lever rule, exterior beam

0.744 moment distribution factor by STAAD, exterior beam

$DF_{me} := 0.80$ design moment distribution factor, exterior

0.974 shear distribution factor by STAAD

$DF_{v} := 0.96$ design shear distribution factor

A.2.11 Live Load Moments at Centerline

{4.6.2.2}

Truck Load

$$e_{tr} := \frac{1}{2}\cdot\frac{32k\cdot 14ft - 8k\cdot 14ft}{2\cdot 32k + 8k} \qquad e_{tr} = 2.33ft$$

location of center axle with respect to midspan for maximum moment

$$R := \frac{32\cdot k\cdot(0.5\cdot L + 14ft - e_{tr}) + 32\cdot k\cdot(0.5\cdot L - e_{tr}) + 8\cdot k\cdot(0.5\cdot L - 14ft - e_{tr})}{L}$$

$$R = 37.5k$$

bearing reaction

$$M_{tr} := R\cdot(0.5\cdot L + e_{tr}) - 32k\cdot 14ft \qquad M_{tr} = 1704ft\cdot k$$

truck moment

Tandem Load

$$e_{tr} := \frac{1}{2}\cdot\frac{25k\cdot 4ft}{2\cdot 25k} \qquad e_{tr} = 1.00ft$$

location of one axle with respect to midspan for maximum moment

$$R := \frac{25\cdot k\cdot(0.5\cdot L + e_{tr}) + 25\cdot k\cdot(0.5\cdot L - 4\cdot ft + e_{tr})}{L} \qquad R = 24.5k$$

bearing reaction

$$M_t := R\cdot(0.5\cdot L - 1ft) \qquad M_t = 1325ft\cdot k$$

tandem moment

Lane Load

$$M_l := \frac{0.64klf\cdot L^2}{8} \qquad M_l = 968ft\cdot k$$

lane moment

Live Load

With ADTT below 100, 90% of force effect is used.

{3.6.1.1.2}

$$M_{ll} := 0.90\,DF_{mi}\cdot\left(M_l + \frac{4}{3}\cdot\max(M_{tr}, M_t)\right) \qquad M_{ll} = 2187ft\cdot k$$

live load moment interior

$$M_{ll2} := 0.90\,DF_{me}\cdot\left(M_l + \frac{4}{3}\cdot\max(M_{tr}, M_t)\right) \qquad M_{ll2} = 2332ft\cdot k$$

live load moment exterior

A.2.12 Flexural Service Stresses at Centerline

Top of Slab

$$f_{s1} := \frac{(M_o + M_b)\cdot c_{1c}}{I_c} \qquad f_{s1} = 0.42\text{ksi}$$ overlay + barrier loads

$$f_a := 0.4\, f_{cs} \qquad < \quad f_a = 1.80\text{ksi}$$

$$f_{s2} := f_{s1} + \frac{M_{ll}\cdot c_{1c}}{I_c} \qquad f_{s2} = 2.07\text{ksi}$$ overlay + barrier + live loads

$$f_a := 0.6\, f_{cs} \qquad < \quad f_a = 2.70\text{ksi}$$

Top of Beam

$$f_{t1} := \frac{P_f}{A} + \frac{P_f\cdot e\cdot c_t}{I} + \frac{(M_{bm} + M_{sl})\cdot c_{tt}}{I_t} + \frac{(M_o + M_b)\cdot c_{2c}}{I_c}$$

$$f_{t1} = 4.89\text{ksi}$$ prestress + permanent loads

$$f_a := 0.45\, f_c \qquad < \quad f_a = 12.60\text{ksi}$$

$$f_{t2} := \frac{1}{2}\cdot f_{t1} + \frac{M_{ll}\cdot c_{2c}}{I_c} \qquad f_{t2} = 3.46\text{ksi}$$ 1/2 (prestress + permanent) + live loads

$$f_a := 0.4\, f_c \qquad < \quad f_a = 11.20\text{ksi}$$

$$f_{t3} := f_{t1} + \frac{M_{ll}\cdot c_{2c}}{I_c} \qquad f_{t3} = 5.90\text{ksi}$$ prestress + permanent + live loads

$$f_a := 0.6\, f_c \qquad < \quad f_a = 16.80\text{ksi}$$

Bottom of Beam

$$f_b := \frac{P_f}{A} + \frac{P_f\cdot e\cdot c_b}{I} + \frac{(M_{bm} + M_{sl})\cdot c_{bt}}{I_t} + \frac{(M_o + M_b)\cdot c_{bc}}{I_c} + \frac{0.8\cdot M_{ll}\cdot c_{bc}}{I_c}$$ prestress + permanent + 0.8 live loads

$$f_b = -0.94\text{ksi}$$

$$< \quad f_{at} = -1.00\text{ksi}$$

A.2.13 Flexural Ultimate Strength

$\phi_f := 0.85$ {5.5.4.2}

Interior, controlled by strand

$M_n := 10014.6\,ft\cdot k$ interior strength by UHPC

$\phi_f \cdot M_n = 8512\,ft\cdot k$ design moment strength

$M_u := \eta_i \cdot \left[1.25\left(M_{bm} + M_{sl} + M_b\right) + 1.5 \cdot M_o + 1.75 \cdot M_{ll}\right]$ {3.4}

$> \quad M_u = 7107\,ft\cdot k$ ultimate moment interior

Exterior, controlled by slab

$M_{n2} := 8967.5\,ft\cdot k$ exterior strength by UHPC

$\phi_f \cdot M_{n2} = 7622\,ft\cdot k$ design moment strength

$M_{u2} := \eta_i \cdot \left[1.25\left(M_{bm} + M_{sl} + M_b\right) + 1.5 \cdot M_o + 1.75 \cdot M_{ll2}\right]$ {3.4}

$> \quad M_{u2} = 7349\,ft\cdot k$ ultimate moment exterior

Table A.1. Analysis of strains and curvatures at flexural capacity of exterior bridge beam.

Value	Total Load	Live Load	Dead Load
Top Strain	1.21E-03	1.04E-03	1.72E-04
Bottom Strain	-5.84E-03	-6.37E-03	5.32E-04
Curvature (1/in.)	1.68E-04	1.77E-04	-8.57E-06

Table A.2. Analysis of strands at flexural capacity of exterior bridge beam.

Position (in.) {12}	Number of Strands {13}	Area of Strand ($in.^2$) {14}	Area ($in.^2$) 13x14 {15}	Total Strain {16}	Stress (ksi) {17}	Tensile Force (kips) 15x17 {7}	Compressive Force (kips) 15x17 {8}	12x18 {9}	1x8 {10}
2.00	8	0.217	1.74	-1.10E-02	-270	-468.7	0.0	-937.4	0.0
2.00	4	0.217	0.87	-1.10E-02	-270	-234.4	0.0	-468.7	0.0
4.00	6	0.217	1.30	-1.06E-02	-270	-351.5	0.0	-1406.2	0.0
4.00	6	0.217	1.30	-1.06E-02	-270	-351.5	0.0	-1406.2	0.0
6.00	6	0.217	1.30	-1.02E-02	-270	-351.5	0.0	-2109.2	0.0
6.00	4	0.217	0.87	-1.02E-02	-270	-234.4	0.0	-1406.2	0.0
8.00	4	0.217	0.87	-9.84E-03	-270	-234.4	0.0	-1874.9	0.0
8.00	2	0.217	0.43	-9.84E-03	-270	-117.2	0.0	-937.4	0.0
10.00	2	0.217	0.43	-9.47E-03	-270	-117.2	0.0	-1171.8	0.0
10.00	1	0.217	0.22	-9.47E-03	-270	-58.6	0.0	-585.9	0.0
8.00	1	0.217	0.22	-9.84E-03	-270	-58.6	0.0	-468.7	0.0
6.00	1	0.217	0.22	-1.02E-02	-270	-58.6	0.0	-351.5	0.0
4.00	1	0.217	0.22	-1.06E-02	-270	-58.6	0.0	-234.4	0.0
2.00	1	0.217	0.22	-1.10E-02	-270	-58.6	0.0	-117.2	0.0
40.00	2	0.217	0.43	-3.92E-03	-112	-48.5	0.0	-1940.0	0.0

Table A.3. Analysis of UHPC and conventional concrete at flexural capacity of exterior bridge beam.

Position (in.) {1}	Base (in.) {2}	Height (in.) {3}	Area ($in.^2$) 2x3 {4}	Total Strain {5}	Stress (ksi) {6}	Tensile Force (kips) 4x6 {7}	Compressive Force (kips) 4x6 {8}	1x7 {9}	1x8 {10}
0.21	26.92	0.42	11.31	-5.81E-03	-1.10	-12.4	0.0	-2.6	0.0
0.63	27.76	0.42	11.66	-5.74E-03	-1.11	-12.9	0.0	-8.1	0.0
1.05	28.00	0.42	11.76	-5.66E-03	-1.11	-13.1	0.0	-13.8	0.0
1.47	28.00	0.42	11.76	-5.59E-03	-1.12	-13.2	0.0	-19.4	0.0
1.89	28.00	0.42	11.76	-5.52E-03	-1.13	-13.3	0.0	-25.2	0.0
2.31	28.00	0.42	11.76	-5.45E-03	-1.14	-13.4	0.0	-31.0	0.0
2.73	28.00	0.42	11.76	-5.38E-03	-1.15	-13.5	0.0	-36.9	0.0
3.15	28.00	0.42	11.76	-5.31E-03	-1.16	-13.6	0.0	-42.9	0.0
3.57	28.00	0.42	11.76	-5.24E-03	-1.17	-13.7	0.0	-49.0	0.0
3.99	28.00	0.42	11.76	-5.17E-03	-1.18	-13.8	0.0	-55.2	0.0
4.41	28.00	0.42	11.76	-5.10E-03	-1.19	-13.9	0.0	-61.5	0.0
4.83	28.00	0.42	11.76	-5.03E-03	-1.19	-14.0	0.0	-67.8	0.0
5.25	28.00	0.42	11.76	-4.96E-03	-1.20	-14.2	0.0	-74.3	0.0
5.67	27.27	0.42	11.45	-4.89E-03	-1.21	-13.9	0.0	-78.8	0.0
6.09	25.48	0.42	10.70	-4.82E-03	-1.22	-13.1	0.0	-79.7	0.0
6.51	23.68	0.42	9.95	-4.75E-03	-1.23	-12.3	0.0	-79.9	0.0
6.93	21.89	0.42	9.19	-4.68E-03	-1.24	-11.4	0.0	-79.2	0.0
7.35	20.10	0.42	8.44	-4.61E-03	-1.25	-10.6	0.0	-77.8	0.0
7.77	18.30	0.42	7.69	-4.54E-03	-1.26	-9.7	0.0	-75.5	0.0
8.19	16.51	0.42	6.93	-4.47E-03	-1.27	-8.8	0.0	-72.4	0.0
8.61	14.71	0.42	6.18	-4.39E-03	-1.29	-7.9	0.0	-68.4	0.0
9.03	12.97	0.42	5.45	-4.32E-03	-1.30	-7.1	0.0	-63.7	0.0
9.45	11.57	0.42	4.86	-4.25E-03	-1.31	-6.4	0.0	-60.0	0.0
9.87	10.43	0.42	4.38	-4.18E-03	-1.32	-5.8	0.0	-57.0	0.0
10.29	9.48	0.42	3.98	-4.11E-03	-1.33	-5.3	0.0	-54.5	0.0
10.71	8.66	0.42	3.64	-4.04E-03	-1.34	-4.9	0.0	-52.2	0.0
11.13	7.94	0.42	3.34	-3.97E-03	-1.35	-4.5	0.0	-50.2	0.0
11.55	7.32	0.42	3.08	-3.90E-03	-1.37	-4.2	0.0	-48.5	0.0
11.97	6.78	0.42	2.85	-3.83E-03	-1.38	-3.9	0.0	-47.0	0.0
12.39	6.31	0.42	2.65	-3.76E-03	-1.39	-3.7	0.0	-45.7	0.0
12.81	5.91	0.42	2.48	-3.69E-03	-1.40	-3.5	0.0	-44.6	0.0
13.23	5.56	0.42	2.33	-3.62E-03	-1.42	-3.3	0.0	-43.7	0.0
13.65	5.26	0.42	2.21	-3.55E-03	-1.43	-3.2	0.0	-43.1	0.0
14.07	5.02	0.42	2.11	-3.48E-03	-1.44	-3.0	0.0	-42.8	0.0
14.49	4.82	0.42	2.03	-3.41E-03	-1.46	-2.9	0.0	-42.7	0.0
14.91	4.67	0.42	1.96	-3.34E-03	-1.47	-2.9	0.0	-43.0	0.0
15.33	4.57	0.42	1.92	-3.27E-03	-1.48	-2.9	0.0	-43.7	0.0
15.75	4.51	0.42	1.90	-3.20E-03	-1.50	-2.8	0.0	-44.8	0.0
16.17	4.50	0.42	1.89	-3.13E-03	-1.51	-2.9	0.0	-46.3	0.0
16.59	4.50	0.42	1.89	-3.05E-03	-1.53	-2.9	0.0	-48.0	0.0
17.01	4.50	0.42	1.89	-2.98E-03	-1.55	-2.9	0.0	-49.7	0.0
17.43	4.50	0.42	1.89	-2.91E-03	-1.56	-3.0	0.0	-51.4	0.0
17.85	4.50	0.42	1.89	-2.84E-03	-1.58	-3.0	0.0	-53.2	0.0
18.27	4.50	0.42	1.89	-2.77E-03	-1.59	-3.0	0.0	-55.1	0.0
18.69	4.50	0.42	1.89	-2.70E-03	-1.61	-3.0	0.0	-56.9	0.0
19.11	4.50	0.42	1.89	-2.63E-03	-1.63	-3.1	0.0	-58.9	0.0
19.53	4.50	0.42	1.89	-2.56E-03	-1.65	-3.1	0.0	-60.8	0.0
19.95	4.50	0.42	1.89	-2.49E-03	-1.67	-3.2	0.0	-62.8	0.0
20.37	4.50	0.42	1.89	-2.42E-03	-1.69	-3.2	0.0	-64.9	0.0
20.79	4.50	0.42	1.89	-2.35E-03	-1.70	-3.2	0.0	-66.8	0.0
21.21	4.50	0.42	1.89	-2.28E-03	-1.70	-3.2	0.0	-68.1	0.0
21.63	4.50	0.42	1.89	-2.21E-03	-1.70	-3.2	0.0	-69.5	0.0
22.05	4.50	0.42	1.89	-2.14E-03	-1.70	-3.2	0.0	-70.8	0.0
22.47	4.50	0.42	1.89	-2.07E-03	-1.70	-3.2	0.0	-72.2	0.0
22.89	4.50	0.42	1.89	-2.00E-03	-1.70	-3.2	0.0	-73.5	0.0
23.31	4.50	0.42	1.89	-1.93E-03	-1.70	-3.2	0.0	-74.9	0.0
23.73	4.50	0.42	1.89	-1.86E-03	-1.70	-3.2	0.0	-76.2	0.0
24.15	4.50	0.42	1.89	-1.79E-03	-1.70	-3.2	0.0	-77.6	0.0

Table A.3. Analysis of UHPC and conventional concrete at flexural capacity of exterior bridge beam.

Position (in.) {1}	Base (in.) {2}	Height (in.) {3}	Area ($in.^2$) 2x3 {4}	Total Strain {5}	Stress (ksi) {6}	Tensile Force (kips) 4x6 {7}	Compressive Force (kips) 4x6 {8}	1x7 {9}	1x8 {10}
24.57	4.50	0.42	1.89	-1.71E-03	-1.70	-3.2	0.0	-78.9	0.0
24.99	4.50	0.42	1.89	-1.64E-03	-1.70	-3.2	0.0	-80.3	0.0
25.41	4.50	0.42	1.89	-1.57E-03	-1.70	-3.2	0.0	-81.6	0.0
25.83	4.50	0.42	1.89	-1.50E-03	-1.70	-3.2	0.0	-83.0	0.0
26.25	4.50	0.42	1.89	-1.43E-03	-1.70	-3.2	0.0	-84.3	0.0
26.67	4.50	0.42	1.89	-1.36E-03	-1.69	-3.2	0.0	-85.1	0.0
27.09	4.50	0.42	1.89	-1.29E-03	-1.66	-3.1	0.0	-85.2	0.0
27.51	4.50	0.42	1.89	-1.22E-03	-1.64	-3.1	0.0	-85.4	0.0
27.93	4.50	0.42	1.89	-1.15E-03	-1.62	-3.1	0.0	-85.5	0.0
28.35	4.50	0.42	1.89	-1.08E-03	-1.60	-3.0	0.0	-85.5	0.0
28.77	4.50	0.42	1.89	-1.01E-03	-1.57	-3.0	0.0	-85.5	0.0
29.19	4.50	0.42	1.89	-9.39E-04	-1.55	-2.9	0.0	-85.5	0.0
29.61	4.50	0.42	1.89	-8.68E-04	-1.53	-2.9	0.0	-85.5	0.0
30.03	4.50	0.42	1.89	-7.98E-04	-1.50	-2.8	0.0	-85.4	0.0
30.45	4.50	0.42	1.89	-7.27E-04	-1.48	-2.8	0.0	-85.3	0.0
30.87	4.53	0.42	1.90	-6.57E-04	-1.46	-2.8	0.0	-85.6	0.0
31.29	4.59	0.42	1.93	-5.86E-04	-1.44	-2.8	0.0	-86.7	0.0
31.71	4.71	0.42	1.98	-5.15E-04	-1.41	-2.8	0.0	-88.6	0.0
32.13	4.87	0.42	2.04	-4.45E-04	-1.39	-2.8	0.0	-91.4	0.0
32.55	5.08	0.42	2.13	-3.74E-04	-1.37	-2.9	0.0	-94.9	0.0
32.97	5.33	0.42	2.24	-3.04E-04	-1.34	-3.0	0.0	-99.3	0.0
33.39	5.64	0.42	2.37	-2.33E-04	-1.32	-3.1	0.0	-104.6	0.0
33.81	6.01	0.42	2.52	-1.63E-04	-1.27	-3.2	0.0	-108.6	0.0
34.23	6.43	0.42	2.70	-9.23E-05	-0.72	-1.9	0.0	-66.7	0.0
34.65	6.92	0.42	2.91	-2.17E-05	-0.17	-0.5	0.0	-17.1	0.0
35.07	7.48	0.42	3.14	4.88E-05	0.38	0.0	1.2	0.0	42.0
35.49	8.12	0.42	3.41	1.19E-04	0.93	0.0	3.2	0.0	113.0
35.91	8.86	0.42	3.72	1.90E-04	1.48	0.0	5.5	0.0	198.4
36.33	9.71	0.42	4.08	2.60E-04	2.04	0.0	8.3	0.0	301.8
36.75	10.71	0.42	4.50	3.31E-04	2.59	0.0	11.6	0.0	427.9
37.17	11.91	0.42	5.00	4.01E-04	3.14	0.0	15.7	0.0	583.6
37.59	13.40	0.42	5.63	4.72E-04	3.69	0.0	20.8	0.0	780.7
38.01	15.43	0.42	6.48	5.43E-04	4.24	0.0	27.5	0.0	1045.4
38.43	19.66	0.42	8.26	6.13E-04	4.79	0.0	39.6	0.0	1521.1
38.85	26.50	0.42	11.13	6.84E-04	5.35	0.0	59.5	0.0	2311.6
39.27	32.00	0.42	13.44	7.54E-04	5.90	0.0	79.3	0.0	3112.7
39.69	32.00	0.42	13.44	8.25E-04	6.45	0.0	86.7	0.0	3440.3
40.11	32.00	0.42	13.44	8.95E-04	7.00	0.0	94.1	0.0	3774.0
40.53	32.00	0.42	13.44	9.66E-04	7.55	0.0	101.5	0.0	4114.0
40.95	32.00	0.42	13.44	1.04E-03	8.10	0.0	108.9	0.0	4460.2
41.37	32.00	0.42	13.44	1.11E-03	8.66	0.0	116.3	0.0	4812.7
41.79	32.00	0.42	13.44	1.18E-03	9.21	0.0	123.7	0.0	5171.3
42.25	48.00	0.50	24.00	1.08E-03	4.19	0.0	100.5	0.0	4245.4
42.75	48.00	0.50	24.00	1.17E-03	4.53	0.0	108.7	0.0	4645.2
43.25	48.00	0.50	24.00	1.26E-03	4.87	0.0	116.8	0.0	5053.3
43.75	48.00	0.50	24.00	1.35E-03	5.21	0.0	125.0	0.0	5469.5
44.25	48.00	0.50	24.00	1.44E-03	5.55	0.0	133.2	0.0	5893.9
44.75	48.00	0.50	24.00	1.53E-03	5.89	0.0	141.4	0.0	6326.4
45.25	48.00	0.50	24.00	1.61E-03	6.23	0.0	149.6	0.0	6767.1
45.75	48.00	0.50	24.00	1.70E-03	6.57	0.0	157.7	0.0	7216.1
46.25	48.00	0.50	24.00	1.79E-03	6.91	0.0	165.9	0.0	7673.2
46.75	48.00	0.50	24.00	1.88E-03	7.25	0.0	174.1	0.0	8138.4
47.25	48.00	0.50	24.00	1.97E-03	7.59	0.0	182.3	0.0	8611.9
47.75	48.00	0.50	24.00	2.06E-03	7.93	0.0	190.4	0.0	9093.5
48.25	48.00	0.50	24.00	2.14E-03	8.28	0.0	198.6	0.0	9583.3
48.75	48.00	0.50	24.00	2.23E-03	8.62	0.0	206.8	0.0	10081.3
49.25	48.00	0.50	24.00	2.32E-03	8.96	0.0	215.0	0.0	10587.5

A.2.14 Dead Load Shear at Abutment

Shear at Abutment

$V_{bm} := \frac{u \cdot A \cdot L}{2}$ $V_{bm} = 30.52k$ shear due to beam

$V_{sl} := \frac{u_s \cdot (S \cdot t_n + h \cdot b_t) \cdot L}{2}$ $V_{sl} = 53.61k$ shear due to slab

$V_b := \frac{2 \cdot b_a \cdot L}{n_b \cdot 2}$ $V_b = 11.61k$ shear due to barrier

$V_o := \frac{f_{ws} \cdot W \cdot L}{n_b \cdot 2}$ $V_o = 8.80k$ shear due to overlay

A.2.15 Live Load Shear at Abutment {4.6.2.2}

Truck Load

$$V_{tr} := \frac{32 \cdot k \cdot \left(L - \frac{H}{2}\right) + 32 \cdot k \cdot \left(L - \frac{H}{2} - 14ft\right) + 8 \cdot k \cdot \left(L - \frac{H}{2} - 28ft\right)}{L}$$

$V_{tr} = 64.7k$ truck shear

Tandem Load

$$V_t := \frac{25 \cdot k \cdot \left(L - \frac{H}{2}\right) + 25 \cdot k \cdot \left(L - \frac{H}{2} - 4ft\right)}{L}$$ $V_t = 48.3k$ tandem shear

Lane Load

$V_l := \frac{0.64\,klf \cdot L}{2}$ $V_l = 35.20k$ lane shear

Live Load

With ADTT below 100, 90% of force effect is used. {3.6.1.1.2}

$V_{ll} := 0.90\,DF_v \cdot \left(V_l + \frac{4}{3} \cdot \max(V_{tr}, V_t)\right)$ $V_{ll} = 105.0k$ live load shear

A.2.16 Shear Service Strength

Table A.4. Service shear design quantities constant over length of bridge.

Variable	Value	Variable	Value
P_f (k)	1482	c_{t3} (in)	-2.22
A (in^2)	512.3	c_{c1} (in)	0
I (in^4)	123654	c_{c2} (in)	-5.04
I_t (in^4)	126078	c_{c3} (in)	-9.04
I_c (in^4)	228251	b_w (in)	4.5
y (in)	18.72	Q_{t1} (in^3)	1839
y_t (in)	18.22	Q_{t2} (in^3)	2680
y_c (in)	25.04	Q_{t3} (in^3)	3422
h_1 (in)	25.04	Q_{c1} (in^3)	10440
h_2 (in)	20	Q_{c2} (in^3)	10383
h_3 (in)	16	Q_{c3} (in^3)	10256
c_1 (in)	6.32	w_{bm} (k/in)	0.0462
c_2 (in)	1.28	w_{sl} (k/in)	0.0812
c_3 (in)	-2.72	w_b (k/in)	0.0176
c_{t1} (in)	6.82	w_o (k/in)	0.0133
c_{t2} (in)	1.78	w_{lane} (k/in)	0.0533

Table A.5. Service shear design quantities variable over length of bridge.

x (in)	σx1 (ksi)	σx2 (ksi)	σx3 (ksi)	γxy1 (ksi)	γxy2 (ksi)
25	2.29	2.71	3.04	1.28	1.38
75	2.52	2.65	2.75	1.20	1.29
125	2.74	2.59	2.47	1.12	1.20
175	2.93	2.54	2.22	1.04	1.11
225	3.11	2.49	2.00	0.96	1.02
275	3.27	2.45	1.80	0.87	0.93
325	3.42	2.42	1.62	0.79	0.84
375	3.55	2.39	1.47	0.71	0.75
425	3.66	2.37	1.35	0.63	0.66
475	3.75	2.35	1.25	0.55	0.57
525	3.82	2.35	1.17	0.47	0.48
575	3.43	2.25	1.32	0.42	0.43
625	3.45	2.25	1.30	0.34	0.34
x (in)	γxy3 (ksi)	σp11 (ksi)	σp12 (ksi)	σp13 (ksi)	σp1 (ksi)
25	1.46	-0.57	-0.58	-0.59	-0.59
75	1.37	-0.48	-0.52	-0.56	-0.56
125	1.27	-0.40	-0.47	-0.53	-0.53
175	1.17	-0.33	-0.42	-0.50	-0.50
225	1.07	-0.27	-0.37	-0.47	-0.47
275	0.98	-0.22	-0.31	-0.43	-0.43
325	0.88	-0.18	-0.26	-0.38	-0.38
375	0.78	-0.14	-0.22	-0.34	-0.34
425	0.68	-0.11	-0.17	-0.29	-0.29
475	0.59	-0.08	-0.13	-0.23	-0.23
525	0.49	-0.06	-0.10	-0.18	-0.18
575	0.44	-0.05	-0.08	-0.13	-0.13
625	0.34	-0.03	-0.05	-0.09	-0.09

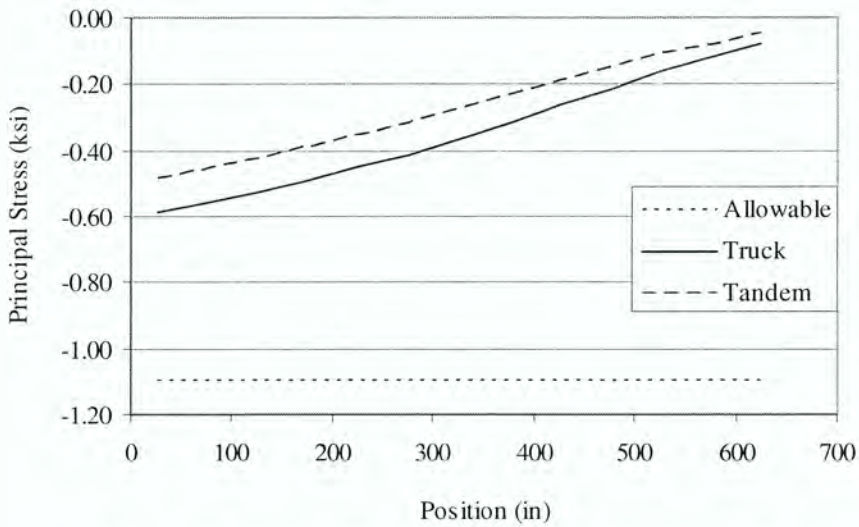

Figure A.1. Variation of principal and allowable stresses along length of bridge calculated at service level loads.

A.2.18 Shear Ultimate Strength

Table A.6. Ultimate shear design quantities constant over length of bridge.

Variable	Value
A_b (in^2)	315
d_c (in)	45.24
jd (in)	40
d (in)	37.24
N_u (k)	0
E_s (ksi)	0
A_s (in^2)	0
E_p (ksi)	28500
E_c (ksi)	7820
b_w (in)	4.5
f_{max} (ksi)	-1.7
f_{cr} (ksi)	-1.1
ε_{max}	-0.0024
Φ	0.85
M_{cr} (in-k)	36396.52
M_n (in-k)	104274

Table A.7. Ultimate shear design quantities variable over length of bridge.

x (in)	A_p (in^2)	A_{pbf} (in^2)	θ (rad)	F_{bf} (k)	ε_x	ε_{xall}
25	7.16	5.64	0.22	0	0.00108	0.00081
75	8.90	7.38	0.24	0	0.00093	0.00065
125	10.63	9.11	0.24	0	0.00072	0.00060
175	10.63	9.11	0.31	-25	0.00040	0.00028
225	10.63	9.11	0.4	-73	0.00011	-0.00003
275	10.63	9.11	0.51	-115	-0.00022	-0.00037
325	10.63	9.11	0.62	-152	-0.00057	-0.00070
375	10.63	9.11	0.73	-184	-0.00090	-0.00103
425	10.63	9.11	0.83	-210	-0.00120	-0.00133
475	10.63	9.11	0.91	-230	-0.00144	-0.00156
525	10.63	9.11	0.98	-245	-0.00162	-0.00175
575	10.63	9.11	1.02	-255	-0.00172	-0.00186
625	10.63	9.11	1.03	-259	-0.00176	-0.00189

x (in)	Δεx	V_{n1} (k)	V_{n2} (k)	V_n (k)	ΦV_n (k)	V_u (k)
25	0.00027	1368	449	449	381	294
75	0.00028	1250	449	449	381	275
125	0.00013	1250	449	449	381	256
175	0.00012	955	449	449	381	238
225	0.00014	724	449	449	381	219
275	0.00015	547	449	449	381	201
325	0.00013	429	449	429	364	182
375	0.00013	342	449	342	291	163
425	0.00013	280	449	280	238	145
475	0.00012	238	449	238	202	126
525	0.00014	205	449	205	174	107
575	0.00014	188	449	188	160	89
625	0.00013	184	449	184	156	70

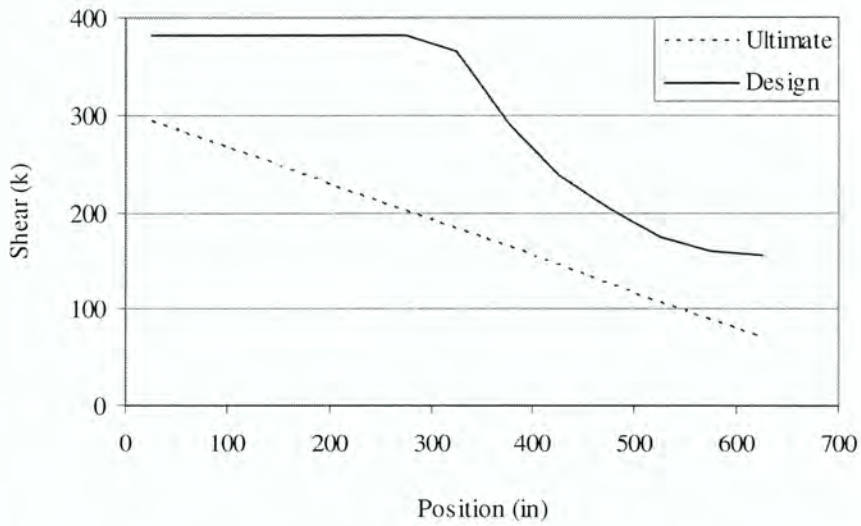

Figure A.2. Variation of ultimate and design shear forces along length of bridge.

A.3 SMALL-SCALE BEAMS

Small-Scale Beam Parameters

$f'_c := 25ksi$		compressive strength
$w_{web} := 1.75in$		width of web
$S_1 := 15in$		short span
$S_2 := 18in$		long span
$H := 10in$		height of beam

Loading

$P := 135k$	iteratate until the strut fails	total applied load

Geometry

$C_t := 0.731in$	iterative	distance from top or bottom of beam to centroid of node
$C_b := 2in$		
$h := H - C_t - C_b$	$h = 7.269in$	strut height
$L_1 := \sqrt{h^2 + S_1^2}$	$L_1 = 16.668in$	length of short strut
$L_2 := \sqrt{h^2 + S_2^2}$	$L_2 = 19.412in$	length of long strut
$R := \frac{S_1}{S_2}$	$R = 0.833$	ratio of strut loads

$$P = P_1 \cdot \frac{h}{L_1} + P_2 \cdot \frac{h}{L_2}$$

$$P = P_1 \cdot \frac{h}{L_1} + P_1 \cdot R \cdot \frac{h}{L_2}$$

$$P_1 := \frac{P}{\frac{h}{L_1} + R \cdot \frac{h}{L_2}} \qquad P_1 = 180.448\text{k}$$ load on short strut

$$P_2 := P_1 \cdot R \qquad P_2 = 150.374\text{k}$$ load on long strut

Strength of Node

$\beta_n := 0.85$ factor

$f_{cu} := 0.85 \beta_n \cdot f'_c \qquad f_{cu} = 18.063\text{ksi}$

Geometry of Top Node

$$a := \frac{P}{f_{cu} \cdot w_{web}} \qquad a = 4.271\text{in}$$ horizontal dimension of node

$$a_1 := a \cdot \frac{P_1}{P} \qquad a_1 = 5.709\text{in}$$ short strut dimension of node

$$a_2 := a \cdot \frac{P_2}{P} \qquad a_2 = 4.757\text{in}$$ long strut dimension of node

$$\alpha_1 := 90\text{deg} - \operatorname{atan}\left(\frac{h}{S_1}\right) \qquad \alpha_1 = 64.145\text{deg}$$ node angle

$$z_h := \frac{a}{2} - \frac{a_1}{2}\cos(\alpha_1) \qquad z_h = 0.891\text{in}$$ nodal dimension

$$z_v := z_h \cdot \tan(\alpha_1) \qquad z_v = 1.838\text{in}$$ nodal dimension

$$C_t := \frac{a_1}{2}\cdot\sin(\alpha_1) - z_v \qquad C_t = 0.731\text{in}$$ distance from top of beam to centroid of node

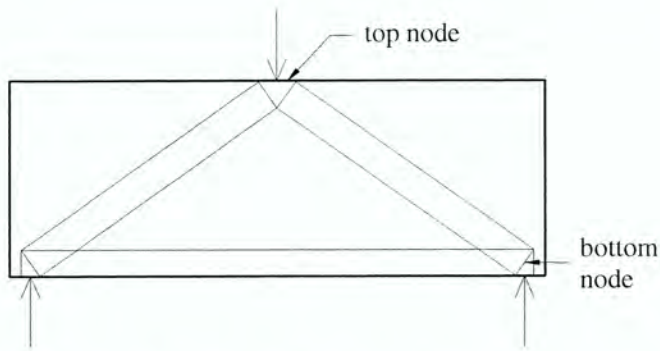

Figure A.3. Strut and tie model of small-scale test beam.

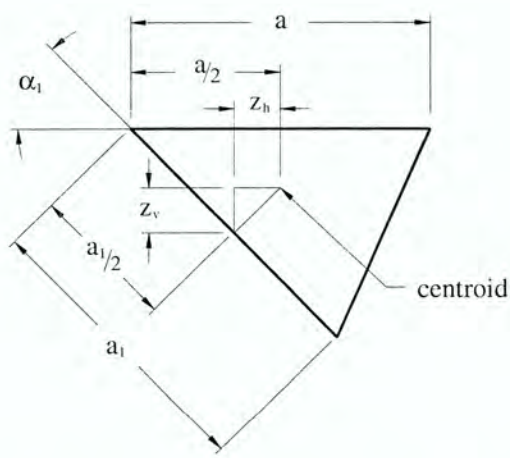

Figure A.4. Top node geometry of small-scale test beam for use in a strut and tie model.

Geometry of Bottom Node

$$\frac{P_1 \cdot \cos(\alpha_1)}{f_{cu} \cdot w_{web}} = 2.49\text{in}$$

This less than the two times the two inches from the bottom of beam to the strands. Therefore, the geometry is satisfactory for the bottom node.

Strength of Strut

$\beta_s := 0.85$

$f_{cu} := 0.85 \beta_s \cdot f'_c$ $\quad f_{cu} = 18.063\text{ksi}$

$A_c := w_{web} \cdot a_1$ $\quad A_c = 9.99\text{in}^2$

$F_{ns} := f_{cu} \cdot A_c$ $\quad F_{ns} = 180.448\text{k}$

$P_1 = 180.448\text{k}$

Strength of Tie

$P_{tie} := P_1 \cdot \cos(\alpha_1)$ $\quad P_{tie} = 78.692\text{k}$

$A_s := 3 \cdot 0.153\text{in}^2$

$fy := 270\text{ksi}$

The final prestressing force was estimated to be 45k.

$A_s \cdot fy - 45\text{k} = 78.93\text{k}$